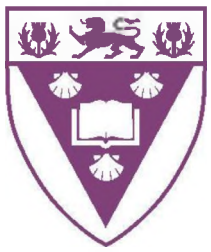

RHODES UNIVERSITY

Grahamstown • 6140 • South Africa

Mineralogy and geochemistry of structurally-controlled metasomatic alteration of carbonate-rich manganese ore at Mamatwan Mine, Kalahari Manganese Field.

A thesis submitted in partial fulfillment of the requirements for the degree of Master of Sciences (by coursework and thesis) in Economic Geology,
Department of Geology, Rhodes University

By

Esau Tonderai Harawa

Supervisor: Prof H. Tsikos

Co-supervisor: Prof J. Harmer

July 2016

ABSTRACT

The Kalahari Manganese Field (KMF) located in the Northern Cape Province about 700km south west of Johannesburg contains 80% of the world manganese ore reserves. Mamatwan Mine is hosted within the low grade Mamatwan type ore and is located in the southernmost tip of the KMF. This mine is an open pit mine which is divided into three benches namely the top cut, middle cut and bottom cut. These three benches are structurally controlled by faults which influence the overall grade of the manganese ore. This study is a follow up work to the previous two studies carried out at Wessels Mine and Mamatwan Mine by (Gutzmer and Beukes) in 1995 and 1996 respectively with regards to alteration processes around fault controlled systems in which they concluded that epithermal fluids caused local reduction and bleaching of ore followed by oxidation and carbonate leaching of manganese ore through ascending oxidized groundwater.

Metasomatic activity around fault controlled systems is controlled by three main processes namely redistribution, enrichment and depletion. These processes are determined by mobility/immobility of elements from the fault which are introduced into the pre-existing braunite carbonate rich ore. Elements such as Ca, Mg, Si, Fe, C and Mn interact with pre-existing ore due to temperature, fluid pressure, physico-chemical property of fluid gradient. Structurally, faulting and folding contribute to the movement of elements as one end of the system gets depleted the other end of the system gets enriched and vice versa.

To better understand this metasomatic activity, it is crucial to conduct mass balance studies of these elements. Grant (1986) introduced the isocon diagram which is a modification of Gresen's equation (1967) to ascertain which elements are directly or indirectly related to alteration through enrichment and depletion of Ca, Mg, Si, Fe, C and Mn. As the section approaches from altered to less altered manganese ore the mineral chemistry gradually changes from a manganese rich matrix composed of manganomelane and todorokite to a carbonate rich matrix composed of braunite, dolomite, kutnohorite and Mn-rich calcites.

ACKNOWLEDGEMENTS

I would like to express my gratitude to the whole Rhodes Geology department, particularly Professor Harilaos Tsikos, Ashley Goddard (for her wonderful support) and the Julian Baring Scholarship for assisting me with making this dream a reality. Professor Tsikos was exceptional in his supervision and assistance in funding for my laboratory costs and field costs to Mamatwan Mine and giving me insight into the knowledge of manganese. I personally believe he is one of the best lecturers in South Africa. Special mention goes to Thapelo Moloto and her expertise in assisting me with use of electron microprobe machine. The use of Jeol JXA 8230 Superprobe, instrument sponsored by NRF/NEP grant 40113 (UID 74464) is kindly acknowledged.

Special mention also is extended to the geology staff at South 32 namely Ayanda Ntalo the Chief Geologist at Mamatwan Mine for agreeing to this project and mobilizing all the resources for me to be able to carry out this project.

To my belated parents I wish you were alive to witness this milestone but I trust by faith wherever you are that you can see this. Special thanks goes to Mr Francis Harawa for pushing me this far, I would not have come this far if it was not for you. To my beloved mum and sister, Mrs Ruth Manjolo Harawa and Wezi Harawa thank you for supporting me and being there for me. I deeply appreciate your efforts and your input in my life. To the Gaza and Muzenda family, thank you for supporting me from childhood when I needed your help the most. To my brothers Dennis and Tawanda, if it was weren't for you I will not have managed to even complete my school. I appreciate your encouragement and support and thank you so much for everything.

Lastly to the 3 most important people to my life thank you for being there for me and giving me moral support and encouragement throughout the year while I was undertaking my studies. This is for you Nyasha, Anthony and Matipa, we have done it. Thank you for being supportive and for your endurance. Anthony and Natalie, I hope this will give you encouragement in the near future to surpass this hallmark.

DECLARATION

All material contained in this thesis represents the original work of the author except where specific acknowledgement is made to others.

18 July 2016

Geology Department

RHODES UNIVERSITY

GRAHAMSTOWN - SOUTH AFRICA

"Nhasi ndezvedu ita makorokoto kwatiri wedu wadadisa, wazvinzwa ka"

OLIVER MTUKUDZI
(Reference to acknowledging a successful completion of a project)

Table of Contents

CHAPTER ONE: INTRODUCTION AND GEOLOGICAL SETTING 1

1.1. Geographical setting 1

1.2. General 2

1.3. History of the mine 2

1.4. Production and reserves 3

1.5. Previous work 3

1.5.1. High grade Wessels type ore 3

1.5.2. Summary of key points 7

1.5.3. Low grade Mamatwan type ore 8

1.5.4. Concluding remarks 12

1.6. Aims and objectives 13

1.7. Methodology 14

1.7.1. Overview of the study area 14

1.7.2. Limitations of this study 14

1.7.3. Mapping 15

1.7.4. Sampling 15

1.7.5. Sample widths 17

1.7.6. Petrography 18

1.7.7. Sample preparation 18

1.7.8. XRD 18

1.7.9 Geochemistry 18

1.8. The Kalahari Manganese Field (KMF) 19

1.9. The Transvaal Supergroup in the Northern Cape 19

1.10. The Geology at Mamatwan Mine 24

CHAPTER TWO: MINERALOGY AND PETROGRAPHY 25

2.1. Introduction 25

2.2. X-Ray diffraction 25

2.3. XRD ANALYSIS: Cross section showing mineralogy 26

2.4. XRD ANALYSIS: Relationship between mineralogy and grade 27

2.4.1. Braunite vs Mn_2O_3 27
2.4.2. Calcite vs Mn_2O_3 27
2.4.3. SiO_2 vs Braunite vs Quartz 28
2.4.4. Hematite vs Goethite vs FeO vs Kutnohorite 28
2.4.5. MgO vs Kutnohorite 29
2.4.6. CaO vs Calcite vs Dolomite vs Kutnohorite 29
2.5. EMPA **30**
2.5.1. Mineral chemistry of selected samples 31
2.5.2. List of gangue minerals 31
2.6. Distribution of carbonates **32**
2.7. Compositional maps **33**
2.7.1. Unaltered ore: RW16 33
2.7.2. Altered ore adjacent to the main structure on the right side: RW1 34
2.7.3. Altered ore on the right side: RW8 35
2.7.4. Altered ore on the left side: LSW2 36
2.8. Petrography **37**
2.8.1. EMPA: Back scattered images 37
2.8.2. Evidence of faulting 38
2.8.3. Textures and Mineralogy 39
2.8.4. Replacement textures 41
2.8.5. Evidence of folding 42
2.8.6. Change in matrix composition 43
2.9. Petrological description of ore **44**
2.9.1. Adjacent to the fault 44
2.9.2. Altered ore: Eastern side (Left) 45
2.9.3. Less altered ore: Western side (Right) 46
2.9.4. Unaltered ore: Western side (Right) 46
CHAPTER THREE: GEOCHEMISTRY **47**
3.1. Introduction **47**
3.1.1. Major Oxides 47
3.1.2. Minor Oxides 48
3.2. Bivariate plots **49**
3.3. Lateral geochemical profiles (traverses) **53**

3.3.1. CaO *53*
3.3.2. CaO (without fissures: LSW3, LSW6 and RW5) *53*
3.3.3. MgO *55*
3.3.4. MgO (without fissures LSW3, LSW6 and RW5) *55*
3.3.5. Mn_2O_3 ..... *57*
3.3.6. Mn_2O_3 (without fissures LSW3, LSW6 and RW5) *57*
3.3.7. $K_2O + Na_2O$ *59*
3.3.8. $K_2O + Na_2O$ (without fissures LSW3, LSW6 and RW5) *59*
CHAPTER FOUR: DISCUSSION AND RECOMMENDATIONS **61**
4.1. Introduction **61**
4.2. Mineralogy of the main structure **61**
4.3. Isocon applications: Left side **63**
4.3.1. Mass balance calculations *63*
4.3.2. Chemical redistribution *64*
4.3.3. Net enrichments *64*
4.3.4. Net depletions *65*
4.4. Isocon applications: right side, most altered samples **65**
4.4.1. Chemical redistribution *66*
4.4.2. Net enrichments *66*
4.4.3. Net depletions *67*
4.5. Isocon applications: right side, approaching unaltered ore **67**
4.5.1. Chemical redistribution *68*
4.5.2. Net enrichments *68*
4.5.3. Net depletions *69*
4.6. Summary **69**
4.7. Recommendations **71**
4.7.1. Effect of faulting *71*
4.7.2. Effect of folding *72*
4.7.3. Grade control *73*
4.7.4. Identification in the field *73*
4.7.4. Fissures *74*
4.8. The "SMARTT" event **74**
4.9. Conclusions **75**

REFERENCES **77-82**
APPENDICES **83**
A.1. Part A: Compositional maps **83**
A.1.1. LSW1 ..... *83*
A.1.2. LSW2 ..... *84*
A.1.3. LSW5A *85*
A.1.4. RW1 ..... *86*
A.1.5. RW4 ..... *87*
A.1.6. RW8 ..... *88*
A.1.7. RW12 ..... *89*
A.1.8. RW16 ..... *90*
B.1. EMPA raw data **90**
B.1.1. Oxides *91*
B.1.2. Carbonates *93*
B.1.3. Silicates *96*

CHAPTER ONE: INTRODUCTION AND GEOLOGICAL SETTING

1.1. Geographical Setting

The Mamatwan manganese mine is an open pit mine found in the Northern Cape Province of South Africa. It is part of the Kalahari Manganese Field (hereafter referred to as KMF) which is situated approximately 60 km from the town of Kuruman. The mine is found on the southernmost part of the KMF which is hosted in the low grade sedimentary Mamatwan-type ore (Fig.1.1C).

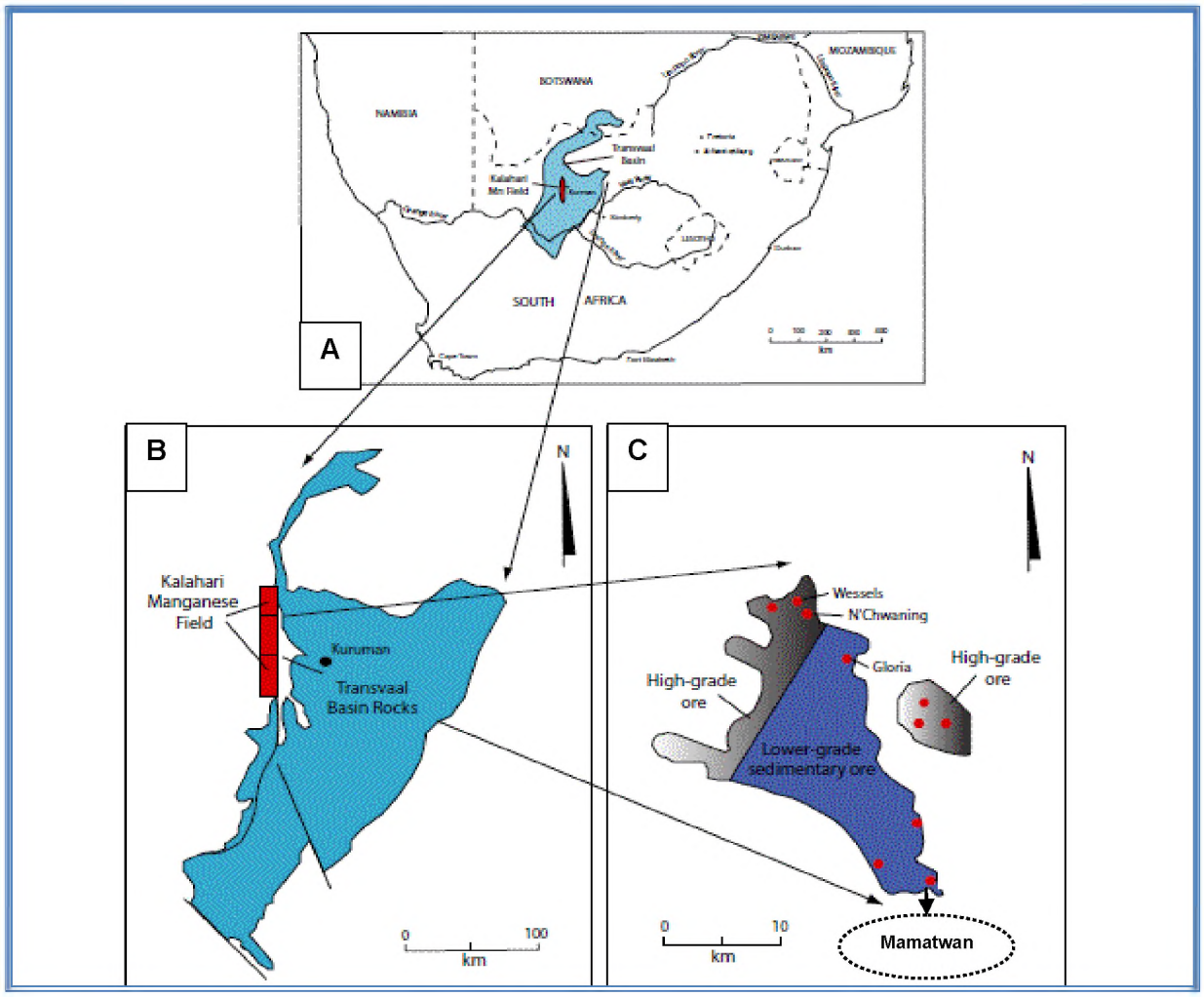

Figure 1.1: Modified from Tsikos and Moore (1998). (A) Map showing the geographical position of the KMF in the Northern Cape Province of South Africa. (B) Map showing the position of the KMF in relation to the Transvaal Basin Rocks. (C) Map showing the enlarged view of the KMF and the location of Mamatwan Mine as well as the distribution of the low grade Mamatwan type ore and the high grade Wessels type ore.

1.2. General

The Mamatwan Mine is owned by South 32 (formerly BHP Billiton) were it controls both the Hotazel Manganese Mines (hereafter referred to as HMM) and Metalloys. South 32 was officially formed in May 2015 by merging lucrative BHP Billiton operations in the southern hemispehere. It has an ownership of 60% in Samancor Holdings and the remaining 40% is owned by Anglo American. This joint venture covers both the mining and processing operations. South 32 has other business interests in other commodities besides manganese on the African continent. In Mozambique it owns the sole aluminium smelter in the entire country which in turn is the second largest aluminium smelter in Africa.

In South Africa it has ventures in other commodities such as aluminium and coal. It owns a world class aluminium smelter in Richards Bay, Hillside in the province of Kwazulu Natal. The energy coal ventures are located in the coal fields of Mpumalanga which consist of 4 coal mining ventures and 3 processing plants.

1.3. History of the Mine

The HMM in the Northern Cape belongs to the District Municipality of John Taolo Gaetsewe. Hotazel was named after World War 2 by land surveyors who described the area as a hot place and named it “Hot as Hell”. On 23 July 1937 Dr H. J van der Bilj formed a company called African Metals Corporation (Amcor). This company focused on production of high carbon ferromanganese (HCFeMn) and pig iron. In 1939 two electric furnaces were established to produce ferro alloys.

Samancor Manganese’s Metalloys plant was initially developed in Vereeniging and was later moved to Meyerton were it was officially commissioned on 11 April 1951. This plant has been functional up to present day. The establishment of this plant generated demand for manganese which motivated the opening of the high grade underground Wessels Mine and the low grade open cut Mamatwan Mine in 1973 and 1964 respectively.

1.4. Production and Reserves

The Mamatwan Mine represents one of the largest manganese reserves in South Africa having estimated reserves of 433 million tonnes of manganese ore grading 40% manganese metal (National Academies, 1981). According to (Samancor, 1994) the Mamatwan Mine has an estimated yearly production tonnage of 1.2 million tons of manganese ore. Approximately 500 000 tons of manganese ore is exported to international markets by ships through the harbor at Port Elizabeth and the remaining ore is fed to local plants at Meyerton and Newcastle.

1.5. Previous work

Not many studies have been done in this area in relation to metasomatic alteration processes around fault controlled systems in the KMF. Two main studies were carried out in the KMF to investigate the alteration changes from the fault zones. The first research was initiated at Wessels Mine on high grade Wessels type ore in 1995 by authors Beukes, N.J, Burger A.M and Gutzmer J at Wessels Mine in the Northern part of the KMF. The second research was done on low grade sedimentary Mamatwan type ore by Gutzmer J, Beukes, N.J and Yah, H.-W at Mamatwan Mine in the Southern part of the KMF in 1996. All these studies were carried out under the affiliation of the Rand Afrikaans University (now University of Johannesburg). The following two studies are a detailed record of their publications and their results:

1.5.1. High grade Wessels type ore

The most important finding was to note the alteration of Mamatwan-type ore to Wessels-type which are fault related. It was noted that the high grade Wessels-type ore is present in the ferruginized fault areas. The process of alterating Mamatwan-type ore to Wessels-type ore is accompanied with an increase in the porosity of ores, recrystallization of the unaltered aphanitic Mamatwan-type ore to a phaneritic size, dissolving of dolomites, Mn-rich calcites and kutnohorites ($CaMn^{2+}(CO_3)_2$ together with discharging of silica from braunites. The name of this alteration is referred to as hydrothermal-metasomatic alteration.

The postulated model suggests that hydrothermal fluids were provided through a channel from fault channel ways into the diagenetic Mamatwan-type ores and this fluid interacted causing alteration and in the end producing high-grade Wessels-type ore. This same model was obtained from Gutzmer & Beukes (1993; in press) in explaining to what caused the alteration of the ores at the Nchwaning Mine.

The initial transformation from primary Mamatwan-type ore and Wessels-type ore furthest away from major fluid conduits along faults shows that the intial indication of alteration is shown by the conversion of kutnahorite into calcite and hausmannite (Mn_3O_4), a reaction as depicted by the following chemical equation:

$$3CaMn(CO_3)_2 + 1/2O_2 \longrightarrow Mn_3O_4 + 3CaCO_3 + 3CO_2$$

As the zone proceeds laterally into areas with intense alteration, silica and calcium are leached out of the ore resulting in braunite initially being converted into braunite II, and then into bixbyite $(Mn, Fe)_2O_3$. The above explanation is shown by the following chemical reaction:

$$\text{braunite} + \text{hematite} + \text{calcite} + O_2 \longrightarrow \text{braunite II} + CO_2 + SiO_2$$

and

$$\text{braunite II} + \text{hematite} \longrightarrow \text{bixbyite} + CaO + SiO_2$$

The following stage involves the formation of ore which is predominantly hausmannite through reducing trivalent manganese to the divalent state. This conversion is associated with desilicification during the replacement of braunite II and braunite (new) by hausmannite. In instances where hausmannite appears pseudomorphic replacement of bixbyite, the conversion process could have involved reduction of some of the trivalent manganese present in the bixbyite.

Wessels-type ore, which constitutes mostly hausmannite, formed in close proximity to the faults which behaved as channel ways for hydrothermal fluids. These ores were possibly enriched by manganese that was released from the zones of enriched with iron along faults.

This ferric iron formed by the reaction above led to the formation of hematite which gives explanation to ferruginization along faults, with manganese being moved further into the manganese bed forming ore which is rich in hausmannite.

The formation of the aphanitic Fe-rich hausmannite by the phaneritic Fe-deficient hausmannite could have been to the establishment of Mn^{2+}-rich fluids. The subsidiary braunite-rich areas, formed between the iron rich (ferruginized) areas and the very high-grade hausmannite-rich ore, could have established by reprecipitation of silica released from braunite in the low-grade ores located in the distal areas away from the channel ways. (Fournier, 1986) suggested that when temperatures of the hydrothermal fluids decreased it led to the impregnation of silica leading to reprecipitation of the SiO_2 either as quartz or the silica component in braunite. This technique could provide reason for the existence of quartz and silicates in some of the ferruginized zones. Dissolved silica could have been re-established as andradite in secondary pores or as a substitute of carbonate ovoids, latter modification could have taken place as explained from the below chemical reaction (Kleyenstüber, 1985):

$$3CaCO_3 + Fe_2O_3 + 3SiO_2 \longrightarrow Ca_3Fe_2Si_3O_{12} + 3CO_2$$

Calcite Hematite Andradite

Calcium discharged from the carbonates led to the formation of secondary calcite, braunite II ($Mn^{2+}Mn^{3+}{}_6SiO_{12}$), marokite ($CaMn^{3+}{}_2O_4$), andradite, and gaudefroyite ($CaMn^{3+}{}_{2.5}(BO_3)_3(CO_3)O_{2.25}(OH)_{0.75}$. Carbon dioxide absolved during the transformation process, reacted with calcium and manganese led to the establishment of secondary calcite and manganoan calcite. Moreover with regards to ferrous iron, some quantities of sodium and potassium were most likely injected by the hydrothermal fluids into the existing set-up, whilst the remaining were redistributed to create gangue minerals such as barite, clinochlore, and andradite. Gutzmer & Beukes (1995) indicated that the following minerals such as potassium feldspar, acmite, richterite, xonotlite, and datolite as further gangue minerals that are closely related with the high grade Wessels-type ore at Nchwaning Mine. Kleyenstüber (1984; 1985) discovered diaspore and hydrogrossularite in veinlets as closely related with Wessels-type ore.

It is crucial to emphasize that the alteration process was explained as a sequence of metasomatic fronts that intruded the Mamatwan-type ore from a channel way along a normal fault.

Consecutive fronts thus imprinted each other sideways as the zone of alteration adjacent to the fault area extended further from the fault channel ways (Khorshinskij, 1970).

When hydrothermal activity was decreasing the metasomatic front moved back, and during that period resilicification and carbonatization occured in the domain of the fault areas with the establishment of secondary braunite ore adjacent to the iron rich (ferruginized) areas and formation of quartz and calcite in the fault zone.

It was proposed that the hydrothermal fluid developed gradually as it percolated the ore bed. "Primary" fluids that shifted along fault channel ways could have been acidic and reducing in order to carry substantial quantities of ferrous iron in solution. The fluids also carried relative quantities of alkalis, and were underfed with silica and carbon dioxide. As the fluids percolated the adjacent Mamatwan-type ore, the dissipated ferrous iron interacted with the trivalent manganese in braunite, causing formation of hematite and disintergration of divalent manganese. The interaction of carbonates in the sedimentary manganese ore (Gutzmer, 1993) most likely caused an elevation in the alkalinity of the fluid intensifying the disintegration of SiO_2. Moreover the fluid temperature would have diminished with increased distance from main channel ways. As hydrothermal activity was decreasing the temperature was also decreasing concurrently, causing fluids to be saturated with silicate. During this period the formation of secondary braunite and quartz adjacent to the fault areas is anticipated.

The exact timing of hydrothermal activity is not known however studies by Kleyenstüber (1985) tried to explain the formation of new minerals during hydrothermal activity caused by thrusting in the KMF. It was postulated that the hydrothermal alteration occurred either during or post the thrusting event. There was no proof present to directly connect the minerals formed during the hydrothermal activity along planes of thrust faults with those closely related with normal faults.

Dixon (1989) used the Rb-Sr method of dating sugilite (KNa_2 (Fe,Mn, Al)$_2Li_3Si_{12}O_{30}$) and Pb-Pb dating of the mineral galena to establish the timing of this hydrothermal alteration event and found out to be around 1350-1250Ma. Bostonite dykes (pinkish alkali feldspars rich intrusive rocks), slightly altered by the hydrothermal process, give a relative Rb-Sr age of 1350 Ma (Dixon, 1989).

The sequence of events in the Kalahari manganese field can thus be outlined as follows: firstly the deposition of primary sedimentary ore occurred around 2240 to 2100 Ma ago. Secondly it accompanied a time of folding, uplift, and erosion before the deposition of the Mapedi red beds and Hartley lava some 1900 Ma ago. Bostonite dykes could have been emplaced post the folding event but before denudation of the Hotazel Formation in pre-Mapedi times. The Mapedi red beds show swift distinctions in thicknesses (Beukes, 1983, Beukes & Smit, 1987) which show indication that deposition occured in a fault environment. The network of normal faults, associated with the enrichment of iron in manganese ores occurred could have been established during deposition of the Mapedi Formation. Reverse faulting occurred during the Kheiss orogeny around 1750 Ma ago (Beukes & Smit, 1987).

1.5.2. Summary of key points

The normal faults acted as channel ways for hydrothermal fluids which regenerated, and thereby enhanced low-grade Mamatwan-type ore to high-grade Wessels-type ore. The manganese ores in close proximity to the faults are rich in hematite, and primary textures and features were completely obliterated. A consistent gradation of textures and minerals is well defined in manganese ore which are in areas closely related to (iron rich) ferruginized fault areas. Areas of ferruginized ore are marked by areas of massive secondary braunite ore, thereby superceded by areas of porous phaneritic high-grade hausmannite-rich ore, partially porous braunite II and concentrated microcrystalline Mamatwan-type ore. Metasomatic alteration was attributed to hydrothermal fluid constituting rich iron in solution, and constituting minor quantities of Na and K.

These fluids caused movement of SiO_2, CO_2 and CaO as they moved through the ore beds. Mn^{2+}, released by reduction of Mn^{3+} by Fe^{2+} with formation of hematite in the fault areas, reprecipitated in the vicinity of the fault areas to establish hausmannite-rich Wessels-type ore.

The gradation of Mamatwan-type ore is associated with kutnohorite being changed to hausmannite and calcite, and silica released from braunite to form braunite II, braunite (new), bixbyite, and hausmannite. The hydrothermal fluids form secondary minerals such as gaudefroyite, clinochlore, barite, and andradite. The source of this hydrothermal fluid could not be established as well the occurrence of this metasomatic process. A study conducted by Dixon (1989) shows that the hydrothermal alteration occurred between 1350 - 1250 Ma ago.

1.5.3. Low grade Mamatwan type ore

The study on Mamatwan fault-controlled alteration discovered four well defined alteration periods which influenced the braunite. Comparative age correlations between these episodes are acknowledged, but the definite timing of the episodes remains uncertain. These four episodes are summarized as follows:

a) Low temperature and low pressure metamorphism which is closely related with metasomatism along specific stratigraphic zones within the ore body.

b) Ore has been reduced around structures such as veins and joints causing deposition of minerals such as hematite calcite-sulphide influenced by epithermal fluids.

c) The pressure from ground water has caused intensive brecciation in the vicinity of the faults.

d) Near - surface weathering across the outcrop of the ore body at the bottom of the Kalahari unconformity by sinking rapid fluids.

The study showed that the faulting of the manganese ore bed has an east-west-trend, and the confined alteration of the ore occurred in the fault areas directly next to them.

The ore has also been locally affected by alteration alongside a set of widely spaced joints transecting the ore bed. Nel et al. (1986) gave a detailed account of the geology of Mamatwan mine and the petrography and geochemistry of the ore body.

The suggested series of episodes that influenced the unaltered manganese ore at Mamatwan mine postulated that the unaltered ore were formed due to stratabound metasomatism related to low grade metamorphism (Kleyenstüber, 1984).

The extent of metasomatism is confined to oxidation of Mn-rich calcites and kutnohorite which in turn are replaced and form secondary minerals such as hausmannite, partridgeite, manganite, and calcite at certain strata.

Kleyenstüber (1984; 1985) and Nel et al. (1986) illustrated this substitution of kutnahorite ovoids by hausmannite and calcite and depicted this finding as late diagenetic or metamorphic oxidation of kutnahorite to hausmannite and calcite.

De Villiers (1983) made the discovery of the mineral partridgeite (Mn_2O_3). He regarded partridgeite as a mineral which is a product of cooling temperatures. The substitution is a result of metasomatism of Mn-calcites and kutnohorite by replacement of secondary minerals such as hausmannite, partridgeite, and manganite (MnO(OH)) causing oxidation of Mn^{2+} to Mn^{3+} and the mineral manganite is hydrated. It is also suggested that the stratigraphic modification of minerals happened as a result of metamorphism that is associated with hydrothermal fluids being confined to specific strata and the deficiency of CO_2 from specific carbonate laminae or ovoids. Metamorphism was superseded by two episodes of fault bound hydrothermal-metasomatic alteration which are structurally related.

The unaltered manganese ore which was affected by the faulting event changed its colour and the manganese ore got reduced. This unaltered ore caused braunite to be substituted by secondary minerals such as jacobsite ($MnFe_2O_4$), hausmannite, and clinochore ($(Mg, Fe^{2+})_5Al[OH)_8/(Si,Al)_4O_{10}]$. The manganese ore became rich in hematite and changed its colour to become redder in appearance as a result of this reduction reaction.

The alteration was associated with the presence of pyrite and quartz and the wallrock alteration was formed as a result of hydrothermal fluids being fed from the veins and joints.

These channel ways of hydrothermal fluids such as joints and veins are impregnated by minerals such as kutnahorite, Mn-calcite, pyrite, and talc. Breccia textures are evidence of deformation occurring at the same time as hydrothermal activity.

The deficiency of Ba, the establishment of pyrite and carbonates such as Mn- rich calcites, kutnohorite and dolomite suggests that alteration occurred in a reduction environment with substantial quantities of H_2S and CO_2. Braunite was initially converted into jacobsite and hausmannite and as the intensity of alteration increased it led to the discharge of manganese in its divalent structure. Pyrite is formed as a result of intense alteration whereas hematite is prevalent at low to medium degrees of wall rock alteration.

H_2S is postulated to be the prevalent sulphur compound as alteration occurred because of the movement of Ba in the altered areas and the existence of the mineral pyrite. Widespread fluid-wallrock alteration is cited to interpret coherent disparities of the stable isotope indication in unaltered and recrystallized carbonates. Recrystallization of unaltered carbonates and increase of porosity between the crystal grains moderated the means of infiltration. The minerals formed in close association with structures such as veins and the reasonably light Delta $^{18}O_{PDB}$ signature of recrystallized carbonates are evidence of near surface temperatures. This definition of hydrothermal fluid is subjective and is not successful to describe the recognizable diminished delta ^{18}O in the jacobsite rich gradation zone of the alteration halo.

The secondary alteration event is prompted by the main structure which has been reactivated. Intense hydrothermal pressure and swift fluid circulation are the causes of widespread brecciation of up to a width of 6.5m in the calcite rich fault breccia. The specks of altered ore constitute the coarse grained part of a matrix primarily composed of calcite and dolomite.

The nature of these fault breccias resemble hydrothermal breccias analogous to carbonate-hosted near surface MVT-type Pb-Zn deposits such as in Griqualand West (Pering, Bushy Park, see Martini et al., 1995).

Percolation of the hydrothermal fluid into the unaltered braunite- carbonate rich ore resulted in widespread alteration portrayed by oxidation of the braunite-carbonate rich manganese ore, the withdrawal of CO_2, and the establishment of alteration minerals such as todorokite (Mn^{2+}, CaMg)$Mn^{4+}{}_3O_7H_2O$) and manganomelane (K,Na, $Ba)_{2-z}(Mn^{2+}$, $Fe^{3+})_{8-z}O_{16-x}(OH)_x$.

Elevated capacity of porosity in altered ore permitted the percolation of the hydrothermal fluid further into the manganese ore body.

The prevalence of alteration minerals such as todorokite is evidence of high oxygen fugacities and low temperatures as alteration was taking place (Frenzel, 1980). There are differences of low the K and Na; and Ca-Mg-rich dominant todorokite and manganomelane as compared to K rich cryptomelane of the late Kalahari near surface weathering along the Kalahari unconformity (Kleyenstüber, 1993). However, it relates closely to the chemistry of the primary Ca-Mg-Mn-carbonates in the Mamatwan-type ore.

The noticeable alteration of todorokite to manganomelane signals continuous discharge of Mg. This transformation is associated with the oxidation of Mn^{2+} and Mn^{3+} to Mn^{4+}, the discharge of substantial quantities of Ca, Mg, and CO_2 and the development of H_2O and SiO_2. The discrepancy of carbon and oxygen isotopes in unaltered and altered carbonates are strong indication for widespread fluid-wallrock processes. An isotope study shows a strong relationship between the carbonates in the fault breccias and the calcrete formed from underground water suggesting that the underground water could be the source of the hydrothermal fluid.

Fluid-wall rock isotope interaction is limited to chemical interactions rates at temperatures below 80 degrees celcius (Zheng & Hoefs, 1993).

This low temperature of below 80 degrees celsius may invalidate the theory as the unaltered carbonates are absorbed chemically by the hydrothermal fluids and the altered carbonates with an isotope marker in between the braunite and the hydrothermal fluids are deposited.

The cause of brecciation maybe due to hydrostatic pressure derived from groundwater as faults are remobilized as the water is ascending through these channel ways. There is a direct correlation of the nature of early and late groundwater as it was oxidized and less fed with CO_2 proving low salinity of ground water. These fault related episodes are dissimilar to each other as compared to the establishment of the Wessels type ores in the north-west part of the KMF (Gutzmer & Beukes, 1995; Beukes et al., 1995).
This emanated in the discharging of CO_2, Ca, Mg, and SiO_2 from the unaltered ore, widespread enrichment of iron along faults, and recrystallization of braunite rich phaneritic crystalline ores dominant in minerals such as hausmannite, braunite II, bixbyite, and andradite (Gutzmer & Beukes, 1995; Beukes et al., 1995).

1.5.4. Concluding remarks

Four late depositional alteration episodes influenced the unaltered manganese ore. Unaltered manganese, constituting of Mn-calcites and kutnohorites, braunite, and hematite, was initially exposed to stratabound metasomatic fluid percolation under greenschist grade of metamorphism, which influenced manganese ore across the KMF. The exact timing of the young alteration episode at Mamatwan mine is evidenced by the presence of the mineral assemblage of pyrite-chalcopyrite-calcite which restricted to vein-type mineralization that resembles the assemblage present at Mamatwan, are recognized from the Wessels, Hotazel, and Gloria mines and intrude the high grade Wessels-type ore.
The exact timing of the Wessels is postulated to be around 1250 Ma (Dixon, 1989).The mineralogy of the two faults controlled alteration episodes are well defined from the alteration in close association to near surface weathering in the vicinity of the Kalahari unconformity. Denudational processes such as weathering resulted in oxidation of unaltered manganese ore to alteration minerals such as cryptomelane, pyrolusite, and goethite.

K and Na were notably established during the denudational process as evidenced by the presence of botryoidal cryptomelane (K_{2-z} (Mn^{2+}, Fe^{3+}) $_{8-z}O_{16-x}$ $(OH)_x$ (De Villiers, 1970; Kleyenstüber, 1993) and Na rich end member of manjiroite (Na ($Mn_7^{4+}Mn^{3+}$) O_{16} (Kleyenstüber, 1993).

The K_2O is absorbed from clays and marls from KMF that have been adsorbed from cryptomelane as proposed by Kleyenstüber (1993). The cryptomelane that is formed near surface is rich in K and Na and is closely aligned to the weathering event in comparison to earlier the fault controlled manganomelane and todorokite formed at low temperatures which is deprived of K and Na but rich in MgO and CaO.

Metasomatic alteration which is fault controlled was preceded by two episodes of metasomatism which is restricted to specific strata. Initially it involved the establishment of near surface fluids along structures causing local reduction and changing the colour of the manganese ore. Thirdly reactivated faults were oxidized and carbonates discharged as groundwater was rising due to its low temperatures and oxidizing ability. Finally as groundwater was sinking it initiated near surface alteration across the KMF forming new minerals such as cryptomelane, pyrolusite and goethite.

1.6. Aims and objectives

The main reasons for this study are as follows:

(1) To provide a detailed characterization of the metsomatic reactions during the upgrading process. This is crucial when working with areas that are intensely faulted north of the KMF.

(2) To provide a correlation of mineralogical and geochemical changes with ore grade.

(3) To add on the existing data that is available from the work done in the KMF mainly by Gutzmer and Beukes in 1995 and 1996. Visually the manganese ore shows no evidence of any major alteration; this research will help to pick up subtle mineralogical and geochemical changes which might have a bearing on the grade of the ore.

(4) To guide the geology department at Mamatwan Mine by having a better understanding on fault related systems as this will assist in demarcating high grade targets for mining.

1.7. Methodology

1.7.1. Overview of the study area

This study area is found on the far western section of the middle cut bench. The intense fracturing is evidenced by the loose material that has accumulated over time as shown in Figure 1.2 below.

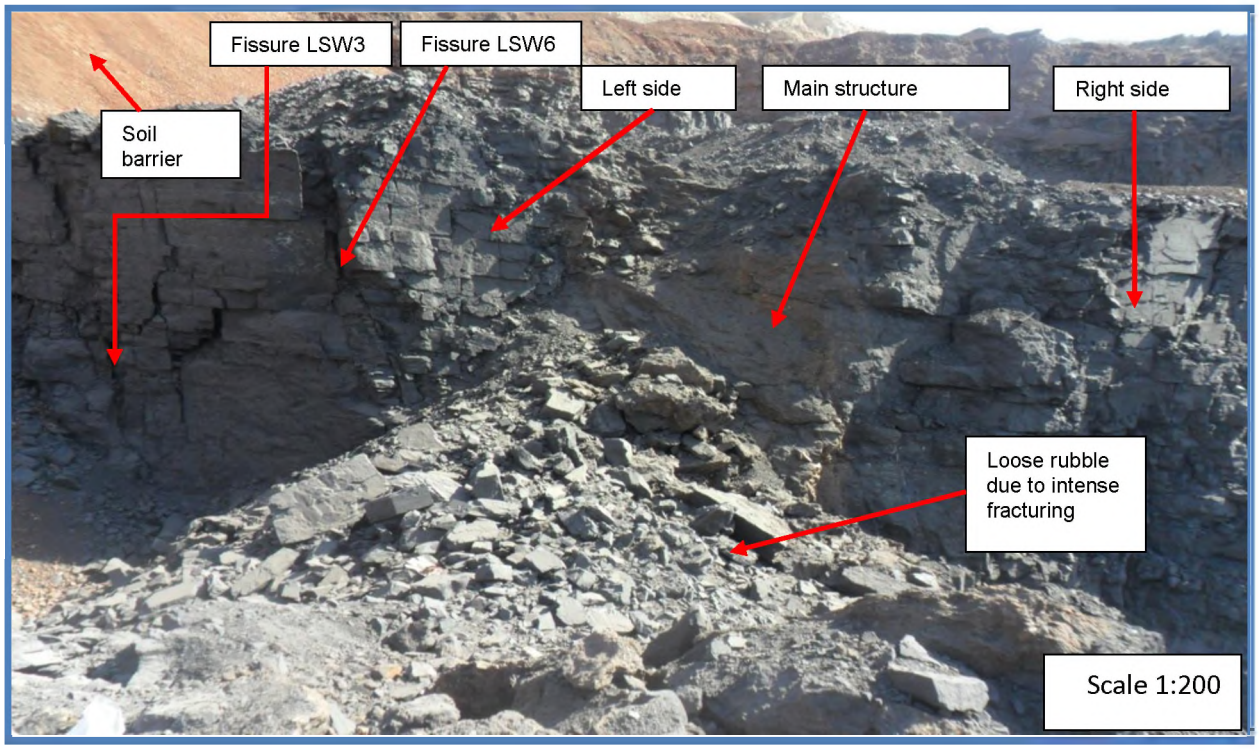

Figure 1.2: Area under study showing the left side, main structure and right side. Note the soil barrier on the left side. Fissure RW5 is located on the right side of the main structure but is not shown on this map.

1.7.2. Limitations of this study

There is no systematic representation on the left side of the main structure from the altered ore to the unaltered ore because of the soil barrier that is shown in Figure 1.2. As a result of this, only the right side showed a clear representation from the altered to the unaltered ore. The intense fracturing that is shown in Figure 1.2 caused a lot of loose bad hangings which meant some sections were limited for safety reasons.

1.7.3. Mapping

The main aim was to demarcate the areas for sampling using colour, texture and intensity of alteration. Secondly it was done to note other secondary structures such as fissures and also the intensity of fracturing at different intervals.

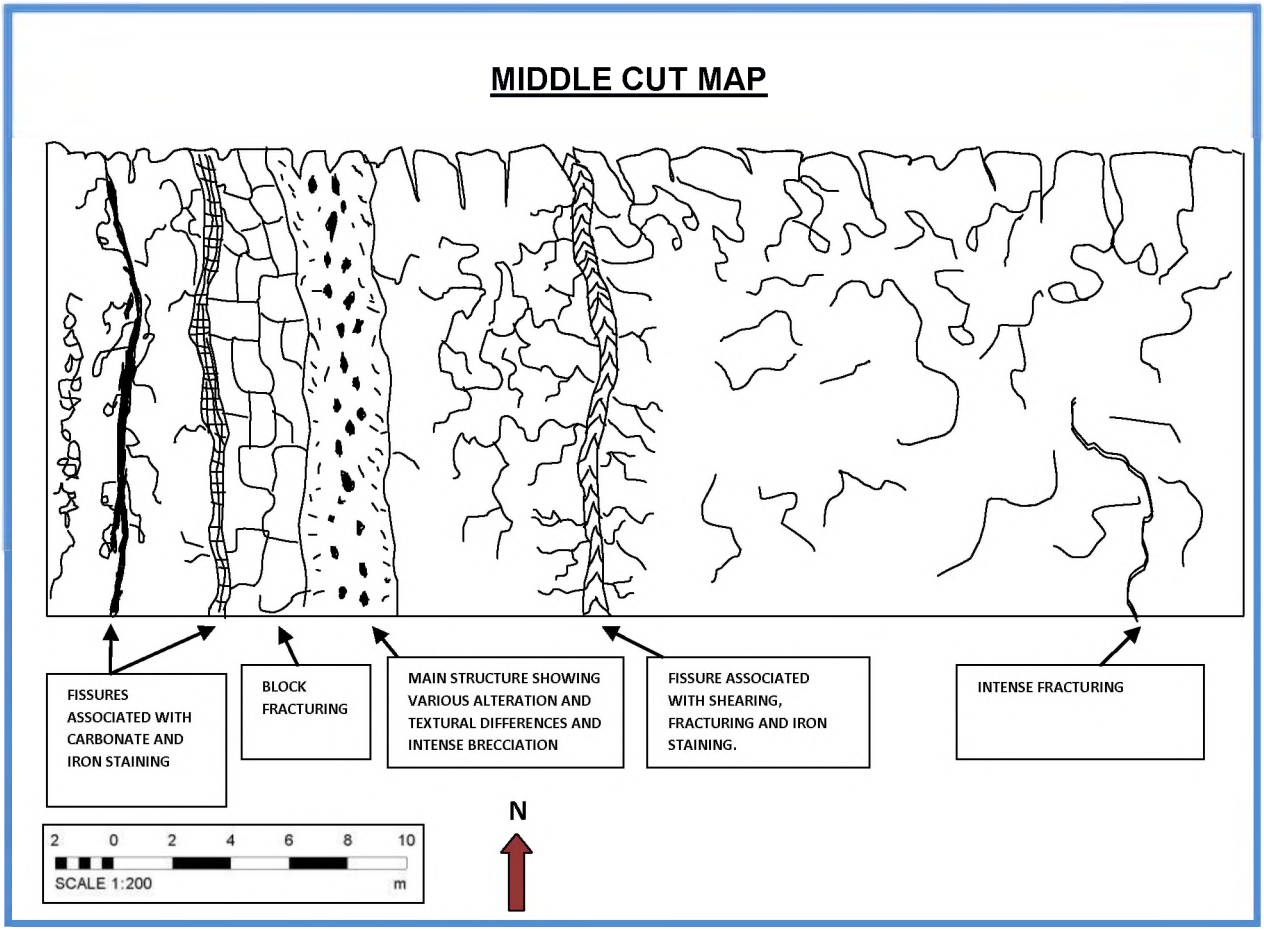

Figure 1.3: Sketch map of sampled area.

1.7.4. Sampling

A total of 30 samples were collected from the left side, the main structure and the right side of the brecciated zone. The width of the sampled zone was not fixed but dependant on the thickness of the zone based on alteration intensity, colour, mineralogy, fracturing intensity and texture.

The main aim was to sample from highly altered zone until the unaltered braunite-lutite zone as shown in figure 1.4. Unaltered was selected on the basis of colour, presence of carbonate minerals and distance from the main fault.

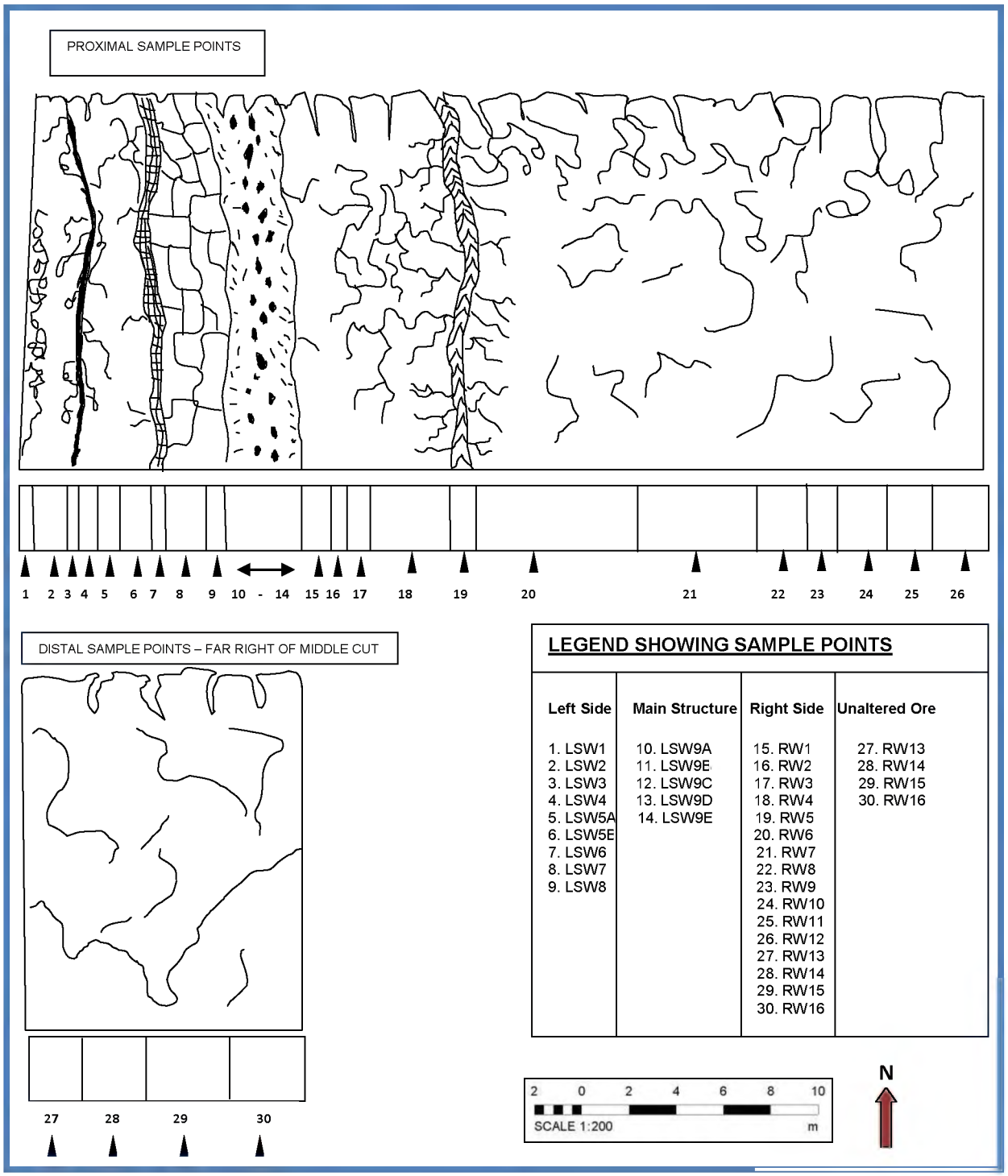

Figure 1.4: Section of sampled area and its associated sample numbers

1.7.5. Sample widths

SAMPLE NAME	WIDTH (M)	LOCATION
LEFT SIDE		
LSW1	0.70	PROXIMAL
LSW2	1.70	PROXIMAL
LSW3	0.33	PROXIMAL
LSW4	0.55	PROXIMAL
LSW5A	1.30	PROXIMAL
LSW5B	1.30	PROXIMAL
LSW6	0.30	PROXIMAL
LSW7	2.30	PROXIMAL
LSW8	0.60	PROXIMAL
MAIN STRUCTURE		
LSW9A	0.40	STRUCTURE
LSW9B	0.30	STRUCTURE
LSW9C	3.00	STRUCTURE
LSW9D	0.15	STRUCTURE
LSW9E	0.20	STRUCTURE
RIGHT SIDE		
RW1	0.90	PROXIMAL
RW2	0.50	PROXIMAL
RW3	1.50	PROXIMAL
RW4	5.10	PROXIMAL
RW5	0.40	PROXIMAL
RW6	7.20	PROXIMAL
RW7	4.20	PROXIMAL
RW8	1.50	PROXIMAL
RW9	3.40	PROXIMAL
RW10	2.70	PROXIMAL
RW11	5.10	PROXIMAL
RW12	3.40	PROXIMAL
UNALTERED ORE		
RW13	3.00	DISTAL
RW14	3.20	DISTAL
RW15	3.30	DISTAL
RW16	3.00	DISTAL

Table 1.1: Sample numbers, sample widths and their locations in relation to the main structure.

1.7.6. Petrography

32 polished round blocks and 7 polished thin sections were carefully selected to represent the main features such as mineralogy, textures and lithostratigraphy. The 32 polished round blocks were observed using transmitted light and the polished thin sections were observed using reflected light microscopy using a Leica microscope.

1.7.7. Sample Preparation

A pulverizer made up of Cr body steel and rings was used in the preparation. Each sample was pulverized for a period of 6 minutes. Quartzite was used to remove the manganese staining and ethanol was used to wipe the interior of the pulverizer to minimize contamination. The resultant powdered samples were used for analysis in tests such as X-Ray diffraction and whole rock geochemistry.

1.7.8. XRD

X-ray powder diffraction patterns were recorded on a Bruker D8 Discover equipped with a proportional counter, using Cu-K Ω radiation (Ω = 1.5405 Å, nickel filter). Data was collected in the range from 2 Ω = 10º to 70º, scanning at 0.5º min^{-1} with a filter time-constant of 1.1 s per step and a slit width of 6.0 mm. Samples were placed on a silicon wafer slide. The X-ray diffraction data was treated using the Eva (evaluation curve fitting) software. Baseline correction was performed on each diffraction pattern by subtracting a spline function fitted to the curved background.

1.7.9. Geochemistry

26 powdered samples weighing 5g each were prepared and the samples were sent to Bureau Veritas Mineral laboratories in Canada to be analysed by XRF analysis.

1.8. The Kalahari Manganese Field (KMF)

The Kalahari basin is a large structurally controlled area caused by tensional forces that dip to the west at angle at average of 7°. This faulted area has a depth that can reach 1.5 km to the west and northwest of the basin. The north of the KMF shows the Hotazel Formation outcropping as a result of thrusting.

The extent of the KMF is approximately 40km and has a width between 5 and 15 km. The manganese is intercalated with banded ironstone comprising 3 segments which are the Lower body, Middle body and the Upper body. The Lower Body is currently being exploited and is approximately 5m thick in the north and up to 45m to the south of the basin. The Middle body and Upper body are uneconomic as the Middle Body is very thin and the Upper Body has low manganese values with an approximate thickness of 5m.

Two major ore types occur in the Main Kalahari Basin: A low grade (av. 37.5% Mn) Mamatwan-type and a higher grade (av. 48% Mn) Wessels-type. The Mamatwan-type represents approximately two-thirds of the total manganese deposit in the Kalahari Basin. Figure 1.1 C shows the distribution of the two ore-types. The transition of the one to the other is not well constrained.

The low grade Mamatwan type is the dominant ore type as it occupies over 60% of the basin and has values averaging 37.5 %. The second type is the Wessels type which occurs in the northern part of the KMF and has a higher grade of approximately 48%.

1.9. The Transvaal Supergroup in the Northern Cape

The HMM is part of the KMF, which is underlain by the early Proterozoic Transvaal Supergroup in Griqualand West. It is located on the western boundary of the Kaapvaal Craton, South Africa. The KMF is upheld in a structural concavity which is created by the Dimoten Synclinorium.

On a larger scale it plunges to the north and northwest between from 3° to 8°. The sequence in the Griqualand West area is plainly sub classified into a chemical-sedimentary unit that forms to a bottom layer known as the Ghaap Group, and a variegated unit that was laid upon a volcanic-clastic-chemical unit known as the Postmasburg Group. The Ghaap and Postmasburg Groups are similar in that they both possess unconformities (Cheney and de la R Winter, 1995). The Postmasburg Group constitutes the following layers, from the bottom to the top: Makganyene diamictite, Ongeluk andesitic lava, Hotazel iron formation with manganese beds intercalated in between and Mooidraai dolomite at the summit. The Hotazel and Mooidraai Formations are classified to belong to the Voëlwater Subgroup. The manganese mined at the high grade Wessels and low grade sedimentary Mamatwan Mines is found within the Hotazel Formation. Deposition of the Transvaal Supergroup was influenced by three prime tectono-sedimentary components (Beukes, 1983, 1987): A superficial water stage on the Kaapvaal Craton, a shelf margin and a profound basin on the Western edge of the Craton. Due to the Postmasburg Group overlying the Ghaap Group this provides evidence that a phase of erosion occurred before the deposition of the Makganyene diamictite. The unconformity penetrates moderately down between the underlying rocks as one lithology progresses from the basin onto the platform.

The Makganyene diamictite constitutes two unique phases. The first phase constitutes intercalated beds referred to as massive diamictite, these layers are stacked with diamictite which has poorly developed beds, conglomerate, sandstone with a pebbly texture, siltstone, varved shale and mudstone (Visser, 1971). The next stage constitutes of a periodic modification of diamictites rich in argillites and arenites, conglomerate, sandstone, subgreywacke, chert and carbonate, limestone with a dolomite end member and laminated jaspilite (de Villiers and Visser, 1977).

Tholeiitic basal andesites are maintained as the Ongeluk lava are released in a semi solid domain within the continental environment of the Kaapvaal Craton (Schutte, 1992). The unconformity is laid upon the Makganyene diamictite and constitutes massive lavas, pillow lavas and hyaloclastic beds. Geophysics conducted by HMM in the Kalahari Basin, advocates a thickness between 1000 and 1200 metres.

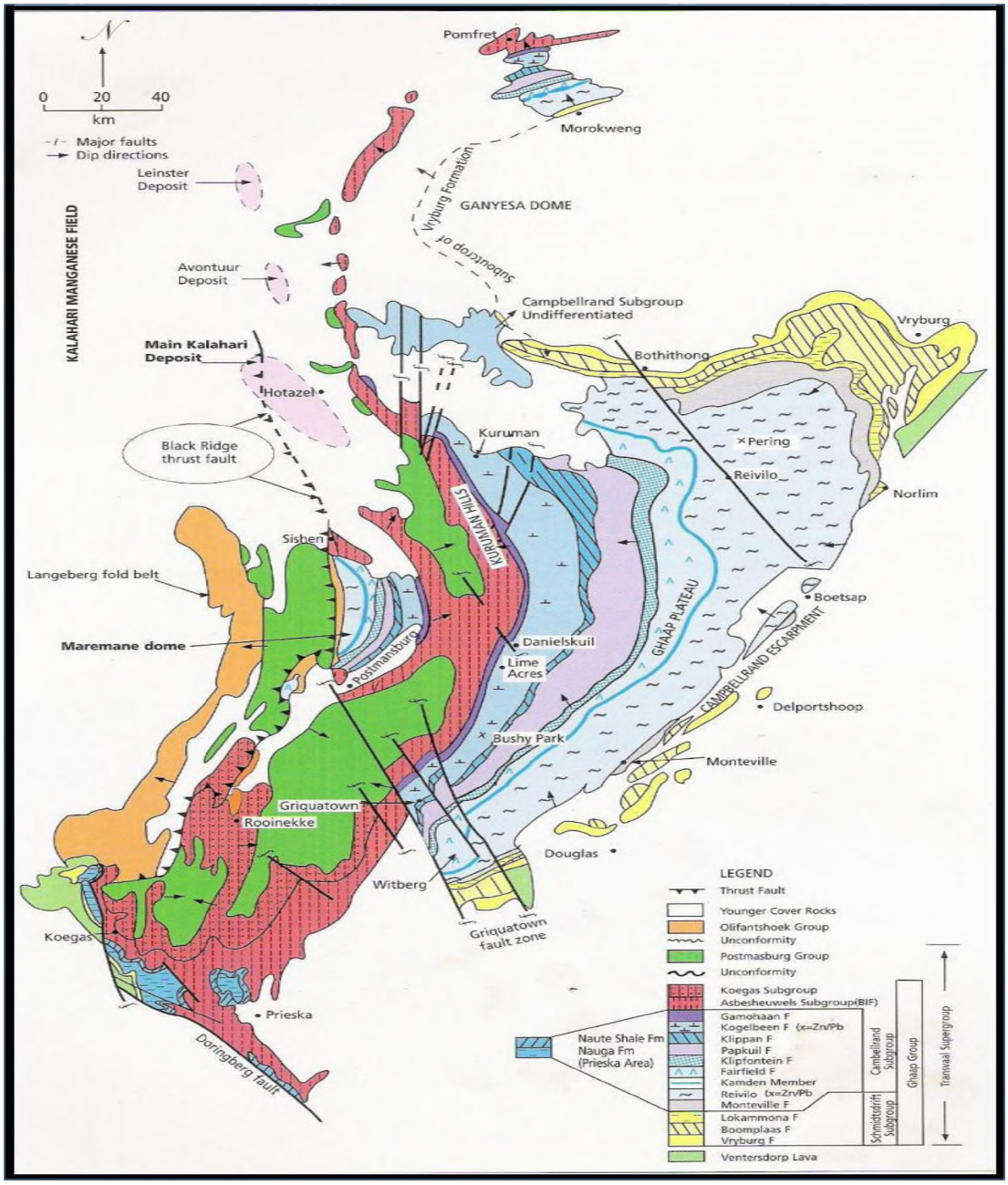

Figure 1.5: Geological map of Transvaal Supergroup in Griqualand West, showing distribution of major stratigraphic units and ore deposits (After Beukes, 1986)

The mining at Wessels Mine to the north of the KMF showed that the Ongeluk lava is the layer of rocks that is at the base of the series; however this bottom layer is not visible to the south of the KMF in areas such as the Mamatwan Mine.

The Ongeluk series is covered conformably by rocks such as jaspilite, banded ironstone and successions of manganese that belong to the Hotazel formation, a sub category of the Voëlwater Subgroup. The Hotazel Formation achieves a thickness that can reach 200 metres as shown in Figure 1.6.

Figure 1.6 shows the Mooidraai dolomite thrust over the Hotazel Formation. The Mooidraai dolomite has been preserved in the Kalahari basin because it is thick but not close to the Wessels Mine where the Mapedi Formation of the Olifantshoek Sequence is thrust upon the Hotazel Formation. The Olifantshoek unconformity is unique in that it distinguishes these two entities. The Mapedi formation is made up of green to maroon shales, secondary shales rich in graphite and narrow bands of quartzite. The Lucknow Formation is a unique sequence which is a phaneritic white orthoquartzite. It has a pebbly coarse texture that is a grey to green sandstone that dominates the Mapedi Formation.

The Dwyka tillite valley is a north-south ancient glacial structure that is situated on the western part of the Kalahari Basin. The Wessels Mine is cut by smaller scale valleys which shorten the manganese horizons towards the north east part of the mine. The Kalahari Formation sediments conformably cover the whole series which constitutes loose sand, calcrete, gravel and clay. The Kalahari Formation sub-outcrops towards the eastern part of the Kalahari Basin which are along the manganese rocks and the banded ironstone of the Hotazel Formation.

(Schütte, 1992) notes that dolerite dykes and sills provide evidence of numerous events of intrusions from Ongeluk to Karoo times. Meta dolerites are evidence of high alteration in the Hotazel Formation that comprises bostonite dykes and sills. These metadolerites have an ENE-WSW trend. The area is classified into two unique fields by a major structure referred to as the Olifantshoek Blackridge thrust.

The footwall of the thrust, in the eastern parts of the Kalahari Basin, is characterized by gently plunging dome and basin structures with gentle dips, normally less than 20°. The footwall of this thrust has dome and basin features which have a dip which is less than 20 °.

Secondly, the parasitic faults formed due to thrusting have a North-South to ENE-WSW trend. All other faults related to this thrusting have a similar trend as well as high angle and extensional structures due to tensional forces.

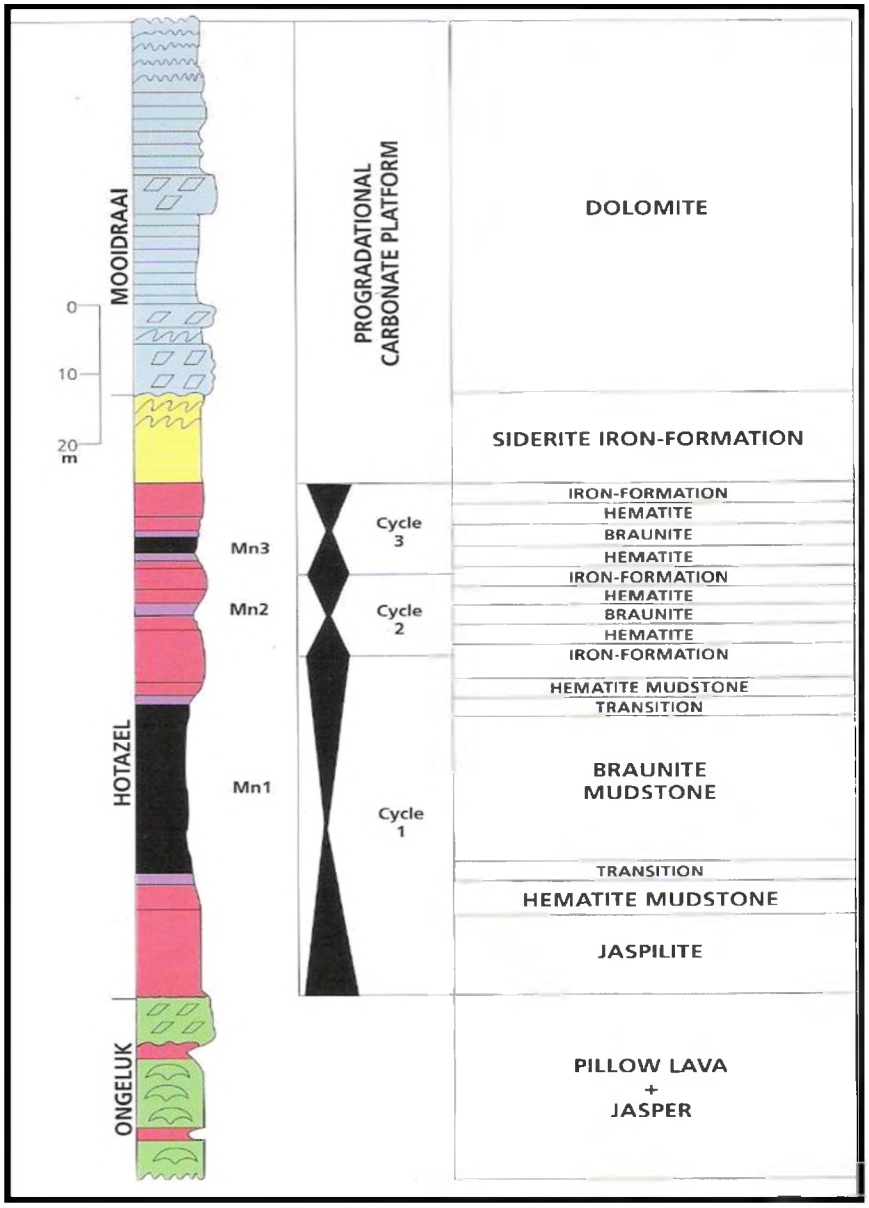

Figure 1.6: Stratigraphic Profile of the Hotazel and Mooidraai Formations in the Kalahari Manganese Field (Beukes, 1986)

1.10 The Geology at Mamatwan Mine

The low grade sedimentary Mamatwan type ore consists predominantly of minerals such as braunite, hausmannite, kutnohorite and jacobsite. This ore visually displays carbonate rich ovoids and laminae as a result of manganese calcites (hereafter referred to as Mn- calcites). In comparison to the higher grade Wessels type ore, the Mamatwan type ore is richer in calcium with lower Mn/Fe ratios. (Beukes, 1983) noted that the manganese ore that is mined at Mamatwan Mine is found at the bottom of the braunite-kutnohorite beds which has intercalations with the iron formation of the Hotazel formation that belong to the Transvaal Supergroup. This lowermost body is 45m thick and for mining purposes it is demarcated into 3 mining benches namely the top, middle and bottom cuts.

The top cut is uneconomic to mine with low manganese values averaging 30% and is approximately 19.5m thick. The middle cut is the economic zone of the mine with manganese values averaging 37.5% and has a thickness of approximately 19.7m. The bottom cut resembles the top cut as it contains approximately the same manganese content of 30% and has a thickness of only 6m. The Mn/Fe ratios of the top, middle and bottom cuts are 8, 7.5 and 5 respectively.

According to (Beukes, 1983; Preston, 2001) undulations of the manganese ore beds are as a result of gentle folding which had compressive forces in an east - west direction that caused thrusting of the Hotazel formation to be repeated in the north western part of the KMF. This manganese ore bed has a shallow dip that averages 7° towards the west below the KMF.

CHAPTER TWO: MINERALOGY AND PETROGRAPHY

2.1. Introduction

This chapter is designed to give an insight of different mineralogical changes that occur across the section from unaltered ore to altered ore. A Leica Microsystems microscope was used to identify minerals through transmissive light microscopy. EMPA and XRD were also the main methods also deployed to ascertain the mineralogy and approximate mineralogical quantities in each sample.

2.2. X – Ray diffraction

X-ray diffraction (hereafter referred to as XRD) was carried out at Rhodes University Chemistry department using X-ray powder diffraction patterns that were recorded on a Bruker D8 Discover equipped with a proportional counter, using Cu-K Ω radiation (Ω = 1.5405 Å, nickel filter). Data were collected in the range from 2 Ω = 10º to 70º, scanning at 0.5º min^{-1} with a filter time-constant of 1.1 s per step and a slit width of 6.0 mm. Samples were placed on a silicon wafer slide. The X-ray diffraction data was treated using the Eva (evaluation curve fitting) software. Baseline correction was performed on each diffraction pattern by subtracting a spline function fitted to the curved background.

Figure 2.1.0 below shows the different XRD data and how the mineralogy varies across the traverse were recorded for the various samples taken from the left side (LSW), the right side (RW) and the main structure (LSW9A-9E). The software used is Match Phase Identification from Powder Diffraction version 3.0.0 Build 17.

The cut off figure of merit (hereafter referred to as FoM) for the samples used was 0.7000; any samples recorded below this FoM were not included.

2.3. XRD ANALYSIS

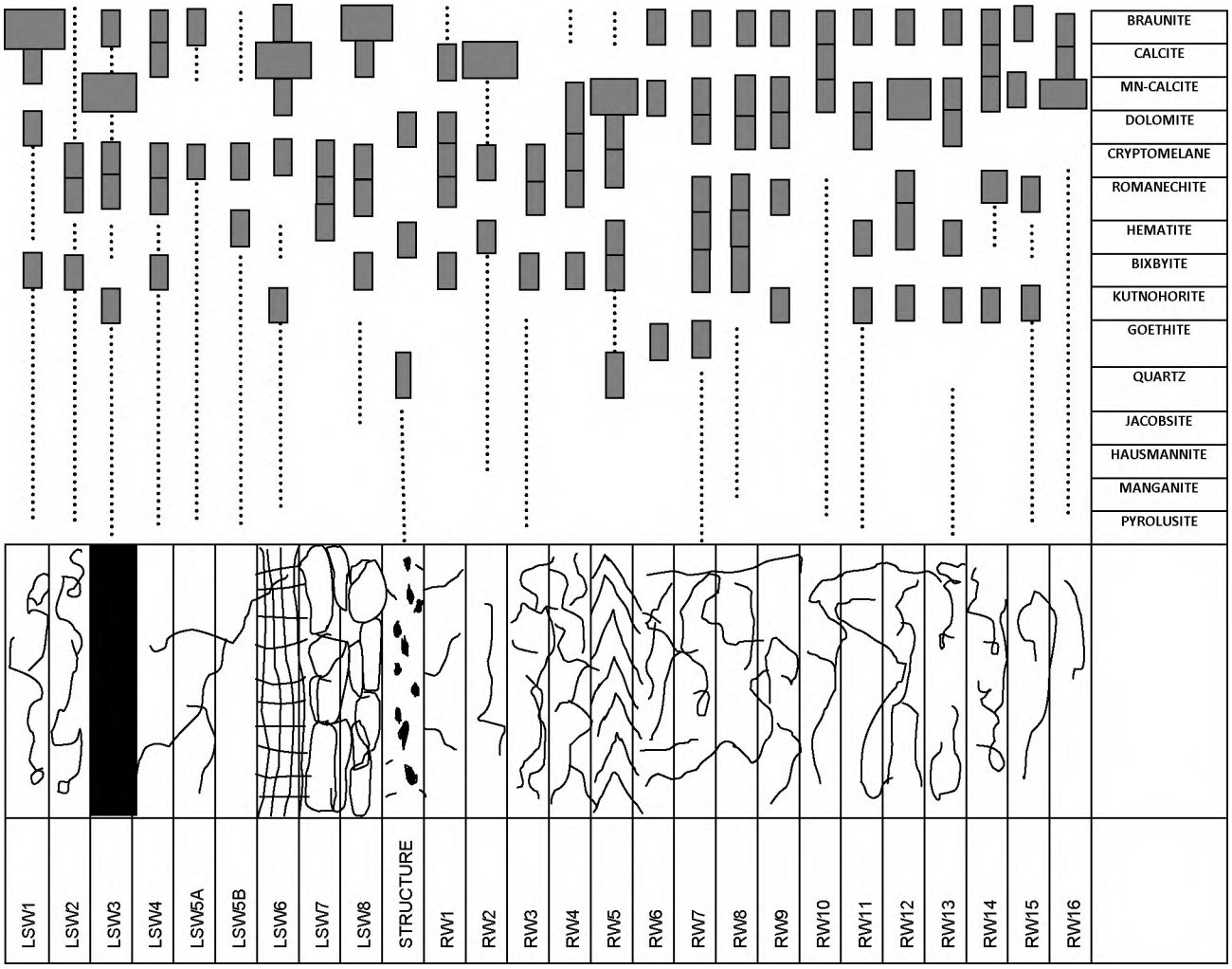

KEY

More than 30% by composition.
10 - 30 % composition.
Less than 10% by composition.

All sample widths have been standardized to the same length for presentation purposes.

Figure 2.1.0: Cross section showing mineralogy on both sides of the main structure.

Manganomelane and todorokite could not be identified by XRD analysis due to their amorphous nature.

2.4. XRD ANALYSIS: Relationship between mineralogy and grade

2.4.1. Braunite vs Mn_2O_3 grade

Figure 2.1.1 shows that Mn_2O_3 broadly correlates with the braunite content and it affects the overall Mn_2O_3 grade especially on the left side of the main structure. Note on the right side there is no correlation close to the structure as braunite is depleted at the expense of alteration minerals such as manganomelane and todorokite. However from RW9 to RW16 there is some correlation as the ore becomes less altered.

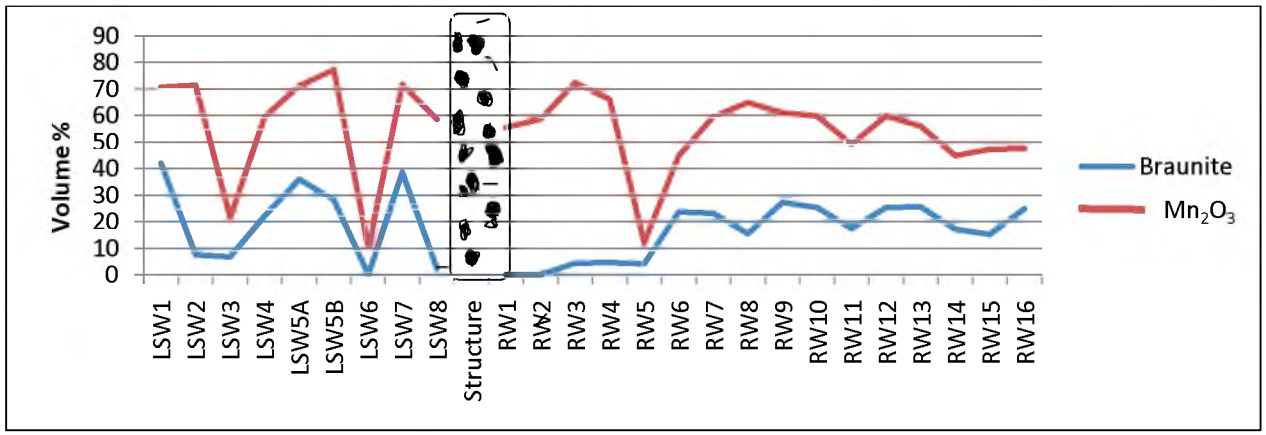

Figure 2.1.1: The relationship of braunite and Mn_2O_3 across the section.

2.4.2 Calcite vs Mn_2O_3

Calcite is the main carbonate mineral that controls the distribution of CaO and the grade of Mn_2O_3 as shown in Figure 2.1.2. An increase in calcite results in a decrease in Mn_2O_3.

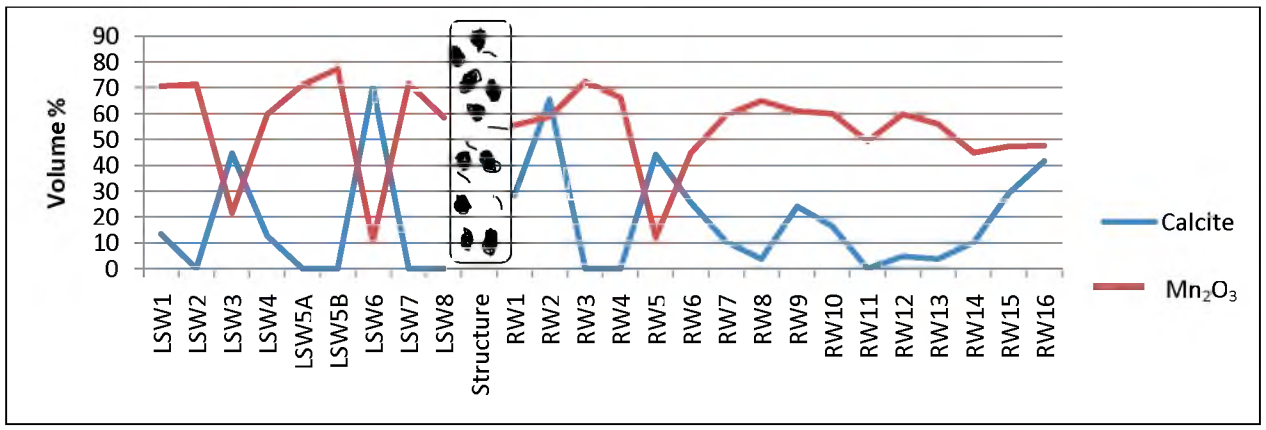

Figure 2.1.2: The relationship between calcite and Mn_2O_3 across the section.

2.4.3. SiO_2 vs Braunite vs Quartz

Figure 2.1.3 shows that quartz has a bigger influence on the overall grade of SiO_2 but the silica content also in braunite which constitutes an average of 10% has also a regulatory effect on the overall SiO_2 grade especially on the right side as the samples approach the less altered ore.

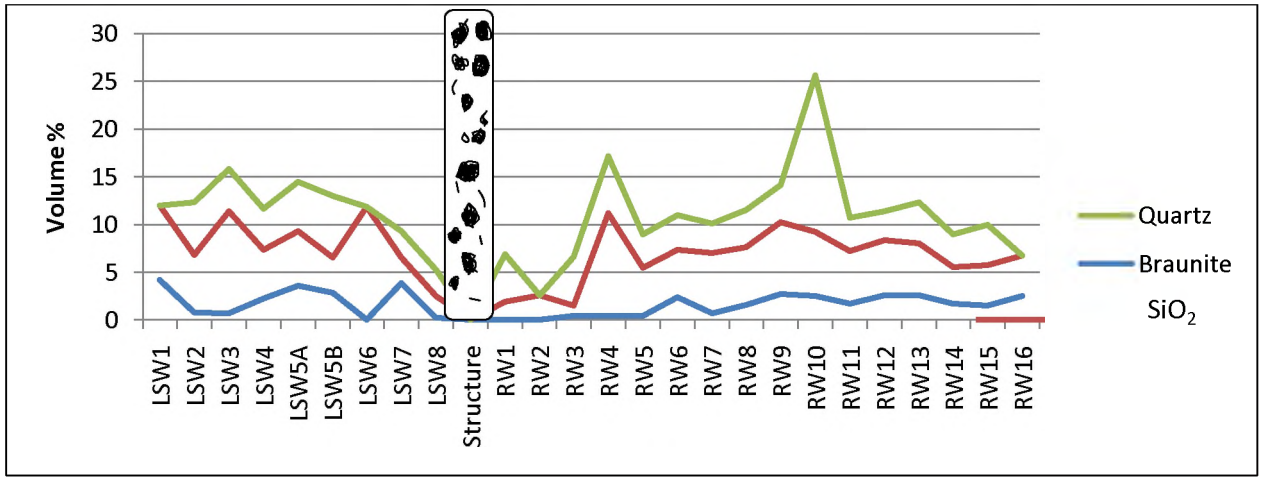

Figure 2.1.3: The relationship of SiO_2, braunite and quartz across the section.

2.4.4. Hematite vs goethite vs FeO vs Kutnohorite

Figure 2.1.4 shows a moderate to weak correlation between hematite and FeO/ Fe_2O_3 grade. On the right side of the main structure, goethite and the Fe content in kutnohorite seem to have a similar pattern and content as the FeO/Fe_2O_3 grade.

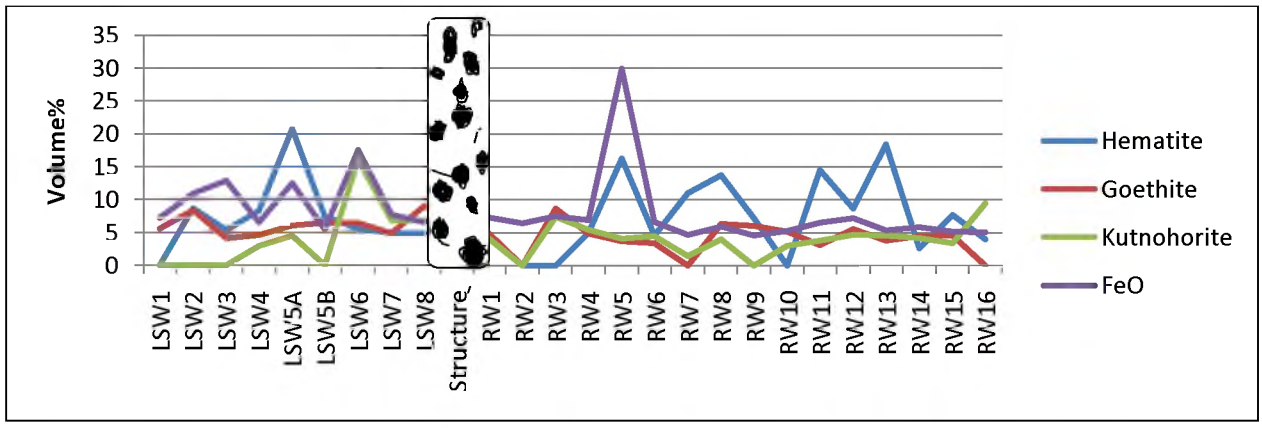

Figure 2.1.4: The relationship of FeO, kutnohorite, goethite and hematite across the section.

2.4.5. MgO vs Kutnohorite

Figure 2.1.5 shows that the distribution of MgO is fairly consistent on both sides and apart from the fissure in LSW6, the Mg content in kutnohorite has the biggest influence and follows a more likely pattern than other Mg rich minerals such as dolomite and manganomelane.

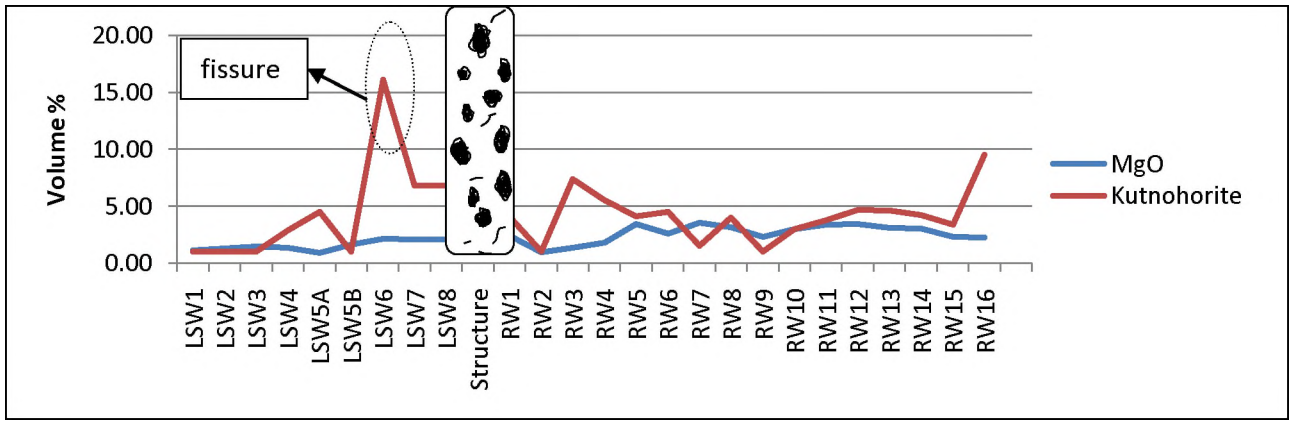

Figure 2.1.5: The relationship of MgO and kutnohorite across the section.

2.4.6. CaO vs Calcite vs Dolomite vs Kutnohorite

Calcite is the carbonate mineral with the most influence in relation to the CaO especially on the left side but on the right side the influence is inconsistent especially towards the less altered ore. On the right side kutnohorite and dolomite appear to have a regulatory effect as their CaO content is the average of the kutnohorite and the dolomite.

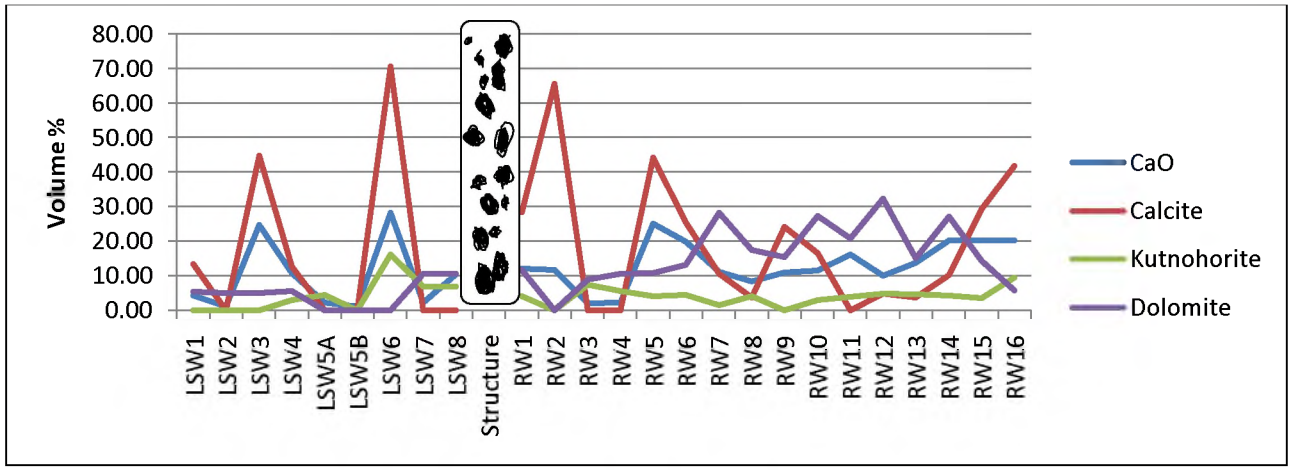

Figure 2.1.6: The relationship of dolomite, kutnohorite, calcite and CaO across the section.

2.5. EPMA

EPMA data acquisition was performed at Rhodes University, Department of Geology, using a Jeol JXA 8230 Superprobe which is equipped with four WD spectrometers. Analytical conditions employed for quantitative analysis were: 15kV for the accelerating voltage, beam current of 20 nA, a spot beam size of >1 micron, and counting times of 10 seconds on peak and 5 seconds on background with the exception of potassium (30 seconds on peak, 15 seconds on background) and chrome (20 seconds on peak, 10 seconds on background). The standards used for quantification of oxides were: Kyanite (Si), Chrome-diopside (Ca), Periclase (Mg), Spinel (Al), Cubic zirconia (Zr), Barite (Ba), Rhodonite (Mn), Chromium oxide (Cr), Hematite (Fe), Plagioclase (Na), Orthoclase (K), and Rutile (Ti).

The following standards were used for quantification of carbonates: Dolomite (Ca and Mg), Barite (Ba), Rhodonite (Mn), Biotite (K), Hematite (Fe),Stronitum titanate (Sr), and Apatite (P).For silicates, the following g standards were used; Chrome-diopside (Si and Ca), Almandine (Al and Fe), Periclase (Mg), Chromite (Cr), Rhodonite (Mn), Biotite (K), Plagioclase (Na), Rutile (Ti), Barite (Ba). The ZAF matrix correction method was used for quantification. The following analytical conditions were used for the qualitative analysis and elemental maps; accelerating voltage of 15 kV, 20 nA probe current, a dwell time of 10 ms, and stage scan mode.

2.5.1. Mineral chemistry of selected samples: EMPA

Sample number	Mineral	Average SiO_2 wt%	Average MgO wt %	Average K_2O wt%	Average Mn_2O_3 wt%	Average Fe_2O_3 wt%	Average BaO wt%	Average Na_2O wt%	Average CaO wt%	CO_2 average wt %
LSW4	Braunite	9.17	0.16	-	83.57	4.28	-	-	1.03	-
LSW6	Mn - Calcite	-	0.67	-	2.89	0.05	-	-	58.26	38.11
LSW3	Calcite	-	0.25	-	0.13	0.21	-	-	55.19	44.22
RW1	Dolomite	-	20.1	-	0.01	-	-	-	36.10	43.73
RW7	Kutnohorite	-	12.88	-	16.89	0.11	0.03	0.02	29.15	40.89
LSW5A	Goethite	-	2.15	0.02	1.50	46.81	0.03	0.02	2.15	-
LSW9D	Manganomelane	1.75	3.46	0.24	78.94	1.56	-	1.15	1.63	-
RW2	Jacobsite	10.20	1.13	0.05	35.76	43.23	-	0.83	0.75	-
RW12	Romanechite	-	0.50	0.01	65.82	0.47	11.67	-	0.59	-
LSW5A	Todorokite	3.94	1.44	0.18	55.32	14.79	0.01	0.39	1.18	-
RW3	Manganite	0.21	1.99	2.49	70.6	1.82	0.03	0.15	1.41	-
RW8	Hausmannite	1.15	0.05	0	83.26	3.68	0.11	0	0.08	-
LSW7	Bixbyite	0.01	-	-	89.27	5.2	-	-	-	-

Table 2.1: Chemical composition of selected minerals identified by EMPA.

2.5.2. List of gangue minerals: EMPA

Sample number	Mineral	Average SiO_2 wt%	Average MgO wt %	Average Al_2O_3 wt %	Average Mn_2O_3 wt%	Average Fe_2O_3 wt%	Average BaO wt%	Average Na_2O wt%	Average CaO wt%	CO_2 average wt %	P_2O_5 average wt %
LSW7	Apatite	-	-	-	0.69	0.04	0.01	-	52.64	4.60	41.89
RW5	Serpentine	47.67	28.78	1.44	1.20	16.63	0.01	0.05	0.09	-	-
LSW9E	Chloritoid	37.02	0.06	21.40	0.10	16.63	0.01	0.05	22.38	-	-

Table 2.2: Chemical composition of gangue minerals identified by EMPA.

The full list of all the samples done using the EMPA is available in the appendix section. The chemistry of the minerals does not alter much from the altered ore to the unaltered except for manganomelane. Manganomelane constantly varies from a Na rich (Manjiroite) to a K rich (cryptomelane) composition.

2.6. Distribution of carbonates

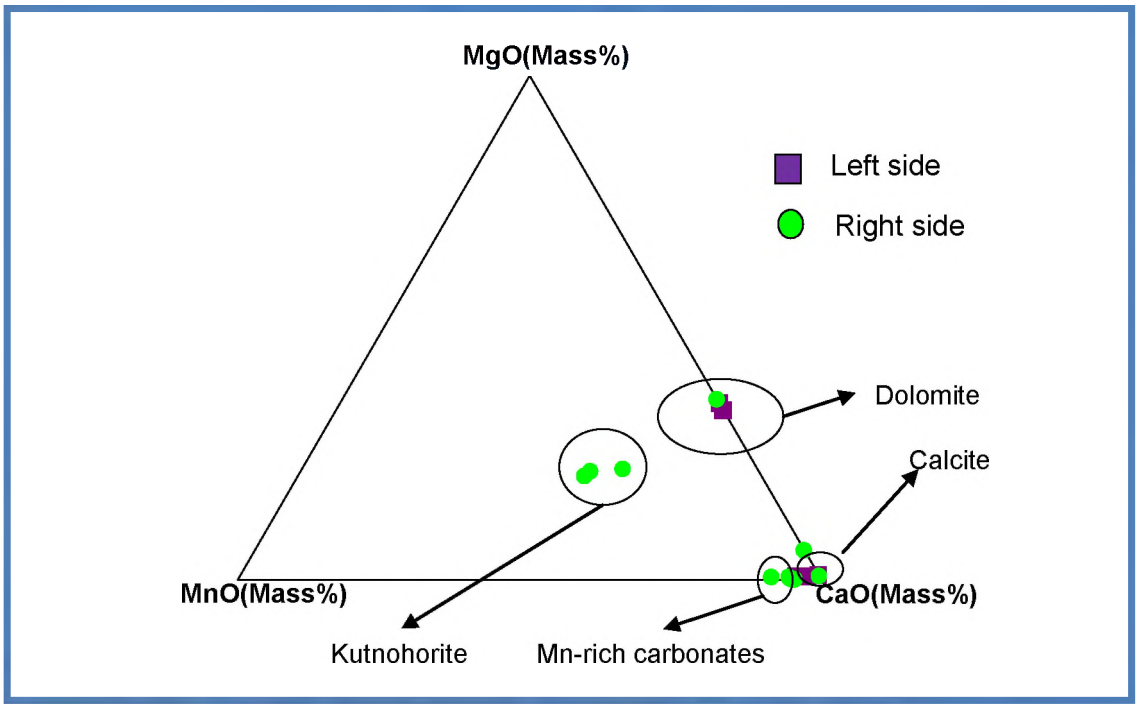

Figure 2.1.7: Ternary plot showing the distribution of carbonates across the section.

The main difference between the left and right side is that kutnohorite is only found on the right side as shown in Figure 2.1.7. The average composition of Mn in the Mn rich calcites as shown in Table 2.1 and 2.2 is between 2 - 5 %. From the ternary plot the Mn-rich calcites on the right side have a higher Mn content than the one the left side. (Preston 2001) notes that the kutnohorite and Mn-rich calcites are formed as a result of early diagenesis to late stage diagenesis processes.

2.7. Compositional maps

The compositional maps confirm the XRD findings and this can be evidenced by the following illustrations:

2.7.1 Unaltered ore: RW16

Figure 2.1.8 shows the direct correlation in the Mn, Si and Fe maps because of braunite. The peaks recorded in the Mg map are because of the mineral kutnohorite. The Ca map shows very high peaks and is evidently the dominant element because of the Mn-rich calcites, kutnohorite and dolomite. The K and Na maps show a low interstitial distribution of the elements.

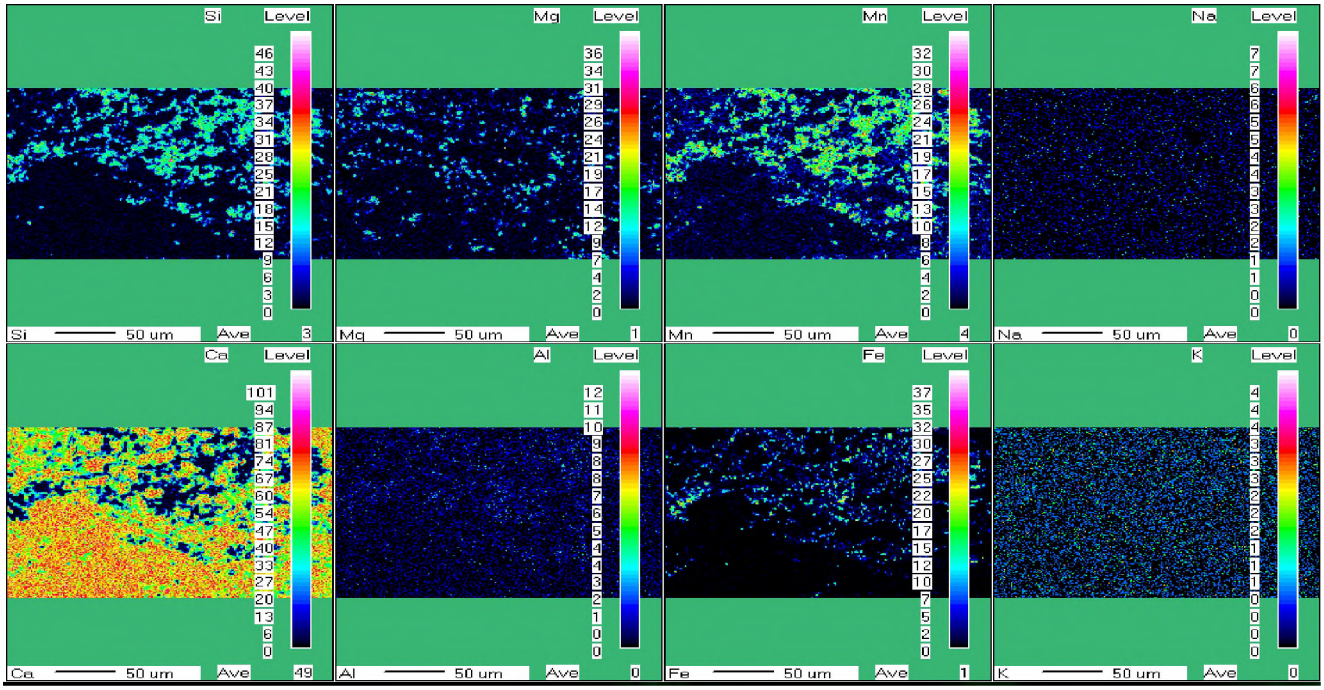

Figure 2.1.8: EMPA scan of a thin section from sample RW16 showing the composition of different elements.

2.7.2. Altered ore adjacent to the main structure on the right side: RW1

Figure 2.1.9 shows the direct correlation between the Mn and K map because of the mineral manganomelane. The Na map does not show any distribution as compared to K elemental map; this implies that cryptomelane is the dominant end member mineral. The Si map has no peaks due to the absence of the mineral braunite next to the main structure, the very low Si distribution are remnants of quartz from the main structure. The Fe is present at the grain boundaries of the cryptomelane as a result of replacement.

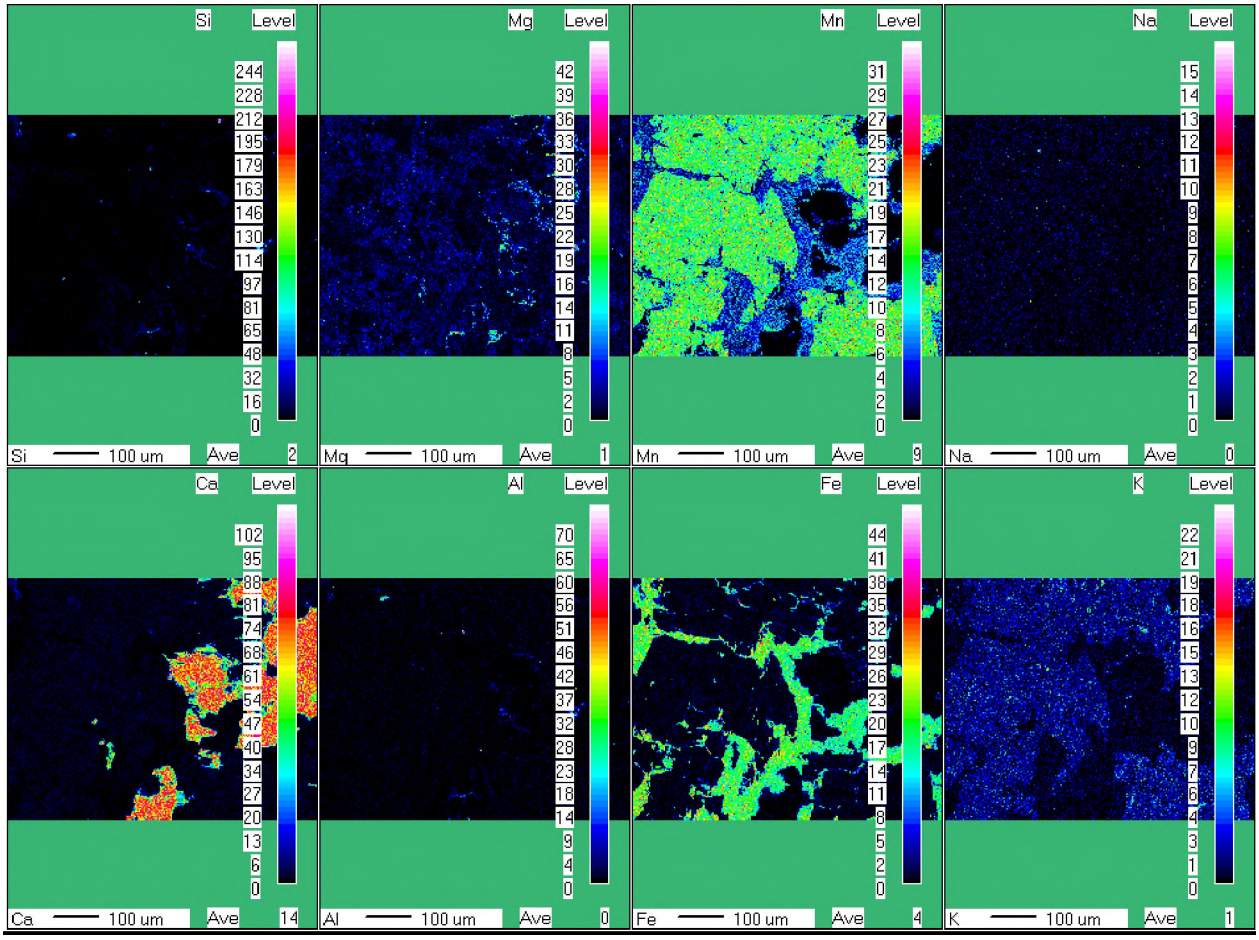

Figure 2.1.9: EMPA scan of a thin section from sample RW1 showing the composition of different elements.

2.7.3 Altered ore on the right side: RW8

The Si, Mn and Fe maps in Figure 2.2.0 provide evidence that braunite is present in a fine grained matrix. The high peaks in the Mg and Ca maps suggest that it could be the mineral dolomite. The presence of kutnohorite is shown as it is closely associated with braunite constituting the fine grained matrix as evidenced by the high distribution of Mn and Ca. The blank maps in the K and Na maps provide evidence that as the ore becomes less altered the presence of manganomelane is obliterated.

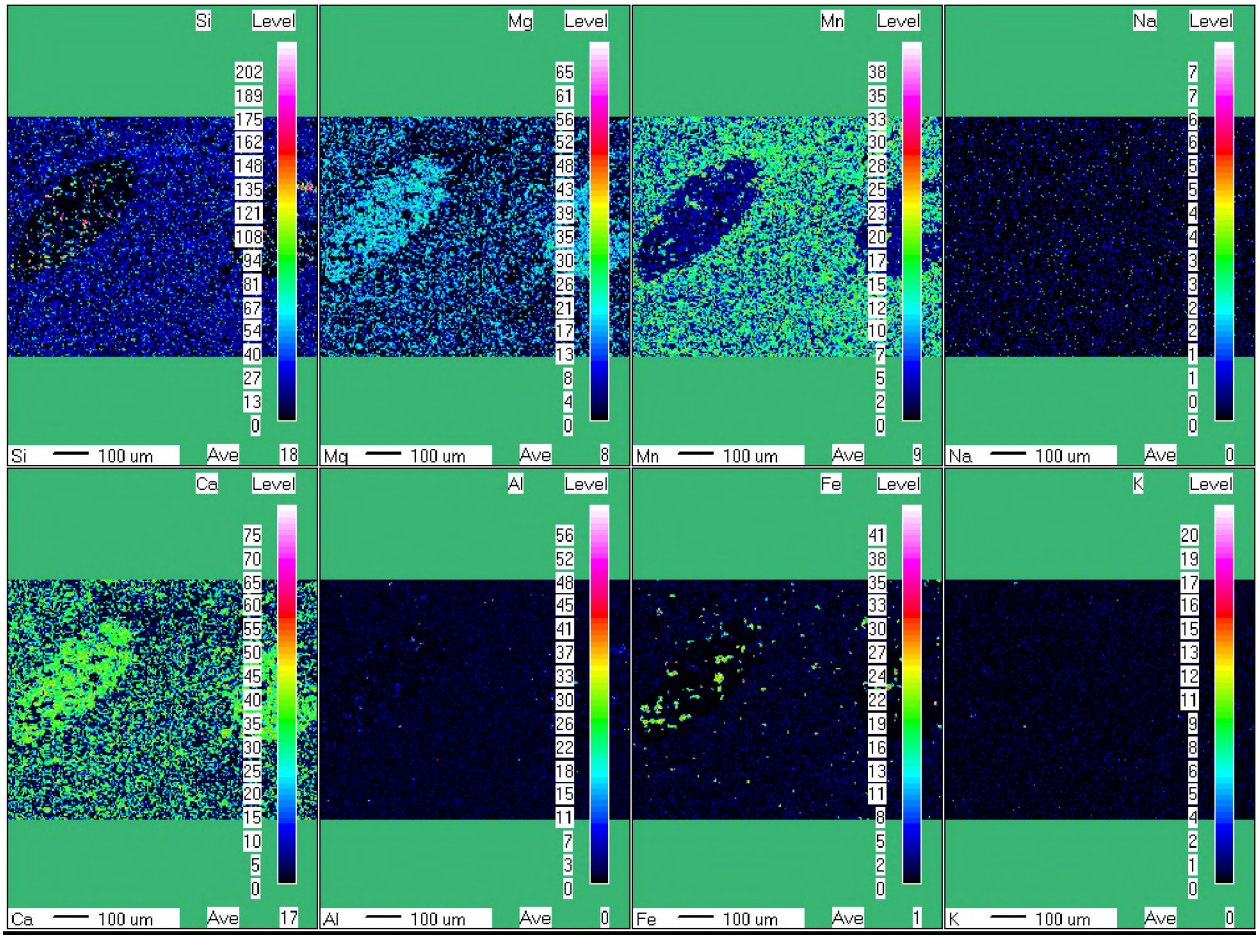

Figure 2.2.0: EMPA scan of a thin section from sample RW8 showing the composition of different elements.

2.7.4. Altered ore on the left side: LSW2

Figure 2.2.1 shows that generally the Ca content is very low except for the fissures see Figure 2.2.2. In intensely altered rocks the braunite content is obliterated as evidenced by the low peaks in the Si and Fe maps. Figure 2.2.1 shows a strong correlation in the K, Mn and Mg maps which suggests the dominance of cryptomelane. The braunite content is low as shown by the low distribution in the Si and Fe maps.

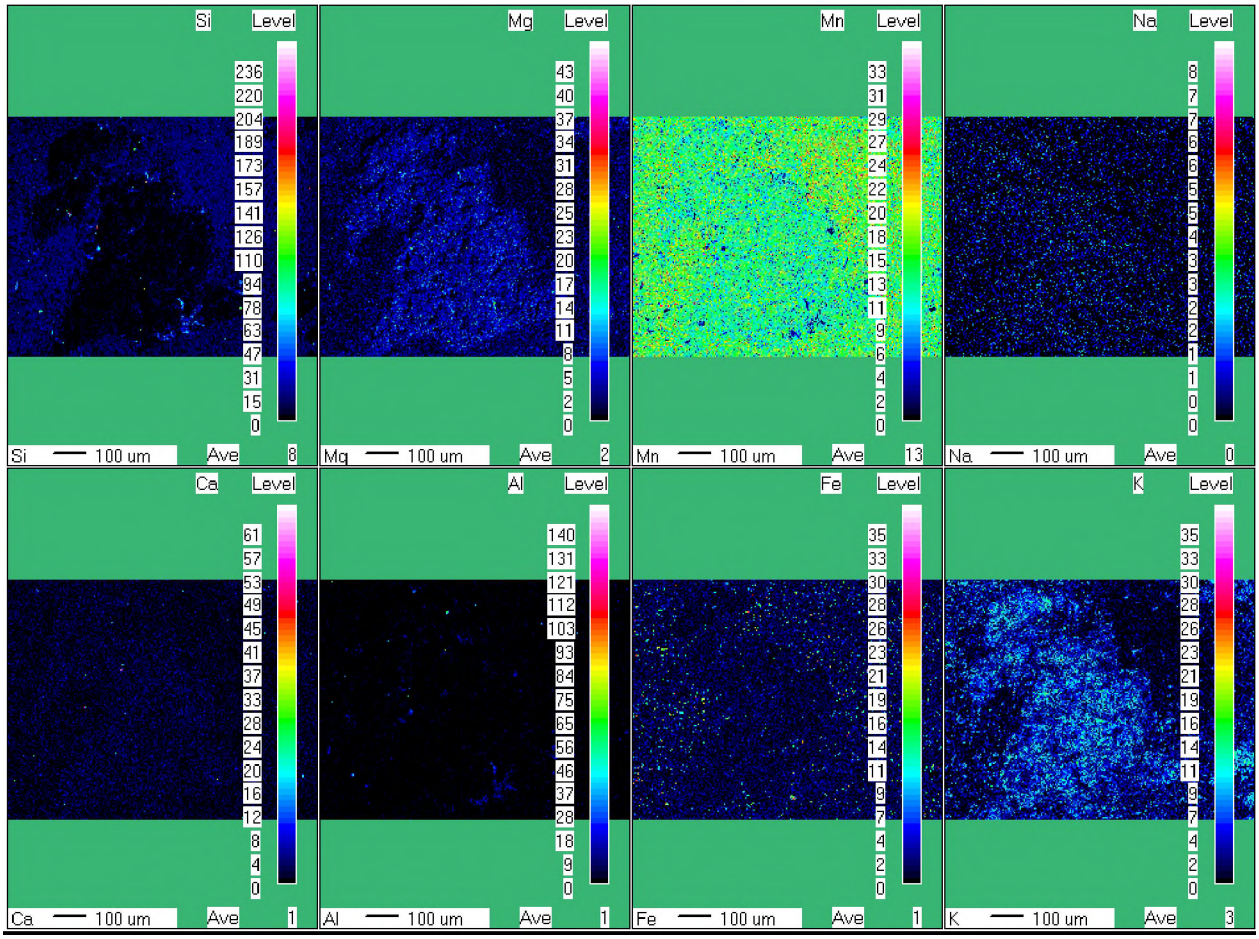

Figure 2.2.1: EMPA scan of a thin section from sample LSW2 showing the composition of different elements.

2.8. Petrography

2.8.1. EMPA: Back scattered images

LSW3 - fissure

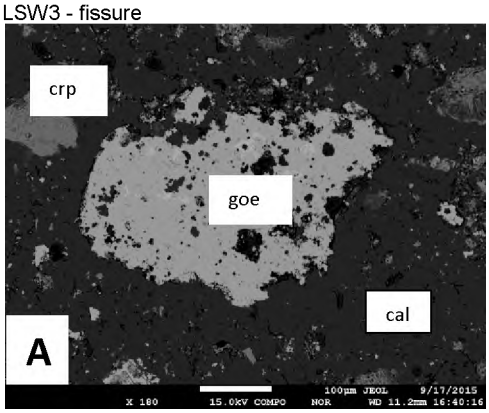

crp – cryptomelane, goe –goethite, cal – calcite

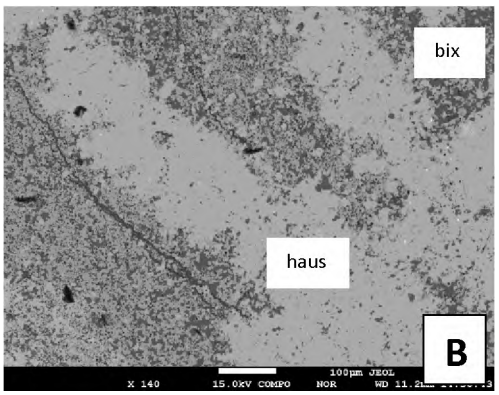

haus- hausmannite, bix – bixbyite.

LSW6 – fissure

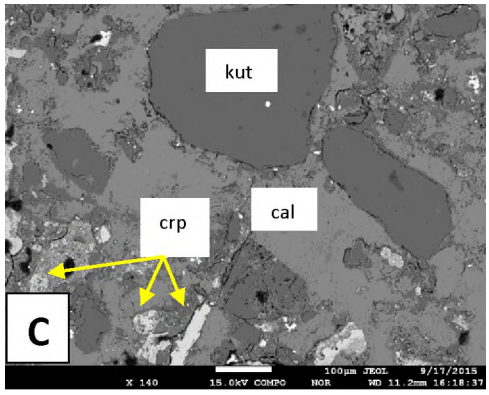

kut – kutnohorite, crp – cryptomelane, cal – calcite

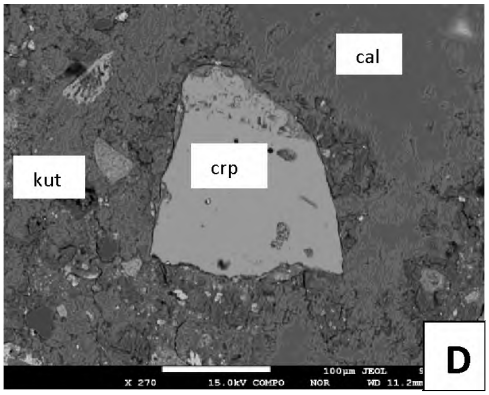

kut- kutnohorite; crp- cryptomelane; cal - calcite

RW5 – fissure

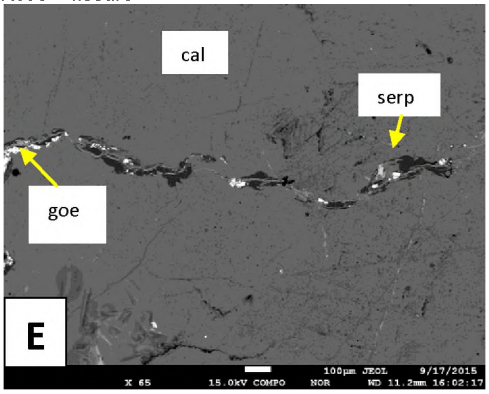

goe – goethite; serp – serpentine; cal – calcite

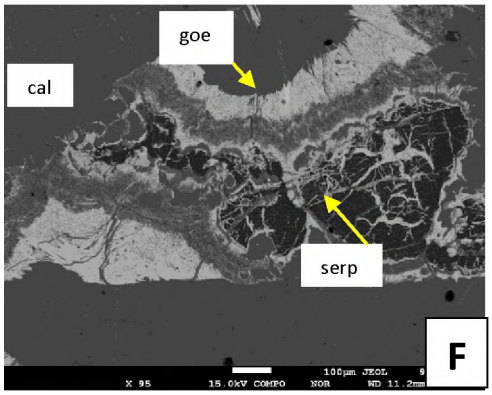

goe – goethite; serp – serpentine; cal – calcite

Figure 2.2.2: Back scattered images showing the different mineralogy.

All the back scattered images of the fissures LSW3, LSW6 and RW5 have calcite and dolomite as the dominant minerals which form the matrix of the samples. The other common minerals present are goethite, manganomelane and quartz. LSW3 provides evidence that displacement took place and as shown in Figure 2.2.3 showing quartz being displaced. Serpentine present in RW5 is closely associated with goethite showing a boytroidal texture. The manganomelane in LSW3 has various shapes from small aggregates to large anhderal crystals. Calcite is being replaced by manganomelane, the manganomelane is being replaced by goethite and hematite. The quartz veins are getting replaced from both the grain boundaries and from the centre by dense aggregates of manganomelane which also fill the faulted areas.

2.8.2. Evidence of faulting

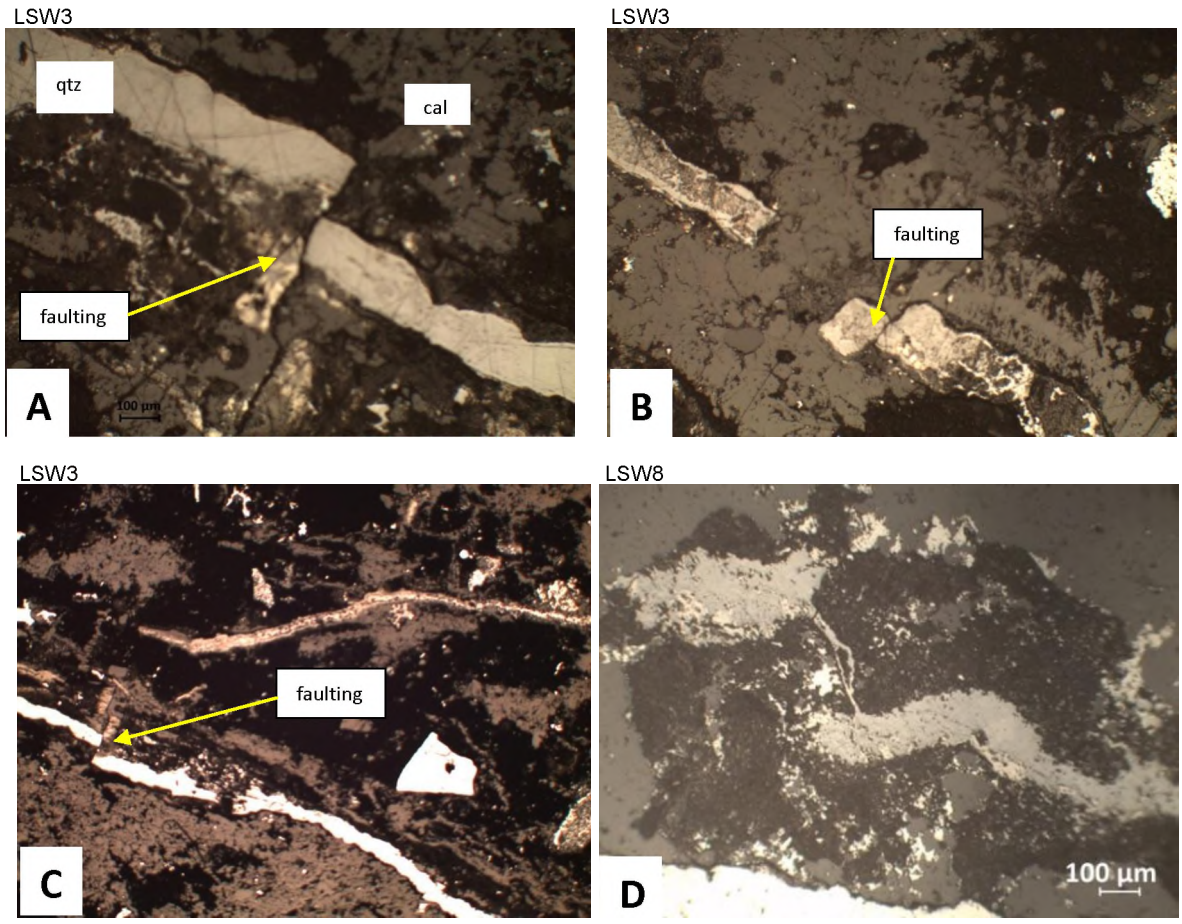

Figure 2.2.3: The displacement of minerals aided in the distribution and movement of different elements.

2.8.3. Textures and Mineralogy

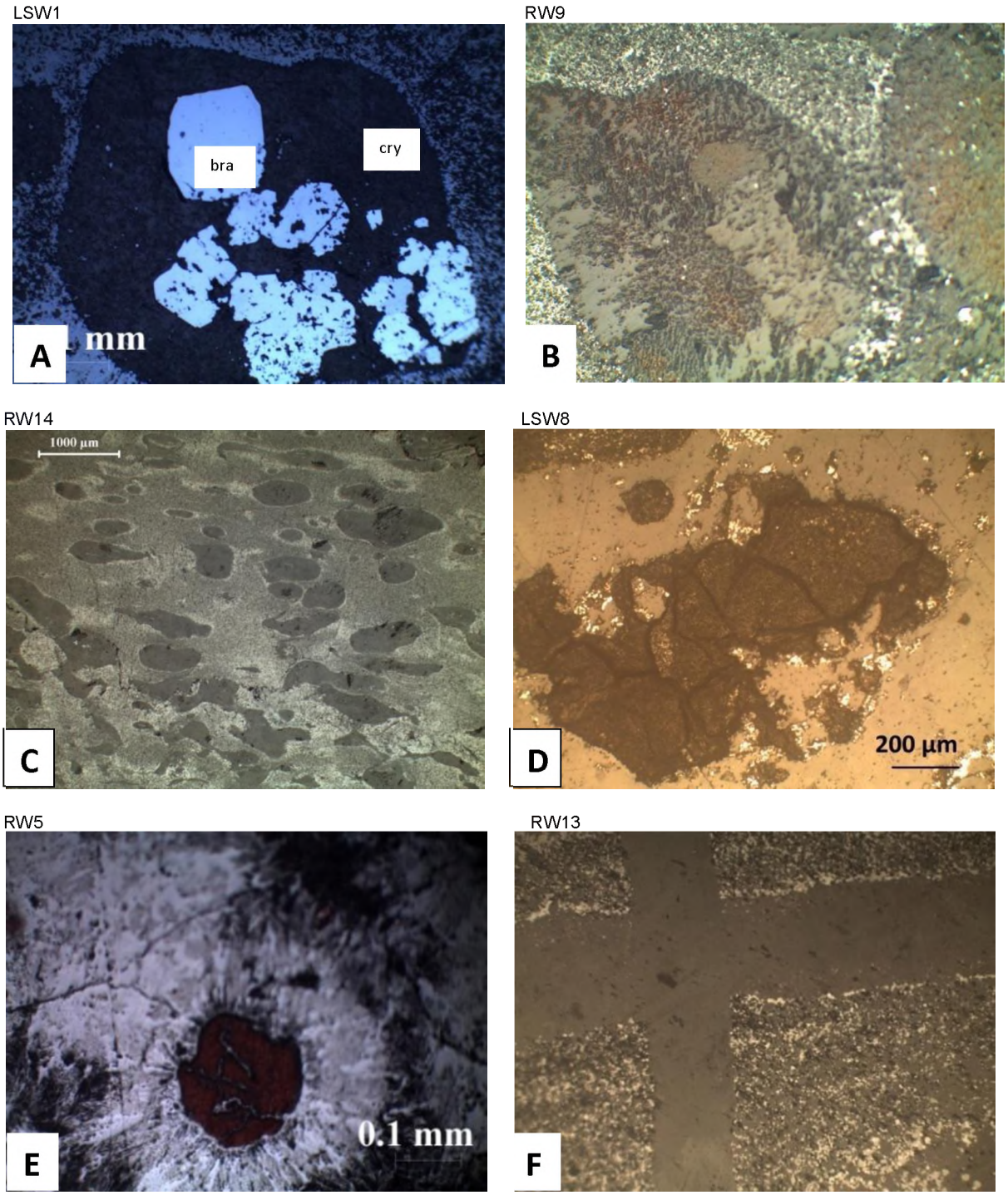

(A) Inclusions of braunite within cryptomelane; the braunite crystals are euhderal to subhedral in shape. Bra - braunite, cry – cyyptomelane (B) Myrmekitic texture shown in the Ca rich minerals calcite and kutnohorite suggesting decomposition of an initially homogenous phase (Craig, James R., 1940) (C) (C)-Oolitc texture been shown in unaltered ore, the ooliths are being defined by the calcite and braunite forms the matrix. (D)- Botryoidal texture in manganomelane (E) Radial texture being exhibited by goethite, todorokite is filling an open fracture (F) Cross cutting relationships of carbonates showing evidence of two depositional events of the carbonates.

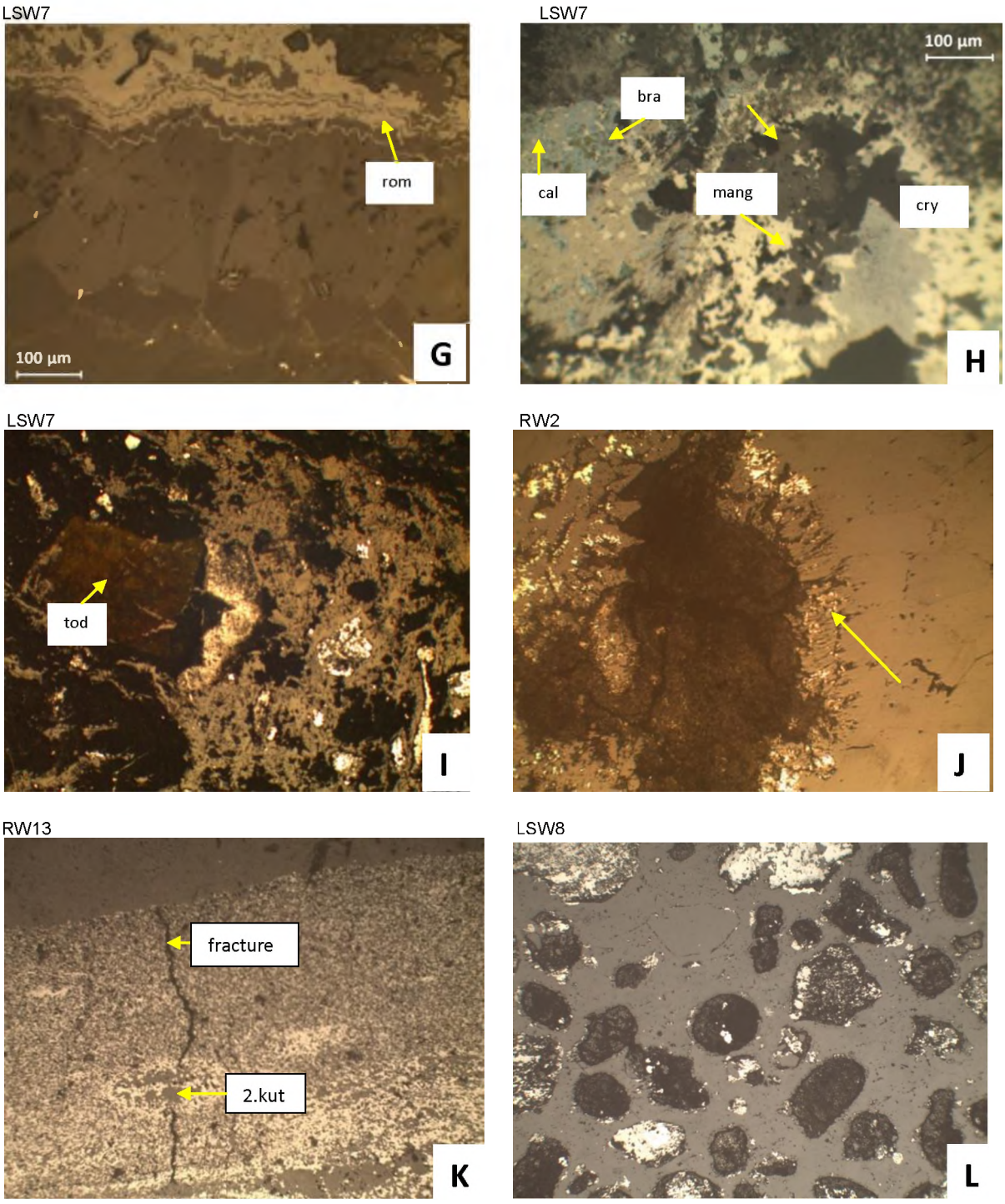

(G) Comb structure showing growth of crystals from fracture walls, calcite crystals are growing from open spaces created by goethite; (H) rom – romanechite; cal – calcite and bra – braunite (I) the difference between todorokite, cryptomelane and manganomelane, tod –todorokite; cry –cryptomelane and mang – manganomelane (J) The yellow arrow shows the margins of manganomelane stretched showing evidence of movement after the alteration of the primary manganese minerals (K) fracture filling by kutnohorite implying deposition of carbonates after a deformation event which emplaced the primary minerals, kutnohorite being replaced by patridgeite; notice 1.Kut – kutnohorite shows no replacement and 2. Kut -kutnohorite showing extensive replacement (L) Rounded to subrounded manganomelane showing extensive movement of samples at the contact of the fault.

Figure 2.2.4: Mineralogy and textures of selected thin sections.

2.8.4. Replacement Textures.

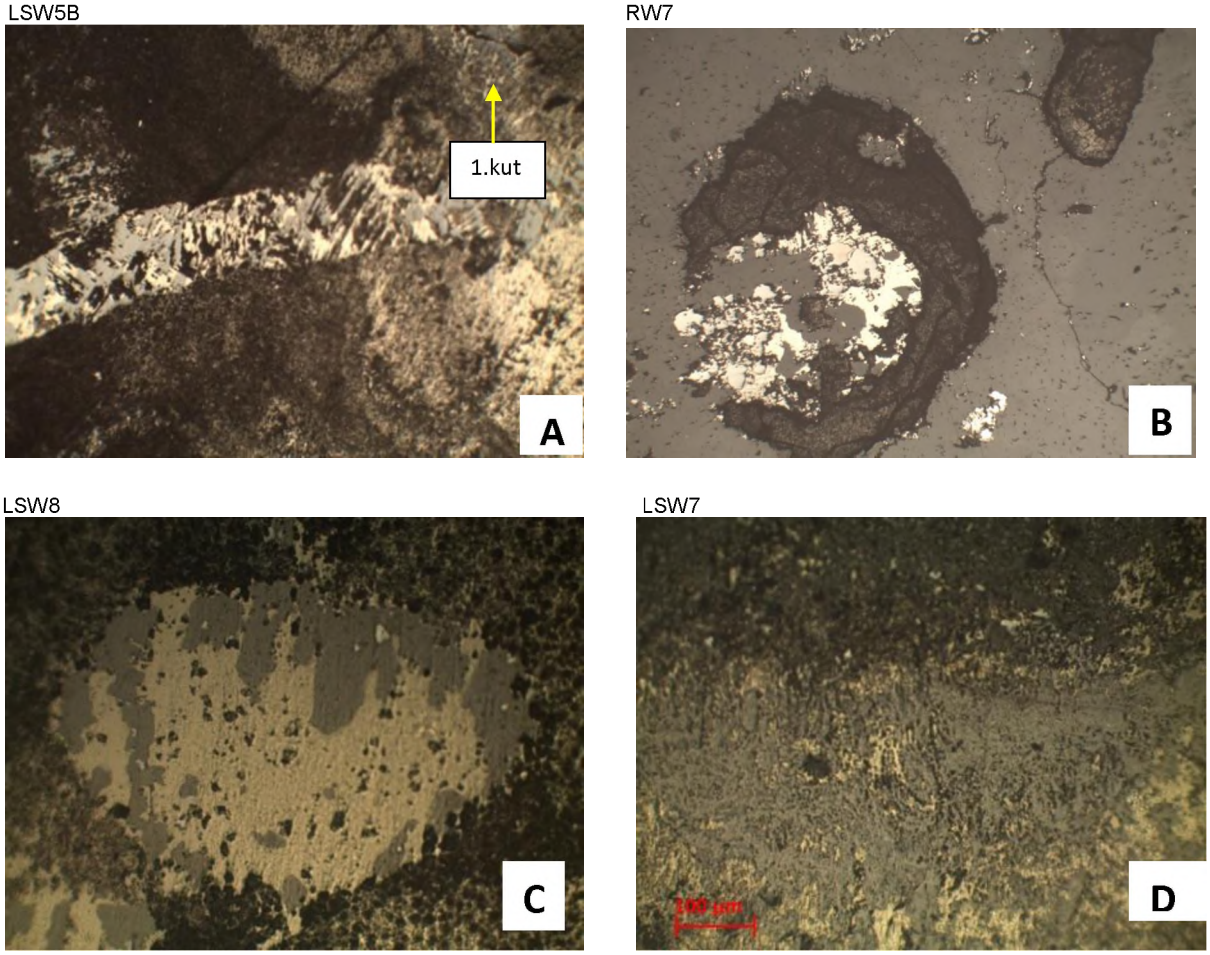

(A) Manganite (grey) and hausmannite (white) being replaced by manganomelane (brown) (B) manganomelane (brown) being replaced by hematite (white) in a matrix of carbonate (grey) (C) - Manganite (grey) being replaced by pyrolusite (yellow brown) in a crystalline dense matrix of manganomelane (brown) (D) romanechite (grey) replacing pyrolusite (yellow brown) and manganomelane surrounded by manganomelane top part (brown)

Figure 2.2.5: Evidence of extensive replacement especially in the intensely altered samples.

2.8.5. Evidence of folding.

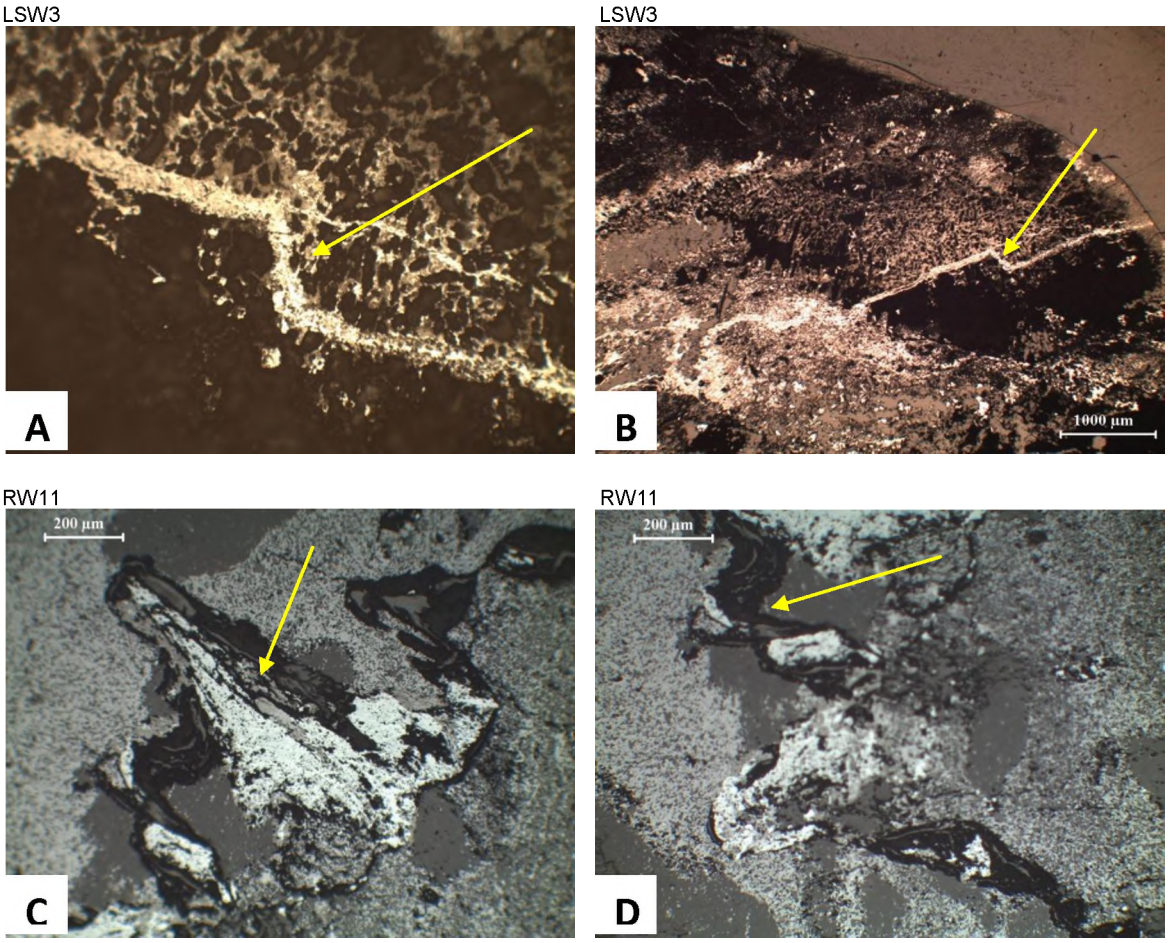

(A) and (B) show parasitic folding as shown by the Z structures (C) and (D) show intense folding shown in calcite and kutnohorite. M folding is shown in (C) and S folding is shown in (D). The white mineral in (C) and (D) is fine grained braunite and kutnohorite and is also affected by this folding.

Figure 2.2.6: The folding aided in the movement of elements due to the shortening and extension of different minerals across the section.

2.8.6. Change in matrix composition.

Figure 2.2.7 shows the transition on the right side from the main structure showing manganese dominated (manganomelane) matrix to a carbonated (kutnohorite, calcite and dolomite) matrix.

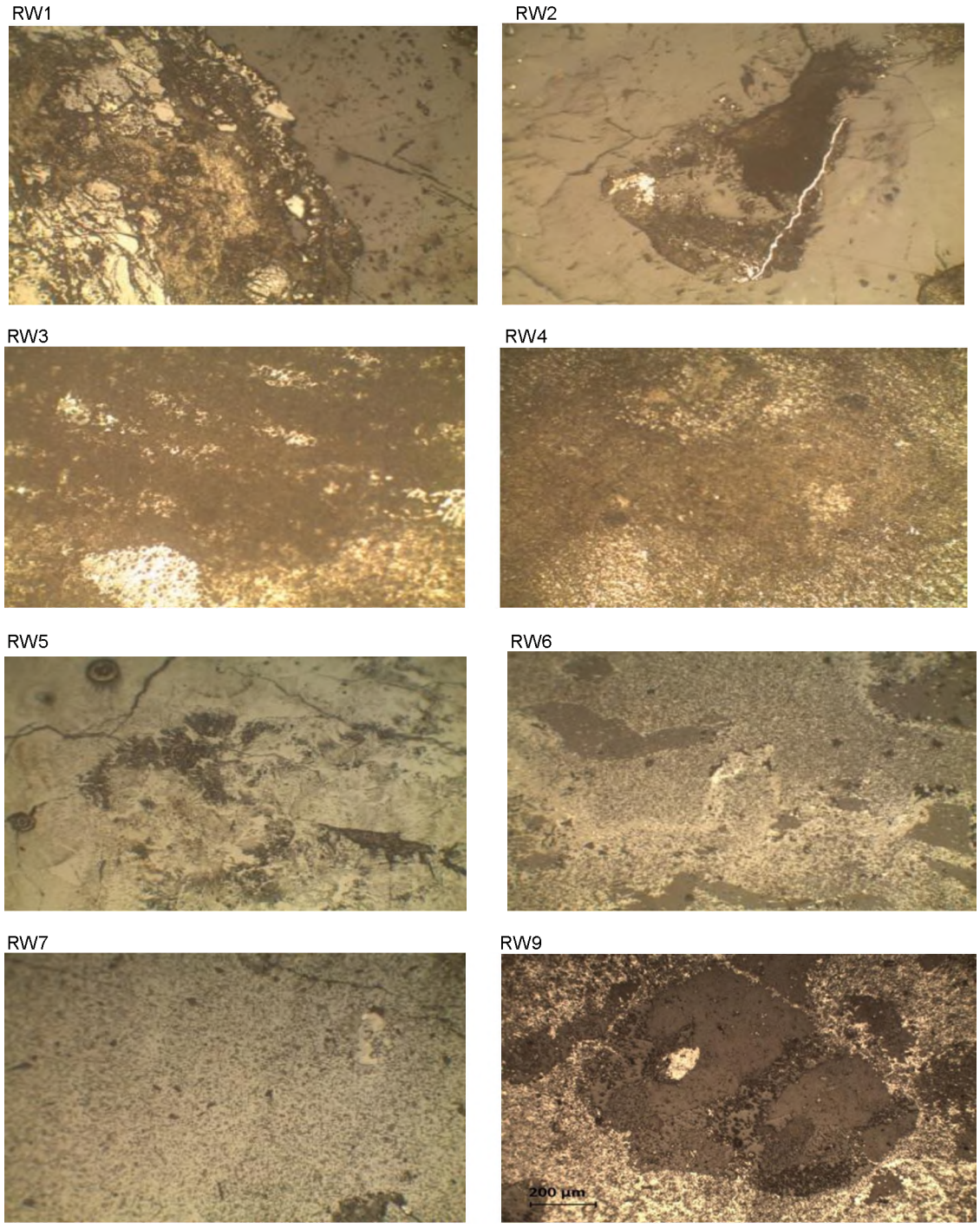

Figure 2.2.7: The change in matrix from altered ore to less altered ore on the right side of the main structure.

RW1 and RW2 are carbonate rich (grey) because of wall rock alteration caused from the main structure which is also dolomite and calcite rich. Notice in RW3, RW4 the dense crystalline manganomelane rich matrix (brown). RW5 which is goethite rich shown by the radial texture, goethite is replacing the manganomelane. RW6 and RW7 have a completely different matrix.

The matrix is composed mostly of very fine grained braunite, calcite and kutnohorite. The zone between RW4 and RW6 marks a sharp contact from the manganese rich matrix to a carbonate rich matrix.

2.9. Petrological description of ore

2.9.1. Adjacent to the fault.

Minerals synonymous with intense alteration in this study include manganomelane, cryptomelane, and romanechite. Samples LSW7, LSW8, RW1 and RW2 are the samples which are adjacent to the main structure and represent the most altered of the samples. These zones are characterized by intense replacement and show evidence of movement and displacement.

The manganomelane from LSW7 is present as small aggregates that are approximately 5 - 10 μm in size. Manganomelane replaces from the centre of the braunite going outwards.

Braunite is subhedral to anhedral in shape and the size ranges from 25 - 50 μm in size and in other cases has much larger sizes. Todorokite is also present as dense aggregates and resembles manganomelane but in some cases it is present as very thin veinlets of approximately 5μm thickness and show a “Z style” pattern typical in s and z folding patterns as shown in Figure 2.2.6.

LSW8 (sample adjacent to structure on the left side) is completely different from LSW7 in that the dominant matrix is predominately dolomite. The todorokite and manganomelane are subhedral to euhedral in shape and the crystal size ranges from 50 - 300 μm in size. Hematite seems to replace the manganomelane crystals, the typical botryoidal texture is displayed by manganomelane.

There are manganomelane crystals which show evidence of extension and resemble veins, the veins show replacement and intense alteration from the centre to the grain boundaries. Areas which have been replaced by hematite in the centre are susceptible to romanechite alteration. The percentage composition is as follows: manganomelane and todorokite 30%, dolomite 50, romanechite 10% and hematite and other manganese minerals occupy 10%.

RW1 is also dolomite rich because of the influence of the main structure which is carbonate rich. Dolomite shows evidence of boudinage folding and displacement. Manganomelane shows spheroidal texture with the spheroids of manganomelane displaying different sizes ranging from 30µm - 350µm. Calcite shows evidence of being intruded by dolomite, the calcite also intrudes the todorokite. This is to suggest that calcite was deposited before dolomite. Todorokite is displaying an anastomising texture forming a network that joins with other minerals through small veinlets.

This also implies that todorokite was most susceptible to deformation as compared to manganomelane because some manganomelane crystals preserve a euhedral shape. The grain boundaries of calcite are the first to be replaced by manganomelane until the whole crystal is entirely replaced. RW2 has a carbonate rich matrix primarily composed of calcite and dolomite. Manganomelane has very large anhedral crystals which are approximately 3000 µm in size. The edges of the crystals show evidence of extension and movement. This sample is carbonate and manganomelane rich.

2.9.2. Altered ore: left side.

Altered samples on the left side excluding the fissures are LSW1, LSW2, LSW4, LSW5A and LSW5B. These samples have a fine grained dense matrix comprised mostly of todorokite and manganomelane as compared to LSW7 and LSW8 which forms anhderal to subhedral crystals. Braunite has euhedral crystals which range from 5 - 20 µm in size.

The braunite occurs as inclusions in the manganomelane crystals. This sample resembles RW3 on the right side.

Calcite is present as very fine crystalline in close association with hematite and dolomite. Hematite is being replaced by romanechite. Hematite replaces the manganomelane from the centre of the crystals.

2.9.3. Less altered ore: right side.

These samples are represented by samples RW6, RW7, RW8, RW9, RW10, RW11 and RW12. The matrix is dominated by a very fine grained matrix of kutnohorite, braunite and dolomite. Mn-rich calcites which range from 0.2mm to 1mm in size constitute the coarse grained ovoids.

Euhedral crystals of manganite are present as inclusions in these ovoids. Crystals which show the most replacement and alteration are associated with intense porosity. The shape of the Mn-rich calcite ovoids changes from ellipsoidal, spherical to anhedral. Manganomelane is present in very trace quantities as part of the carbonate rich matrix and is being replaced by kutnohorite. Romanechite are replaced by manganite, hausmannite and braunite are replaced by partridgeite. Partridgeite noted by (Gutzmer, Beukes 1996) and (Paula Preston 2001) has a distinct yellow tint is also closely associated with romanechite which has a grayish bluish colour.

2.9.4. Unaltered ore: right side.

These samples are represented by samples RW14, RW15 and RW16.

RW16 which is the least altered sample has very little to no ovoids, the calcite in RW16 is present as massive crystals, and the kutnohorite and braunite which are replacing the calcite contribute to the disintergration of these Mn-calcites into small ovoids and also to become part of the fine grained matrix. As the samples move away from the unaltered ore as in RW15 the calcite is present as veinlets which are approximately 0.4mm thick, Mn-rich calcite ovoids become more prominent in RW14 which have a ellipsoidal to spherical shape. The size of braunite crystals increases from RW16 to RW14, the braunite has an euhedral to subhedral shape with an average size of about 10 μm.

CHAPTER THREE: GEOCHEMISTRY

3.1. Introduction

Whole rock geochemical analysis was done on samples collected on the left and right side of the section. 26 samples were crushed, pulverized into pulp samples and prepared into 5g vials. Only samples from the main structure were excluded from this analysis. 26 samples were sent for whole rock geochemical analysis at Bureau Veritas Commodities Limited in Canada. Whole rock by XRF method was conducted on the samples by a method called LF700 by $Li_2B_4O_7/LiBO_2$ fusion discs. The minimum detection limit for all the samples was 0.01% and the maximum being a 100%.

3.1.1. Major oxides (in wt %)

Sample name	Mn_2O_3	SiO_2	Fe_2O_3	CaO	Al_2O_3	MgO	K_2O	Na_2O	LOI	TOTAL
LSW1	70.62	7.78	7.25	4.15	0.33	1.13	0.23	0.35	9.13	***101.04***
LSW2	71.45	6.06	10.89	0.99	0.28	1.32	0.31	0.52	8.57	***100.42***
LSW3	21.63	10.73	12.91	24.72	1.67	1.45	0.19	0.34	25.05	***98.97***
LSW4	59.63	5.13	6.56	10.68	0.22	1.34	0.80	0.24	15.83	***100.53***
LSW5A	71.10	5.70	12.44	2.23	0.22	0.90	0.52	0.42	7.59	***101.19***
LSW5B	77.27	3.74	5.46	1.16	0.28	1.63	0.39	0.45	10.65	***101.10***
LSW6	10.50	11.84	17.52	28.15	1.28	2.14	0.35	0.17	26.66	***98.75***
LSW7	71.66	2.66	7.70	2.27	0.28	2.11	0.42	0.66	14.17	***101.98***
LSW8	58.52	2.25	6.52	10.30	0.44	2.10	0.25	0.54	18.88	***99.94***
RW1	55.49	1.91	7.28	12.06	0.36	2.44	0.21	0.47	19.18	***99.45***
RW2	58.60	2.57	6.45	11.72	0.26	0.98	0.16	0.42	18.44	***99.87***
RW3	72.33	1.08	7.49	2.00	0.32	1.34	0.27	0.78	15.38	***101.17***
RW4	66.10	10.71	6.94	2.27	0.24	1.78	0.93	0.45	11.33	***100.95***
RW5	12.19	5.05	29.91	25.00	0.22	3.45	0.01	0.03	23.38	***99.28***
RW6	44.93	4.99	6.66	19.79	0.23	2.61	0.01	0.02	19.41	***98.69***
RW7	59.55	6.32	4.71	11.04	0.24	3.56	0.01	0.01	14.57	***100.18***
RW8	64.86	6.09	5.98	8.25	0.23	3.18	0.01	0.01	11.92	***100.65***
RW9	61.05	7.47	4.60	10.95	0.21	2.29	0.01	0.01	12.86	***99.90***
RW10	59.91	6.72	5.29	11.43	0.25	3.00	0.01	0.01	13.74	***100.49***
RW11	49.34	5.50	6.49	16.13	0.22	3.38	0.01	0.01	18.11	***99.23***
RW12	59.74	5.83	7.20	10.01	0.24	3.45	0.01	0.01	13.99	***100.61***
RW13	56.06	5.47	5.37	13.61	0.13	3.09	0.01	0.01	16.00	***99.80***
RW14	44.89	3.83	5.81	20.22	0.08	3.05	0.01	0.01	20.98	***98.93***
RW15	47.41	4.25	5.19	20.11	0.12	2.33	0.01	0.01	19.67	***99.23***
RW16	47.44	4.26	5.08	20.27	0.11	2.24	0.01	0.01	19.60	***99.15***
76(control)	1.27	32.87	51.12	5.25	0.08	1.18	0.01	0.01	7.42	***99.17***

Table 4.1: Geochemistry results of major oxides.

3.1.2. Minor Oxides: (in wt %)

Sample name	TiO_2	P_2O_5	Cr_2O_3	Ba
LSW1	0.01	0.07	0.01	0.01
LSW2	0.01	0.07	0.01	0.03
LSW3	0.10	0.01	0.01	0.17
LSW4	0.01	0.07	0.01	0.03
LSW5A	0.01	0.07	0.01	0.01
LSW5B	0.01	0.07	0.01	0.01
LSW6	0.10	0.01	0.01	0.03
LSW7	0.01	0.03	0.01	0.02
LSW8	0.01	0.06	0.01	0.08
RW1	0.01	0.05	0.01	0.01
RW2	0.01	0.04	0.01	0.23
RW3	0.01	0.04	0.01	0.14
RW4	0.01	0.04	0.01	0.16
RW5	0.01	0.03	0.01	0.01
RW6	0.01	0.05	0.01	0.01
RW7	0.01	0.04	0.01	0.15
RW8	0.01	0.05	0.01	0.09
RW9	0.01	0.04	0.01	0.41
RW10	0.01	0.04	0.01	0.11
RW11	0.01	0.04	0.01	0.02
RW12	0.01	0.05	0.01	0.10
RW13	0.01	0.04	0.01	0.03
RW14	0.01	0.05	0.01	0.02
RW15	0.01	0.04	0.01	0.11
RW16	0.01	0.04	0.01	0.10
76(control)	0.04	0.08	0.01	0.01

Table 4.2: Geochemistry results of minor oxides.

3.2. Bivariate plots

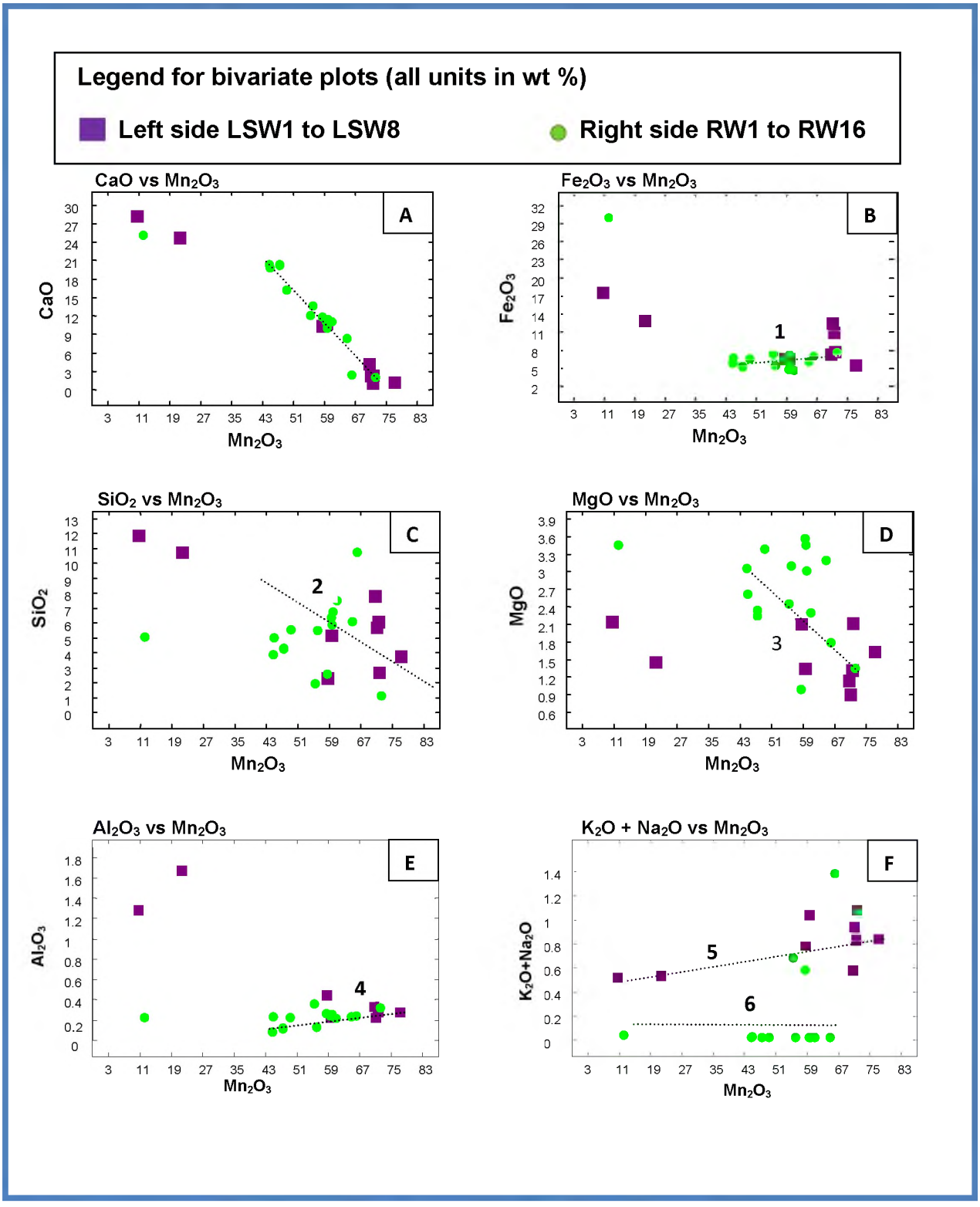

Figure 3.1.0: Correlations showing the relationship between major oxides and Mn_2O_3.

The purpose of bivariate plots in this study is to find correlations between two oxides, whether the relationship between the two oxides is positive or negative. The main oxide under investigation is Mn_2O_3, therefore Figure 3.1.0 plots Mn_2O_3 against the major oxides namely Fe_2O_3, MgO, Al_2O_3, K_2O, CaO, Na_2O and SiO_2. K_2O and Na_2O have been combined together because of their strong relationship and their values are almost similar.

There is a strong negative correlation between CaO and Mn_2O_3, an increase in Mn_2O_3 results in a decrease in CaO as shown in Figure 3.1.0. This is backed up by the petrographic observation in Figure 2.2.2 where the fissures have low manganese values because they are rich in carbonates. Another important plot is diagram F in Figure 3.1.0; line 5 shows a trend of mostly samples on the left side and the first few samples on the right side where an increase in K_2O + Na_2O results in an increase in Mn_2O_3 grade. This correlation in line 5 confirms the presence of manganomelane and todorokite which are associated with high Mn_2O_3 grades. Line 6 in diagram F shows a trend of very low K_2O and Na_2O which have lower Mn_2O_3 grades. The two trends in Line 5 and Line 6 of diagram F show a strong relationship to the petrographic observation in Figure 2.2.7.

Generally the correlations in Figure 3.1.0 are very weak to no correlations at all but using the line of best fit method this can help us to identify the general relationship between the two oxides. Diagram C and D (line 2 and 3) in Figure 3.1.0 show a general negative trend, a decrease in SiO_2 and MgO shows a general increase in the Mn_2O_3. As shown in Chapter 2 Figures 2.1.3 and 2.1.5 that SiO_2 and MgO are influenced by braunite and kutnohorite respectively, unaltered ore rich in braunite and kutnohorite have lower Mn_2O_3 values as compared to altered ore.

Using the line of best fit method, diagrams E shows that an increase in Mn_2O_3 is also associated with an increase in Al_2O_3. The source of Al_2O_3 is chloritoid and from Table 4.1 it shows that generally high Al_2O_3 values are associated with high Mn_2O_3 values. This implies that chloritoid alteration has some influence and association with the grade and alteration of manganese minerals excluding the fissures (LSW3 and LSW6) which have high Al_2O_3 values and low Mn_2O_3 grades.

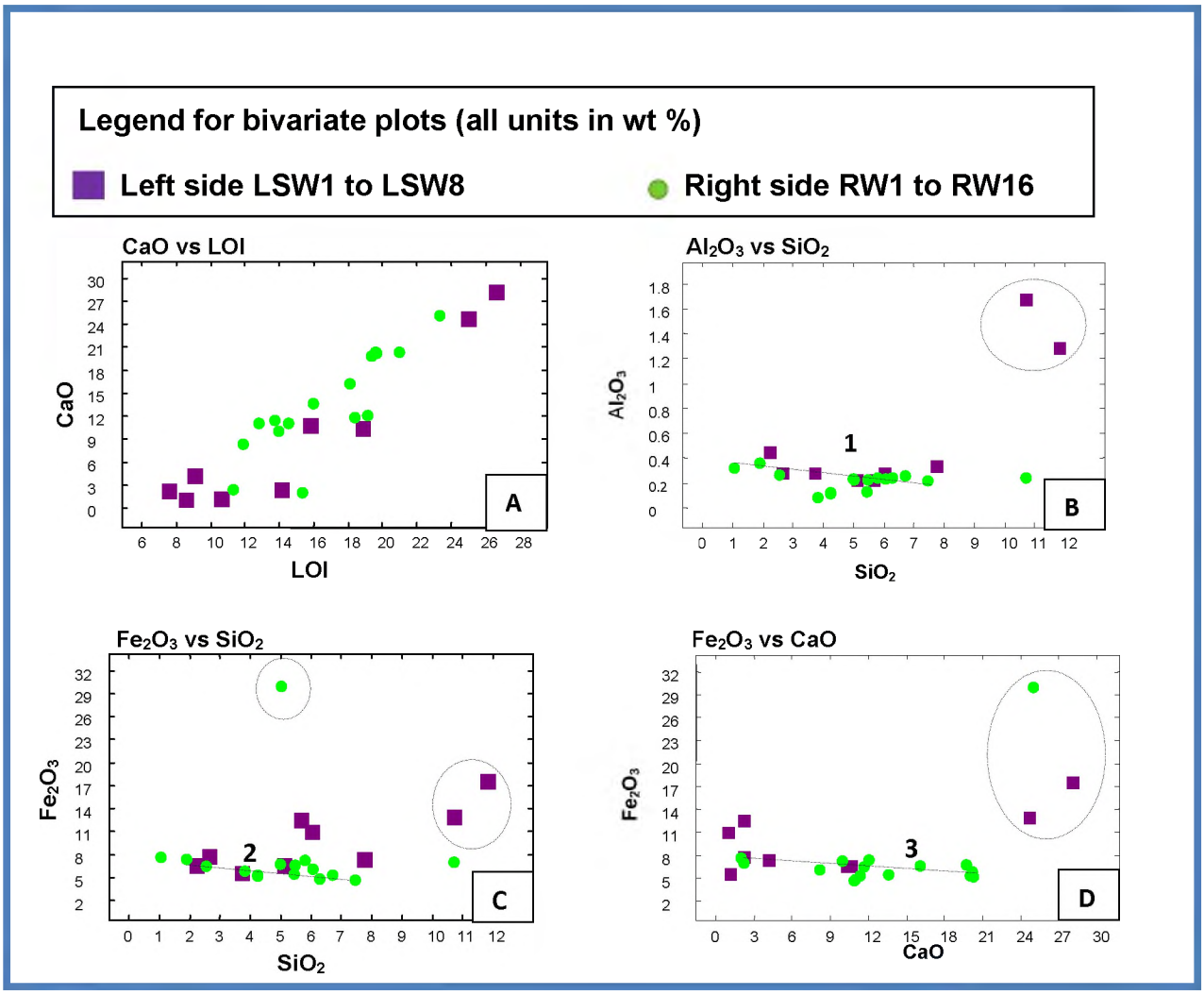

Figure 3.1.1: Correlations of different oxides plotted against each other except for Mn_2O_3.

The diagrams plotted in Figure 3.1.1 aim to show the relationship between two oxides other than Mn_2O_3 that can have a direct or indirect relationship to the overall behavior of Mn_2O_3. Most of the oxides have weak correlations to no correlations however the objective of Figure 3.1.1 is to display plots that have weak correlations to strong correlations as this can give an indication of the general trend being exhibited by the two oxides. The oxides that are not plotted in Figure 3.1.1 do not show any indication of correlation and were omitted.

There is a positive correlation between LOI and CaO as shown in Figure 3.1.1 diagram A. An increase in either of the two results in a direct increase of the other. Observing the diagrams in Figure 3.1.1 it shows that there are generally very weak correlations between oxides.

Using the line of best fit method, diagrams B, C and D in Figure 3.1.1 show a general negative relationship. SiO_2 is the primary manganese element oxide in unaltered ore which has a generally lower grade than altered ore. Line 1 in diagram B of Figure 3.1.1 shows that a decrease in Al_2O_3 results in an increase of SiO_2 except for the two fissures which are circled. Diagram B of Figure 3.1.1 and diagram E of Figure 3.1.0 shows some correlation.

Fe_2O_3 is generally controlled by hematite as shown in Chapter 2 Figure 2.1.4, however hematite is the main replacement mineral of manganomelane as shown in Chapter 2 Figure 2.2.5 diagram B. Essentially an increase in manganomelane results in an increase in hematite presence, therefore high Mn_2O_3 grades are associated with hematite. Unaltered ore with lower Mn_2O_3 grades constitute CaO and SiO_2 (constituent mineral of braunite), therefore diagram C and D confirm that a decrease in Fe_2O_3 is associated with an increase in both CaO and SiO_2. The samples which are circled in diagrams C and D are fissures (LSW3, LSW6 and RW5) which have above average values and therefore were omitted to avoid distortion.

.

3.3. Lateral geochemical profiles (traverses)

3.3.1. CaO

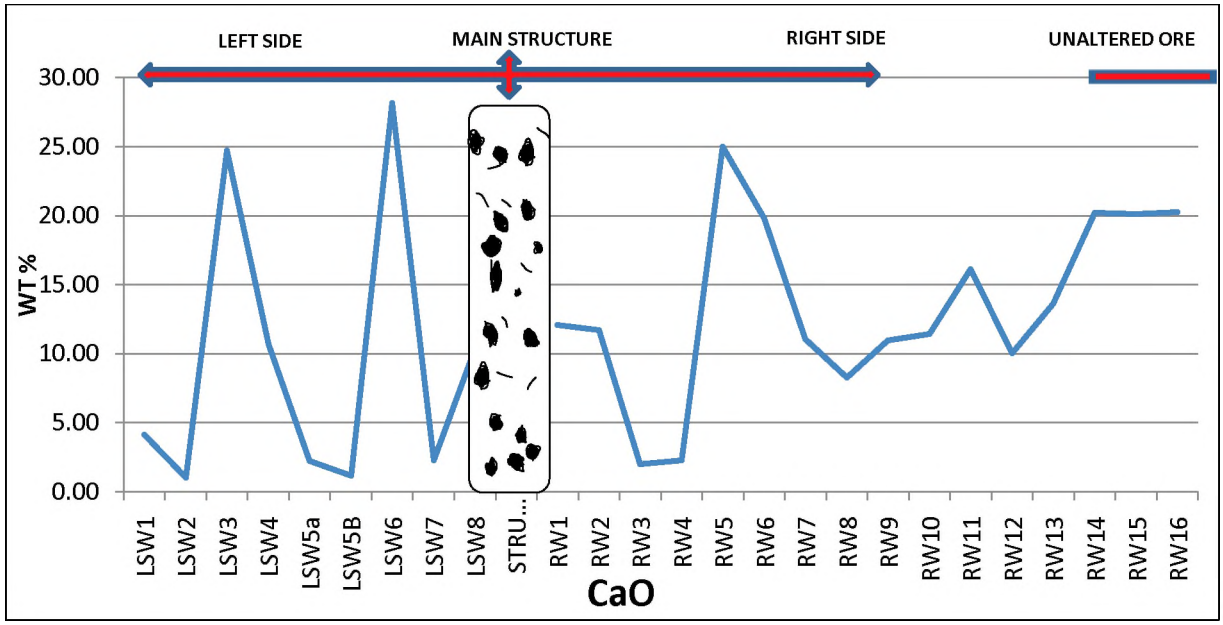

Figure 3.1.2: Geochemical traverse showing the behavior of CaO across the section including the fissures.

3.3.2. CaO (without fissures: LSW3, LSW6 and RW5)

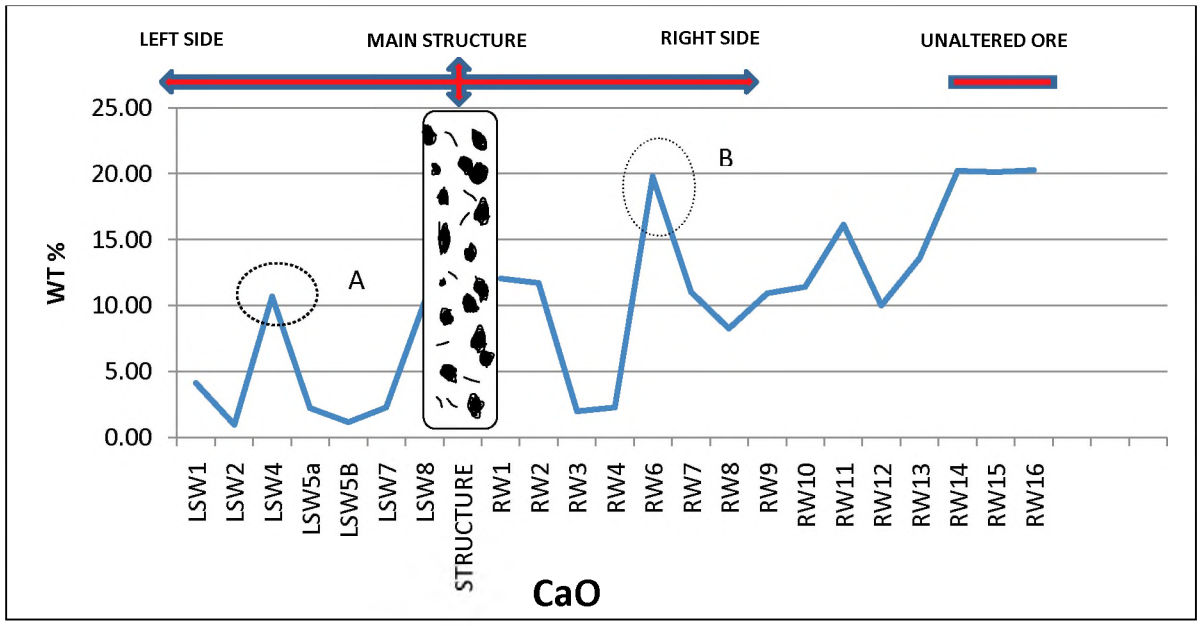

Figure 3.1.3: Geochemical traverse showing the behavior of CaO across the section excluding the fissures.

An increase in CaO is accompanied by a decrease in Mn_2O_3 as by shown the bivariate plot in Figure 3.1.2 which shows a negative correlation between the two oxides. This negative correlation is shown in Figure 3.1.2 and Figure 3.1.6. The three fissures LSW3, LSW6 and RW5 have the highest grades in CaO with 20% content because the dominant matrix is calcite as shown in Figure 2.2.2A, Figure 2.2.2 C and Figure 2.2.2 E respectively.

A and B in Figure 3.1.3 are not fissures but have high CaO content values because of the influence of the fissures which are adjacent to these samples. The CaO generally decreases away from the main structure because of the intense alteration of manganese ore which is associated with alteration minerals such as todorokite and manganomelane. The decline in the CaO content on the right side is less abrupt as compared to the left side because of the presence of the dolomite which originates from the main structure as shown the mineral chemistry of RW1 in the appendix section of the carbonates.

There is a significant increase in the CaO content on sample RW5 because of the transition from a manganese matrix to a carbonate matrix in Chapter 2 Figure 2.2.7. The decrease in CaO content in samples RW8, RW9, RW10 in Figures 3.1.2 and 3.1.3 is because of the increase in the mineral braunite which is one the major constituents of the unaltered manganese ore. Figure 2.1.3 shows a strong relationship between SiO_2 and braunite and how much it influences the grade of CaO especially towards the unaltered ore from sample RW8 to RW10.

The CaO shows another significant increase in its content from sample RW12 to the unaltered ore because of the enrichment of carbonate minerals such as kutnohorite, calcite and dolomite as the ore becomes less altered. The evidence of the abundance of carbonate minerals is shown in Figure 2.2.4 C which displays an oolitic texture where the Mn-calcites form the matrix of the samples. The CaO content becomes constant in samples RW14, RW15 and RW16 because they show very little alteration in the chemical composition of these samples. The only alteration present in these samples is the change in the shape of the Mn- calcite grains. The mineral chemistry of the Mn-calcites is shown in sample RW16 in the appendix section of carbonates.

3.3.3. MgO

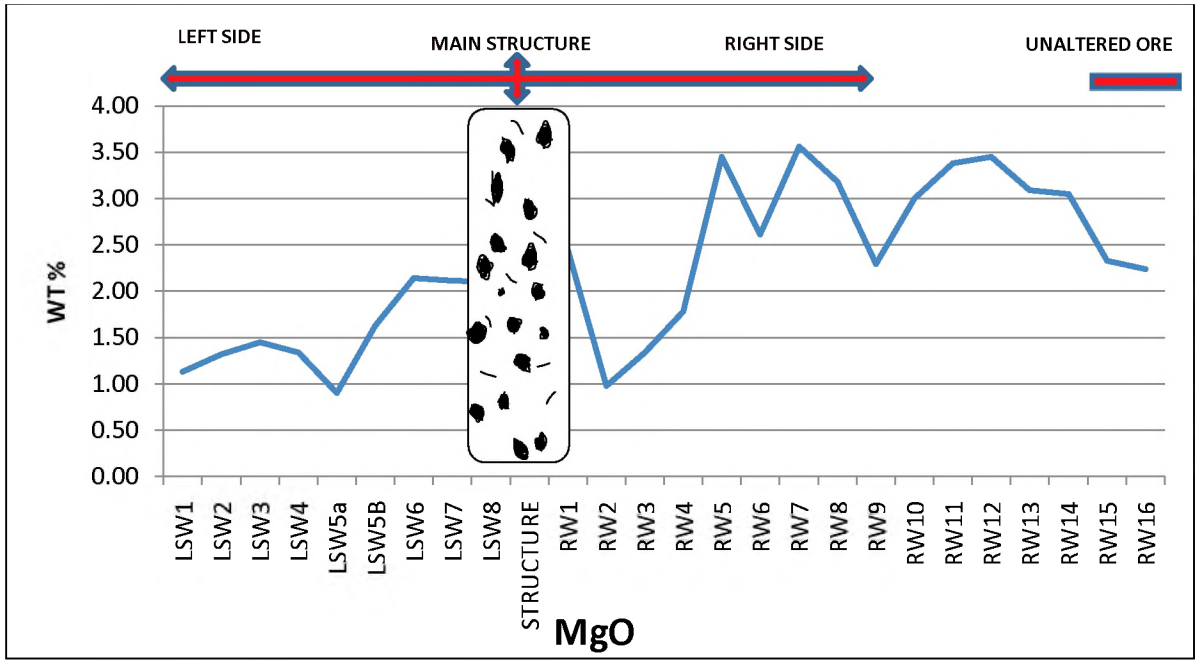

Figure 3.1.4: Geochemical traverse showing the behavior of MgO across the section including the fissures.

3.3.4. MgO (without fissures: LSW3, LSW6 and RW5)

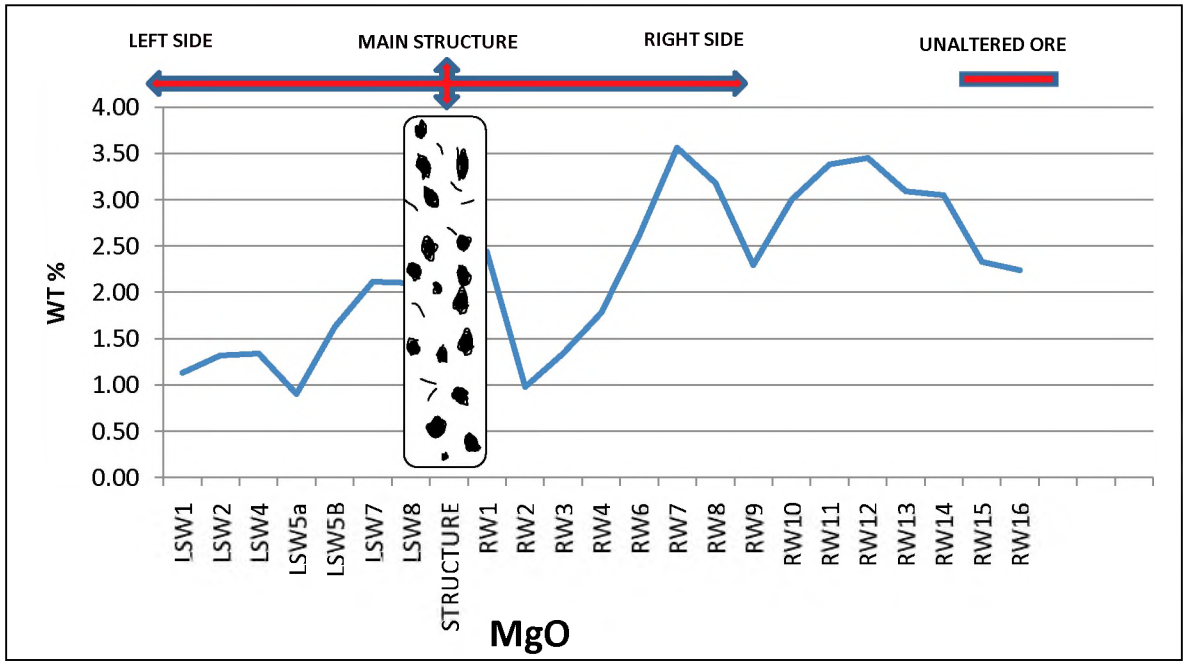

Figure 3.1.5: Geochemical traverse showing the behavior of MgO across the section excluding the fissures.

The Mg distribution across the traverse is influenced by minerals such as kutnohorite, todorokite, dolomite and chlorite. MgO content has at least 1% content on both the left side and right side because of the presence of chlorite as shown in Figure 3.1.4. (Gutzmer; Beukes 1996) noted the presence of clinochore as one of the minerals encountered either through XRD and petrographic studies. Chlorite is a secondary mineral formed as a result of the alteration processes.

The presence of todorokite on the left side of the main structure is synonymous with the degree of alteration which shows the enhanced MgO content to above 2% as shown by samples LSW7 and LSW8 in both Figures 3.1.4 and 3.15. The effect of dolomite on the overall MgO content is very minimal because there is no significant increase in MgO in the samples immediately adjacent to the main structure. However the right has more manganomelane than todorokite which shows the lower MgO content in samples RW2, RW3 and RW5.

As shown in Chapter 2 Figure 2.1.5 that kutnohorite is the main mineral which possesses the biggest influence in the MgO content. The marked increase in MgO from sample RW5 coincides with presence of kutnohorite as shown in Table 2.1 which shows the mineral chemistry of RW7 which has a MgO content of 12.88%. The higher MgO content is as a result of the fine grained kutnohorite and braunite. The MgO content steadily decreases towards the unaltered ore because the Mn-calcites become the more dominant as shown by the ternary plot in Chapter 2 Figure 2.1.7 and the EMPA raw data of sample RW16 in the appendix section of the carbonates.

LSW3, LSW6 and RW5 show an increase in MgO content as shown in Figure 3.1.4 because the fissures are predominantly composed of calcite and kutnohorite as shown in Chapter 2 Figure 2.2.2 C.

3.3.5. Mn_2O_3

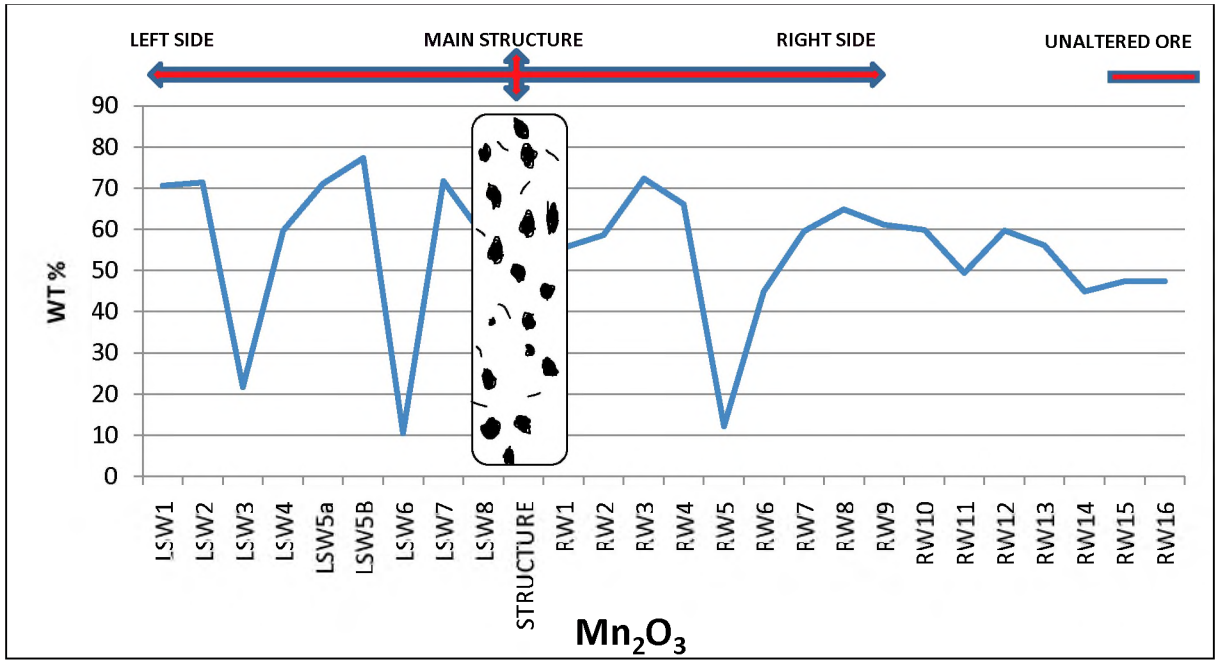

Figure 3.1.6: Geochemical traverse showing the behavior of Mn_2O_3 across the section including the fissures.

3.3.6. Mn_2O_3 (without fissures: LSW3, LSW6 and RW5)

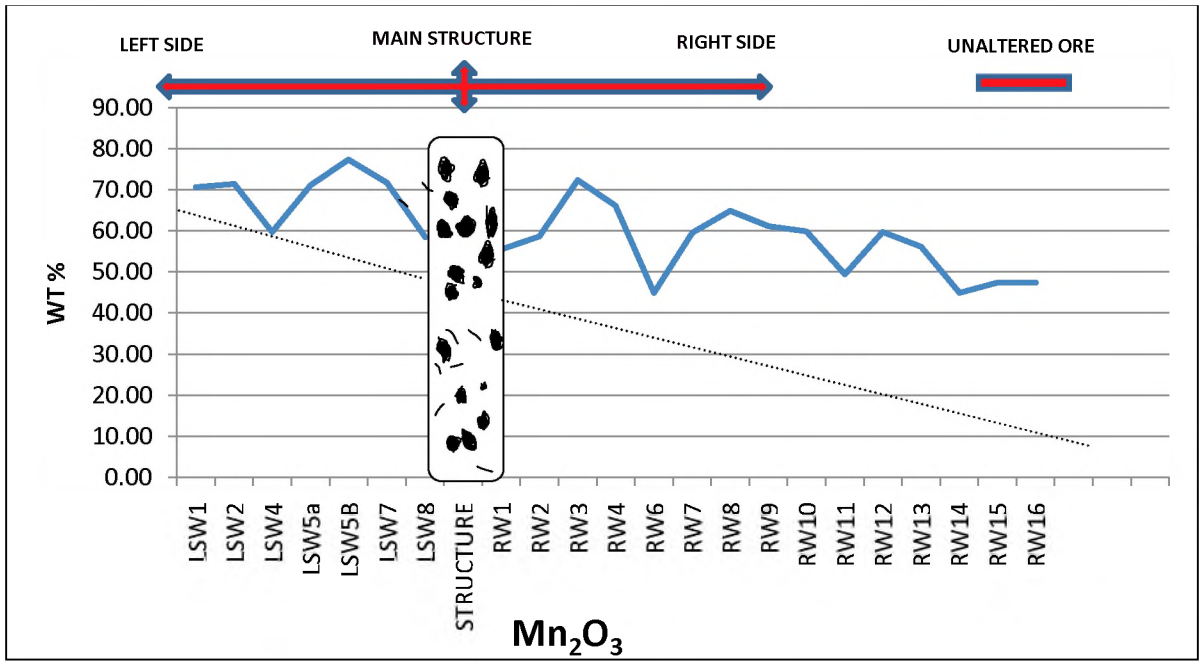

Figure 3.1.7: Geochemical traverse showing the behavior of Mn_2O_3 across the section excluding the fissures.

From the illustrations shown above there is a direct correlation between alteration intensity and grade of manganese. Samples LSW5A, LSW5B, LSW7, RW2 and RW3 are intensely altered as shown in Chapter 2 Figures 2.2.6 and 2.2.7. These intensely altered samples are associated with a manganese content averaging 70% as they are predominantly composed of romanechite, manganomelane and todorokite. Samples LSW3, LSW6 and RW5 are small fissures which are associated with the lowest Mn_2O_3 values as shown in the illustrations above. The reason for the low Mn_2O_3 values is because the samples are rich in carbonate minerals such as calcite which constitutes the matrix of these fissures. The left side of the main structure has higher Mn_2O_3 values than the right side because all the samples on the left side show some degree of alteration as evidenced by the presence of either todorokite or manganomelane in the samples. On the right side the alteration is evident from sample RW1 to RW4 but shows a sharp decline in the Mn_2O_3 content from sample RW5 as the matrix changes to carbonate rich matrix as shown in Chapter 2 Figure 2.2.7.

As the section moves away from the main structure, the Mn_2O_3 content shows a steady decline from sample RW5 and the grade of the ore averages 40%. The behavior of the manganese grade across the traverse is shown by the dotted line in Figure 3.1.7 which shows a clear trend from the left side which is intensely altered to a less altered on the right side.

3.3.7. $K_2O + Na_2O$

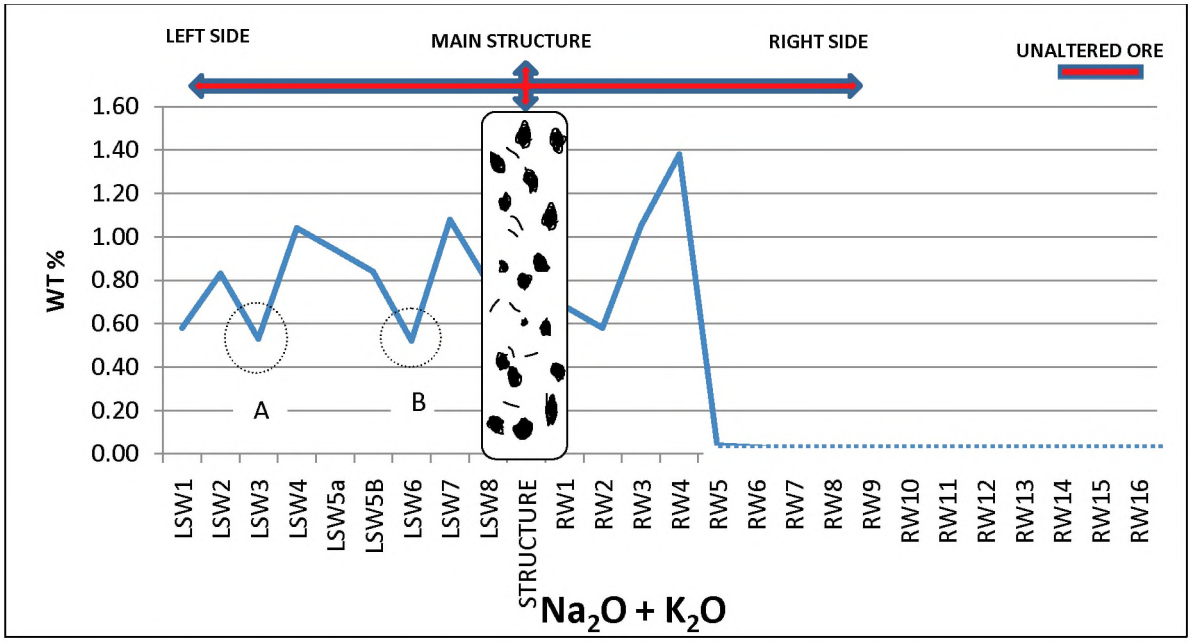

Figure 3.1.8: Geochemical traverse showing the behavior of $Na_2O + K_2O$ across the section including the fissures.

3.3.8. $K_2O + Na_2O$ (without fissures: LSW3, LSW6 and RW5)

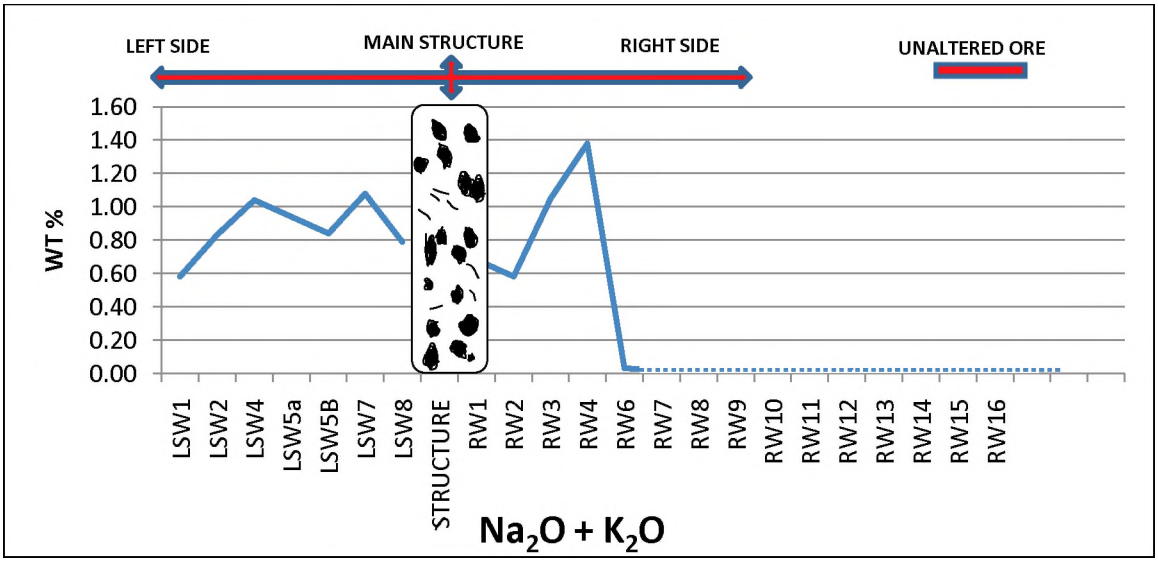

Figure 3.1.9: Geochemical traverse showing the behavior of $Na_2O + K_2O$ across the section excluding the fissures.

The influence and intensity of alteration are influenced by the presence of K and Na. Manganomelane is mainly controlled by the distribution of K and Na as shown in the samples on Figures 3.1.8 and 3.1.9 above which shows the distribution of these two elements across the traverse. A and B in Figure 3.1.8 show a decrease in K and Na because the fissures are predominated with carbonate minerals as shown in Chapter 2 Figure 2.2.2 A and C. Fissures LSW3 and LSW6 have calcite as the dominant matrix minerals as well as coarse grained kutnohorite grains which occupy these intergranular spaces of these fissures.

Generally the intensity of alteration is consistent on the left side as shown by the distribution of K and Na in both Figures 3.1.8 and 3.1.9. The samples on the right side show a decrease immediately after the fault probably due to the influence of the fault which is dolomite rich. As the section progresses further on the right side the intensity of alteration becomes intense and the content of K and Na increase from sample RW2 to RW5 as shown from the samples in Figures 3.1.8 and 3.19.

The section shows a sharp decline of both elements of K and Na from sample RW5 onwards as it approaches the unaltered ore. The explanation is justified in Chapter 2 Figure 2.2.7 which shows a transition from the main structure showing a manganese dominated (manganomelane) matrix to a carbonate rich matrix. Figures 3.1.8 and 3.1.9 shows that sample RW5 marks the contact zone of the manganese matrix and the carbonate matrix. This evidence is a strong relationship to the petrographic observation in Chapter 2 Figure 2.2.7.

CHAPTER FOUR: DISCUSSION AND RECOMMENDATIONS

4.1. Introduction

Geochemical changes across the profile are governed by three main processes which affect the mineralogy and distribution of oxides across the section. These three main processes are redistribution, enrichment and depletion. These three processes can be best illustrated through mass balance diagrams. (Gresens, 1967) designed an analytical method to ascertain variations in volume and concentrations by hydrothermal processes. (Grant, 1986) designed the isocon diagram to estimate chemical differences by analyzing gains and losses in mass transfer. Using these two methods we can analyze the chemical changes that have occurred, when some elements are getting enriched, others are getting depleted and in turn some elements are redistributed to other sections of the profile.

When a new system of fluids (emplacement of fault) is introduced into a pre-existing system this results in various geochemical changes from the main structure to the less altered. It is important to use these diagrams in this study as it helps to understand if there is an increase or decrease in volume/mass of a specific compound when these three processes (redistribution, depletion and enrichment) take place.

4.2. Mineralogy of the main structure

Mineral	Major Elements
Dolomite	Ca, Mg.
Quartz	Si
Chloritoid	Mg, Al, Si.
Jacobsite	Mn, Fe
Hematite and Goethite	Fe
Calcite	Ca
Graphite	C

Table 4.1: Minerals of the main structure and their main elements.

The full mineralogy list of the fault is found in the appendix section, analysis was carried out by EMPA for samples LSW9A, LSW9B, LSW9C, LSW9D and LSW9E.

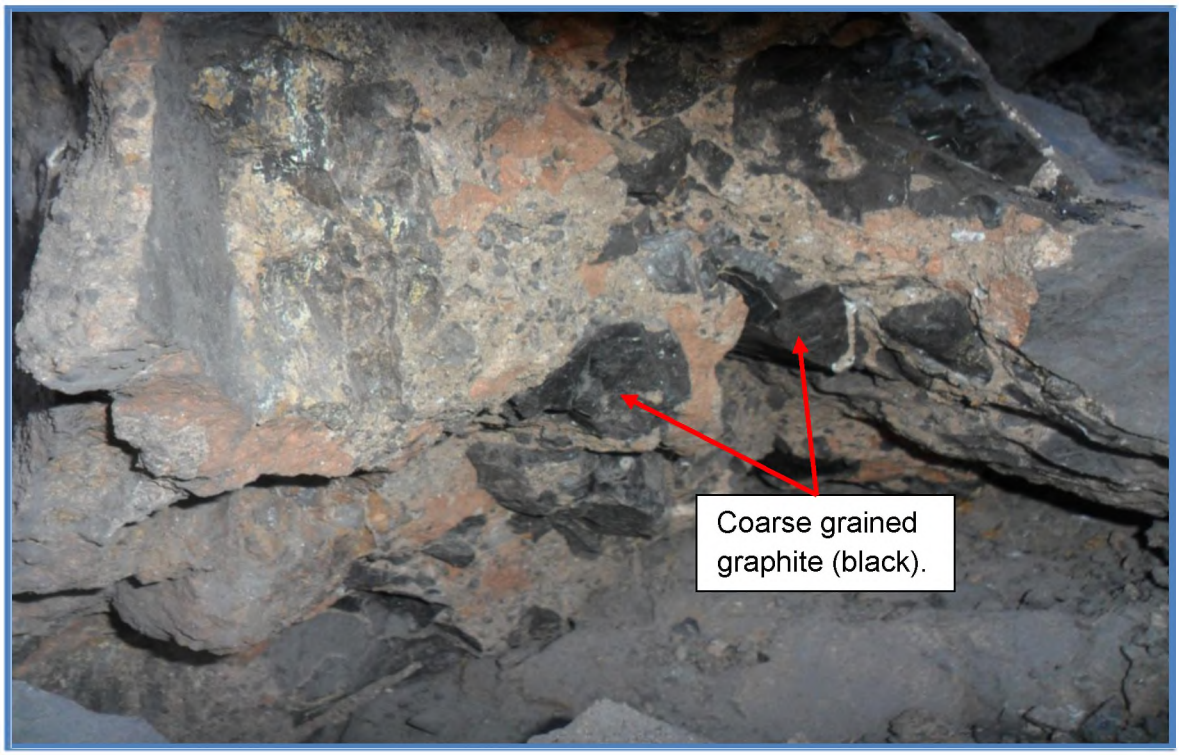

Figure 4.1.0 Evidence of intense brecciation as shown by the coarse grained graphite. The presence of graphite signifies high grade metamorphism in the main structure as result of high temperature and pressure.

The mineralogy of the fault is important to investigate and understand as it is the source of new elements into the pre-existing system. Understanding its mineralogy helps to find how various elements have been distributed across the profile on both the left and right sides when emplacement took place. The main minerals from the fault are summarized in the Table 4.1. The major elements shown in Table 4.1 had interaction with the pre-existing braunite-carbonate rich manganese ore. The mobility/immobility of these elements caused replacement and alteration resulting in new minerals being formed. The new minerals formed were also dependant on the existing conditions present in the environment such as pressure, temperature and oxidation/reduction agents. The distribution of different elements across the section is also affected by faulting and folding as will be described in further detail towards the end of this chapter.

Metasomatism is illustrated by the isocon diagrams which show the behavior of these elements across the section and will result in the 3 processes (1) redistribution (2) enrichment and (3) depletion as already discussed.

4.3. Isocon applications: left side

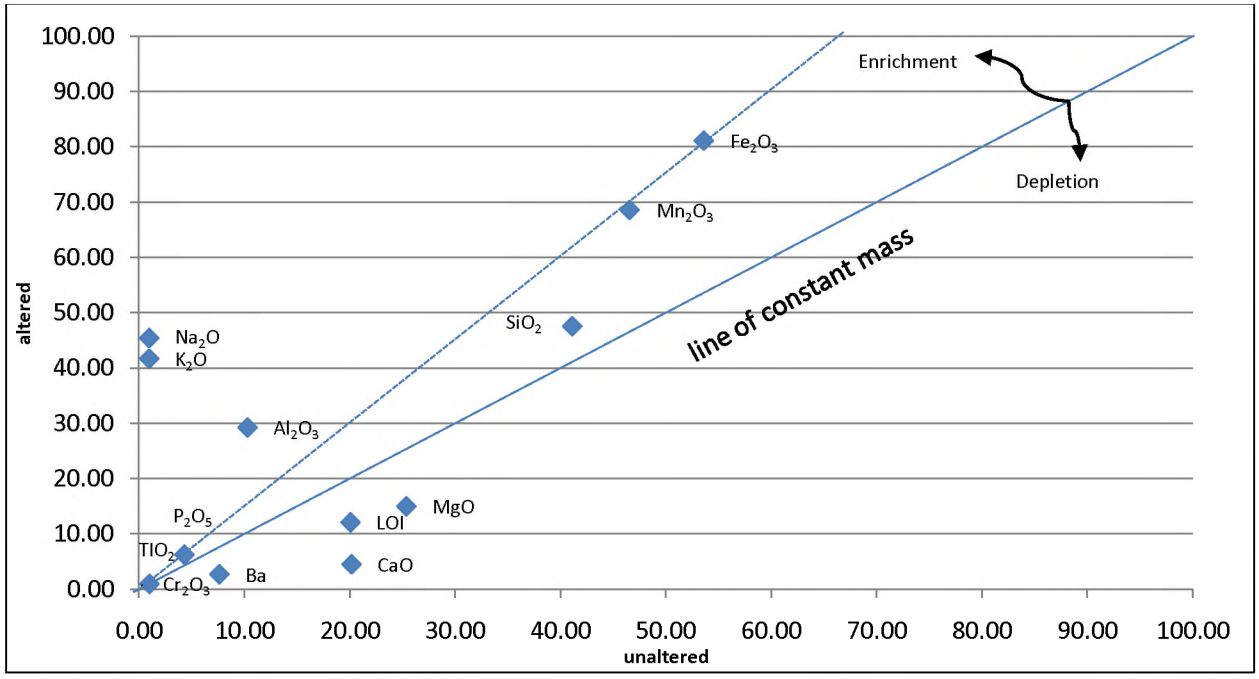

Figure 4.1.1: Isocon map showing the behavior of oxides on the left side.

The protolith or the unaltered samples are represented by the average of the 3 distal unaltered samples which are RW14, RW15 and RW16. Cr_2O_3 is immobile throughout the alteration process and it defines the line of constant mass. All elements plotting above this line represent enrichment and elements which plot below the line represent depletion. The isocon is defined by elements Fe_2O_3, Mn_2O_3 and TiO_2 on the left side of the main structure.

4.3.1. Mass balance calculations

Where C^O_I is the average composition of the unaltered ore, C^A_I is the average composition of the altered ore, C_X is the mass factor (the number of by which the total mass of the unaltered ore should be multiplied to result in the mass of the altered ore), C^O_F is the mass gain or loss from the line of constant mass represented by 1, C^F_X is C^O_F/C_X expressed as a percentage.

Component	Least altered C^O_I	Most altered C^A_I	Slope to data point C^A_I/C^O_I (C_X)	Gain/loss C^O_F	Percentage composition change C^F_X	Gain/loss in wt %
SiO_2	4.11	6.21	1.51	0.51	33.78	2.10
Al_2O_3	0.10	0.56	5.38	4.38	81.47	0.45
Fe_2O_3	5.36	9.69	1.81	0.81	44.78	4.33
CaO	20.20	9.41	0.47	-0.47	-100.94	-10.79
Na_2O	0.01	0.41	41.00	41.00	100.00	0.40
K_2O	0.01	0.38	38.44	38.44	99.99	0.37
P_2O_5	0.04	0.05	1.18	0.18	15.26	0.01
Mn_2O_3	46.58	56.93	1.22	0.22	18.00	10.35
MgO	2.54	1.57	0.62	-0.38	-61.52	-0.97
TiO_2	0.01	0.03	3.00	2.00	66.67	0.02
Cr_2O_3	0.01	0.01	1.00	0.00	0.00	0.00
Ba	0.08	0.04	0.57	-0.43	-76.08	-0.03
LOI	20.08	15.17	0.76	-0.24	-31.77	-4.91

Table 4.2: Mass balance determinations for the left side.

4.3.2. Chemical redistribution

The source of MgO is dolomite from the fault which is redistributed to form todorokite where Mg^{2+} is the major constituent in the mineral todorokite. Todorokite is the major indicator mineral for intense alteration and it is a major constituent in the alteration zone. SiO_2 is also redistributed from the main structure as quartz and some of the Si forms braunite the main manganese mineral as shown in Figure 4.1.1 which controls the grade on the left side of the fault, apart from the fissures LSW3 and LSW6 which are high in quartz is present in quantities of less than 10% composition.

4.3.3. Net enrichments

From the isocon in figure 4.1.1 and Table 4.2 respectively, K_2O and Na_2O represent the compounds with the most enrichment of over 100%. These elements contribute to the formation of manganomelane and todorokite. Manganomelane has a Na rich variety and a K rich variety which are manjiorite and cryptomelane respectively. Intense chlorite alteration is shown by the high content of Al_2O_3 which is 81%.

There is a 45% enrichment of Fe_2O_3 because of the replacement of manganomelane and also the small fissures LSW3 and LSW6 have been further enriched by Fe_2O_3 due to the reactivation and remobilization of fluids.

4.3.4. Net depletions

CaO is the main compound to be depleted on the left side as shown in Table 4.2; its mass loss is over 100%. It is depleted as to the enrichment of Mn_2O_3 as shown in figure 4.1.1. MgO is also depleted because the main mineral which influences its content is kutnohorite which is relatively associated with the unaltered ore. (Gutzmer, Beukes; 1996) suggests that the depletion of Ba could show that the alteration occurred under reducing conditions under considerable amounts of H_2S and CO_2 present, as shown by the decrease of 76%.

4.4. Isocon applications: right side, most altered samples

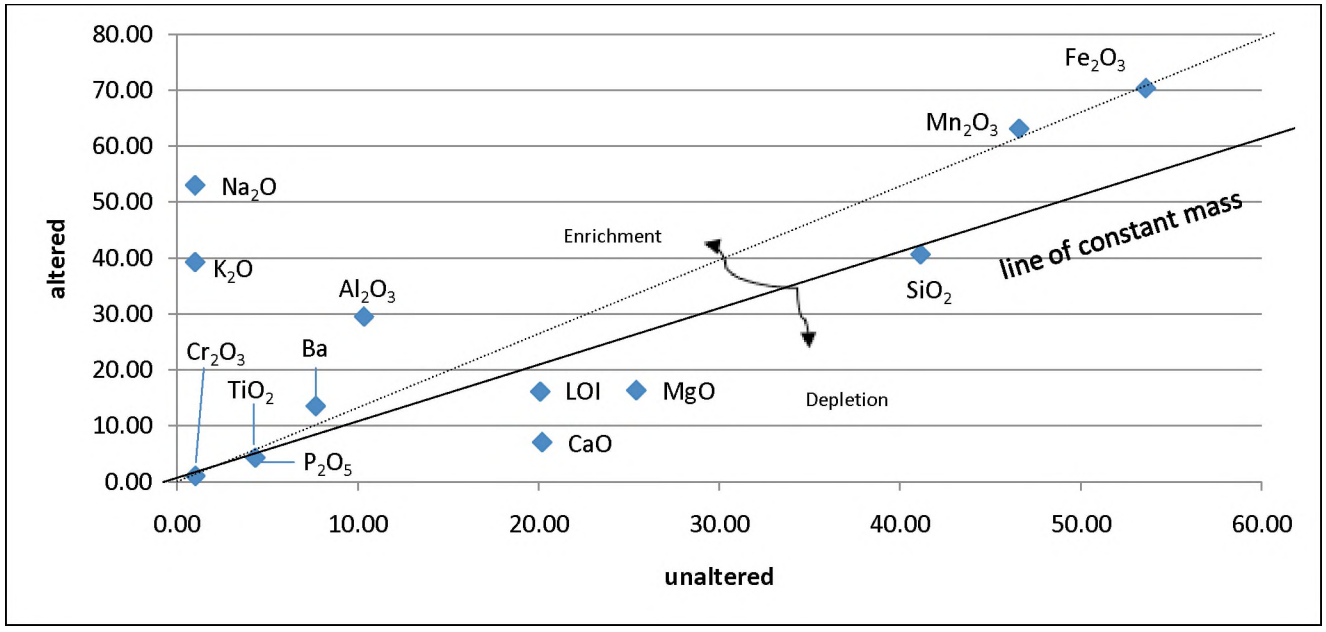

Figure 4.1.2: Isocon map showing the behavior of oxides on the right side immediately after the main structure.

The line of constant mass is defined by immobile elements P_2O_5, Cr_2O_3 and SiO_2. The isocon is defined by the oxides Mn_2O_3 and Fe_2O_3.

The isocon diagram in figure 4.1.2 is derived from samples RW1, RW2, RW3 and RW4 on the right side which are adjacent to the main structure and represent the most altered samples on the right side. The protolith or the unaltered ore is the average of the 3 distal samples which are RW14, RW15 and RW16.

Component	Least altered C^{O}_{I}	Most altered C^{A}_{I}	Slope to data point C^{A}_{I}/C^{O}_{I} (C_X)	Gain/loss relative to C^{O}_{I}	Percentage composition change C^{F}_{X}	Gain/loss in wt %
SiO_2	4.11	4.07	0.99	-0.01	-1.13	-0.05
Al_2O_3	0.10	0.30	2.85	1.85	64.97	0.19
Fe_2O_3	5.36	7.04	1.31	0.31	23.86	1.68
CaO	20.20	7.01	0.35	-0.65	-188.06	-13.19
Na_2O	0.01	0.53	53.00	53.00	98.11	0.52
K_2O	0.01	0.39	39.25	38.25	97.45	0.38
P_2O_5	0.04	0.04	1.00	0.00	1.96	0.00
Mn_2O_3	46.58	63.13	1.36	0.36	26.22	16.55
MgO	2.54	1.64	0.64	-0.36	-55.35	-0.91
TiO_2	0.01	0.01	1.00	0.00	0.00	0.00
Cr_2O_3	0.01	0.01	1.00	0.00	0.00	0.00
Ba	0.08	0.14	1.76	0.76	43.21	0.06
LOI	20.08	16.08	0.80	-0.20	-24.88	-4.00

Table 4.3: Mass balance determinations for the right side, most altered samples.

4.4.1. Chemical redistribution

The presence of low braunite after the main structure is justified by the low SiO_2 content shown by the above table. The SiO_2 is initially present as quartz because of the influence of quartz and it is further redistributed to form the mineral braunite as shown from sample RW3. The first two samples (RW1 and RW2) after the main structure are entirely secondary manganese oxide minerals and devoid of braunite. Mg present from the fault through the mineral dolomite is also redistributed from dolomite to form major constituent in the mineral todorokite.

4.4.2. Net enrichments

There is a 43% enrichment of Ba^{2+} which is present in minerals romanechite and manganomelane shown by Table 4.3.

Similarly from the first isocon as shown in Figure 4.1.1 and Table 4.2 respectively K_2O and Na_2O represent the compounds with the most enrichment. The source of Al_2O_3 is as a result of chlorite alteration, as the intensity of alteration and replacement increases the presence of chlorite increases resulting in more enrichment of Al_2O_3.

Due to its proximity to the main structure there is an 8% increase in the overall grade of Mn_2O_3 from the grade on the left side. This is backed by the evidence in Chapter 3 Figure 3.1.0 diagram E.

4.4.3. Net depletions

MgO is depleted at the expense of todorokite. CaO is depleted by a further mass loss of 88% from the previous section as shown in Tables 4.2 and 4.3 respectively. CaO is replenished at the expense of Mn_2O_3 due to the intense alteration. The CaO is represented as calcite and dolomite.

4.5. Isocon applications: right side, approaching unaltered ore

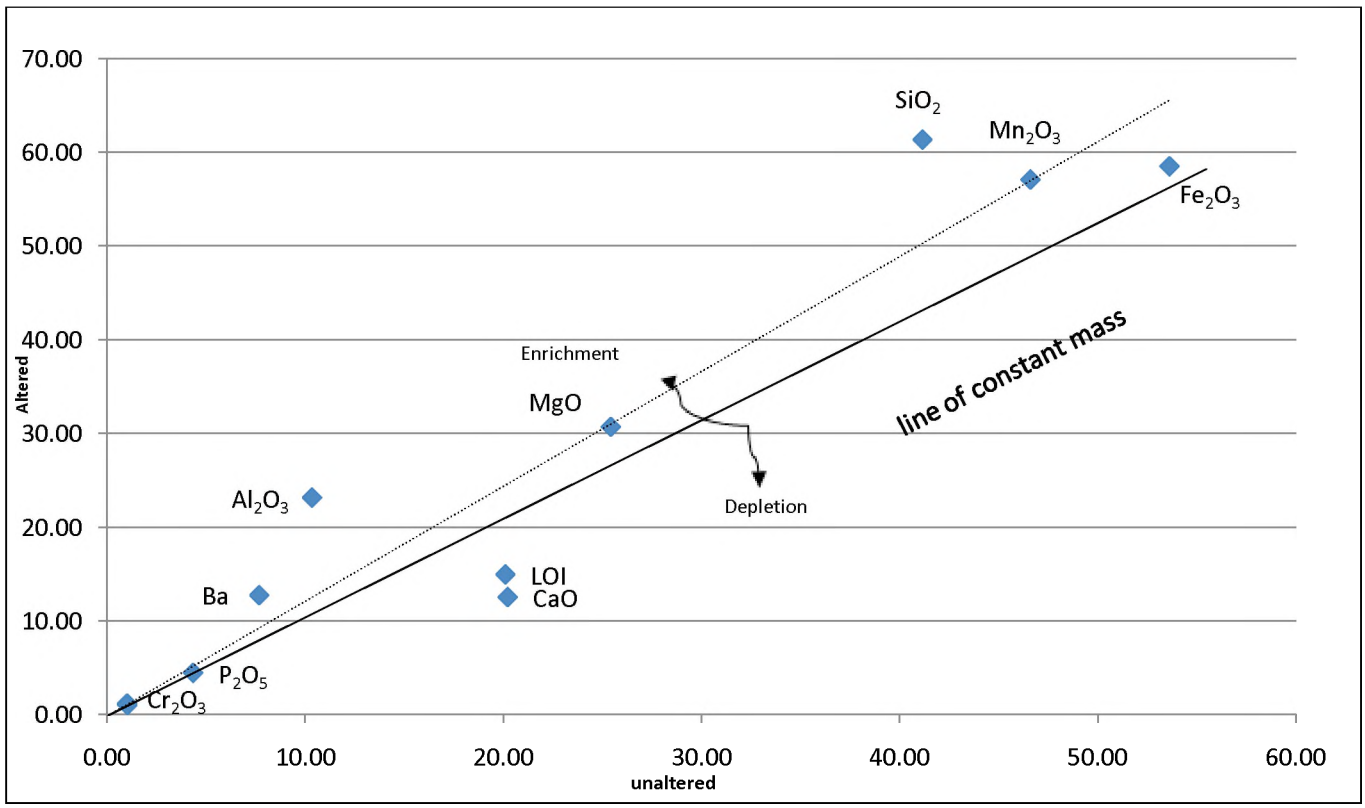

Figure 4.1.3: Isocon map showing the behavior of oxides on the right side from fissure RW6 to the unaltered ore.

The line of constant mass is defined by the immobile elements P_2O_5, Cr_2O_3, TiO_2, K_2O and Na_2O. The isocon is defined by the oxides of Mn_2O_3, MgO, TiO_2, Na_2O and K_2O. The altered samples shown in Figure 4.1.3 are represented by samples RW6, RW7, RW8, RW9, RW10, RW11 and RW12.

These were plotted against the unaltered samples of RW14, RW15 and RW16. These samples are altered by less but not as intense as the samples close to the main structure. The matrix of these samples significantly changes from a manganomelane matrix rich to a carbonate – kutnohorite rich matrix as shown in Chapter 2 Figure 2.2.7.

Component	Least altered C^O_I	Most altered C^A_I	Slope to data point C^A_I/C^O_I (C_X)	Gain/loss relative to C^O_I	Percentage composition change C^F_X	Gain/loss in wt %
SiO_2	4.11	6.13	1.49	0.49	32.86	2.02
Al_2O_3	0.10	0.23	2.24	1.24	56.52	0.13
Fe_2O_3	5.36	5.85	1.09	0.09	8.25	0.49
CaO	20.20	12.51	0.62	-0.38	-61.35	-7.69
Na_2O	0.01	0.01	1.14	0.14	0	0.00
K_2O	0.01	0.01	1.00	0.00	0	0.00
P_2O_5	0.04	0.04	1.02	0.02	0	0.00
Mn_2O_3	46.58	57.05	1.22	0.22	17.96	10.47
MgO	2.54	3.07	1.21	0.21	16.55	0.53
TiO_2	0.01	0.01	1.00	0.00	0	0.00
Cr_2O_3	0.01	0.01	1.00	0.00	0	0.00
Ba	0.08	0.13	1.66	0.66	36.92	0.05
LOI	20.08	14.94	0.74	-0.16	-21.50	-5.14

Table 4.4: Mass balance determinations for the right side, approaching unaltered ore.

4.5.1. Chemical redistribution

K_2O, Na_2O are present as interstitial fillings in the samples in very trace amounts. They now constitute the immobile elements as well as TiO_2, Cr_2O_3 and P_2O_5. There is not much redistribution that takes place at this part of the section.

4.5.2. Net enrichments

The biggest difference as compared to the other two isocons is the enrichment of MgO, which has a 17% increase. MgO is the oxide used to form the mineral kutnohorite.

There is a significant increase in SiO_2 of 32% as compared to samples that are close to the main structure. This shows that the mineral braunite is becoming more prevalent towards the less altered ore at the expense of secondary manganese minerals such as manganomelane and todorokite.

Chlorite alteration shows enrichment but has significantly decreased from 81% to 56%. Fe_2O_3 shows an enrichment of 8% but there is a drop of 37% from the left side due to the absence of manganomelane.

4.5.3. Net depletions

The depletion in CaO is lower at 61% as compared to the other two above which are over 100% because the manganese oxide minerals are being replaced by carbonate minerals.

4.6. Summary

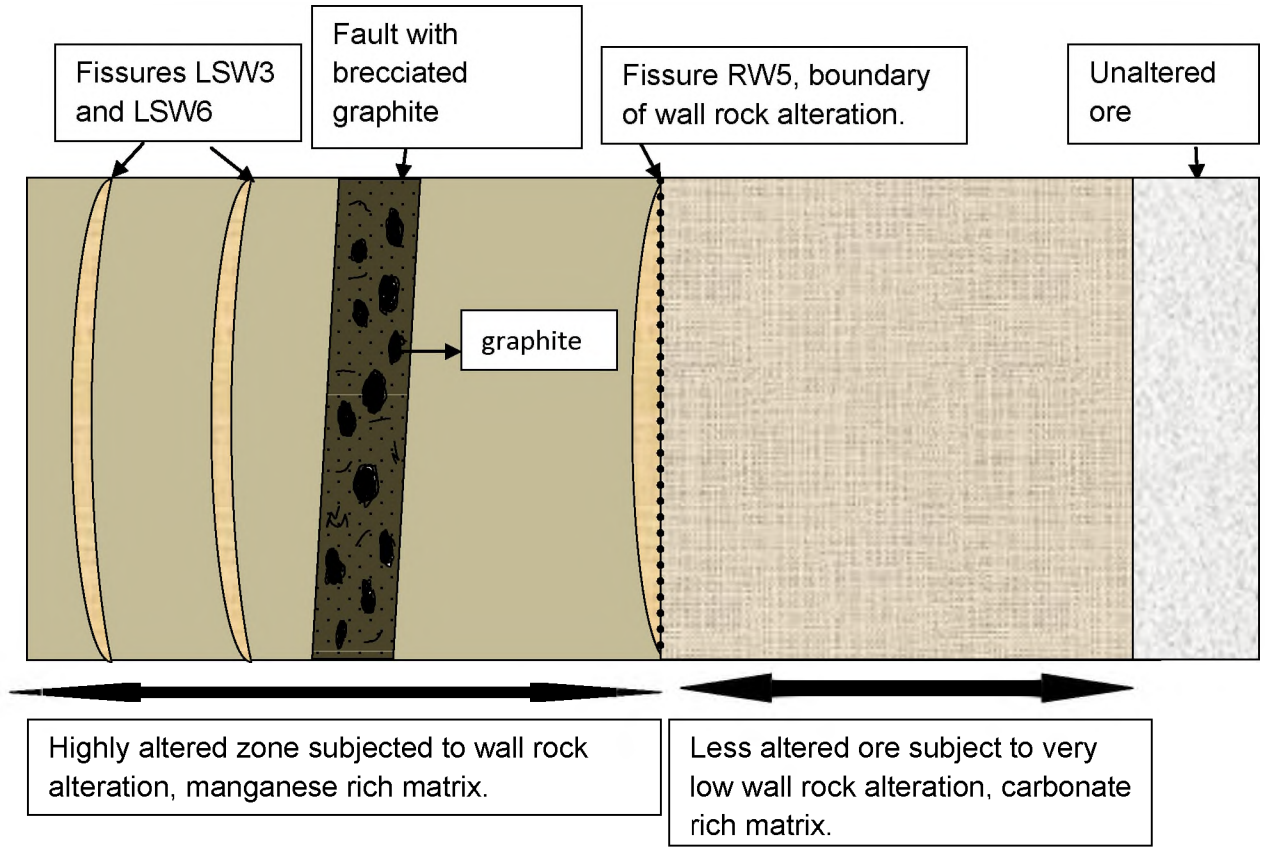

Figure 4.1.4: Section map highlighting the major conclusions of this study.

The main structure is characterized by intense brecciation and the presence of graphite. According to (Beukes, Gutzmer; 1996) they postulate that brecciation occurs under conditions of high pressure and rapid fluid flow. This high pressure was crucial in determining the extent of this wall rock alteration and in this study, the contact for this wall rock alteration is at RW5 on the right side.

CaO is directly related to wall rock alteration, Mn-rich calcites, dolomite and kutnohorite are the carbonate minerals that control the CaO content on the right side from less altered to the unaltered ore. Mn-rich calcites on the left side were only observed in the fissures LSW3 and LSW6.

K and Na are the major elements that have been the determining factors for the abrupt change in the matrix from a manganese dominated matrix to a carbonate rich matrix. These elements are synonymous with alteration and their absence from RW5 on the right side proves this.

Romanechite is present as a replacement mineral of the trace amounts of manganite, hematite and hausmannite and therefore is not directly related to wall rock alteration. This is shown by its presence in less altered ore such as RW9 which has a Ba^{2+} content as well as its low content on the left side of the main structure. As alteration increases the chlorite alteration increases, this is evidenced by Al_2O_3 which plots above the isocon line in all the isocon diagrams shown in this chapter.

Hematite and goethite are the major replacement minerals of manganomelane and therefore Fe_2O_3 enrichment is directly related to wall rock alteration as shown by the steady decrease of its content from the left side to the right side. The other Fe^{2+}/ Fe^{3+} is redistributed in the formation of minerals of jacobsite, bixbyite, chlorite, manganomelane and todorokite.

MgO is also directly related to wall rock alteration, Mg^{2+} seems to be one the most mobile elements in the zone of wall rock alteration as it redistributed from the fault as dolomite to form todorokite. This redistribution of MgO still results in its depletion both on the left side and on the most intensely altered samples on the right side.

The enrichment of MgO is directly related to the kutnohorite rich matrix from sample RW6 on the right side up to the unaltered ore. The mineral chemistry of LSW3, LSW6 and RW5 is very different from the main structure which suggests that the emplacement of these faults were separate events. These small fissures do not cause any significant wall rock alteration adjacent to the samples on either side of them, their alteration is however localized.

4.7. Recommendations

4.7.1. Effect of faulting

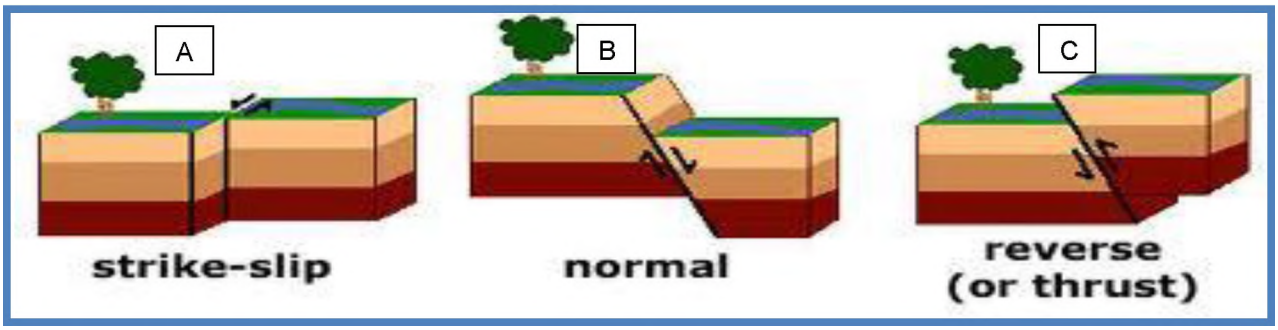

Figure 4.1.5: The different types of faults.

From the microscope images show in Figure 2.2.3 in Chapter 2, it is clear that the main structure is indeed a fault because there is evidence of displacement. However macroscopically displacement is not visible on either side of the fault, the microscopic displacement does not imply that it had no significant bearing on the grade and distribution of elements.

Geochemical analysis has shown no consistency in the grades on both the left and right sides. From Figure 4.1.5 above the faults can neither be B or C because there is no macroscopic evidence to show displacement through upward and downward dip slip movement. It is however safe to assume that displacement could have taken place across the parallel to the strike of the fault as shown by A in Figure 4.1.5 above.

When similar faults are encountered caution has to be exercised when planning for grade control as this may vary significantly on either side of the faults.

If there is no evidence to the naked eye that there is lateral displacement, it is safe to assume a strike slip movement; this can be verified by investigating parallel to the fault by either diamond drilling or channel sampling to confirm the consistency of the grades on either side of the faults.

The displacement effect of the fault also causes movement of minerals which contributes to how elements are distributed across the section as shown in Figure 2.2.9. As displacement occurs either one end of the fault gets enriched while the other end gets depleted and vice versa. A once uniformly distributed system is thus greatly disturbed by the displacement effect.

4.7.2. Effect of folding

Folding is as a result of compressional and extensional forces of the limbs. Figure 2.2.6 provides evidence of folding as shown by the "s" and "z" structures. When folding occurs this is shortening on one limb and extension on the other limb. A once uniformly distributed system is thus greatly affected by this folding as this implies that one limb that is shortened is getting enriched because of the accumulation of elements from different parts of the limb, whereas one limb that is getting extended is becoming depleted as the elements are being squeezed out through extensional forces. However this folding was not visible to the naked eye implying that the folding was at a very small scale.

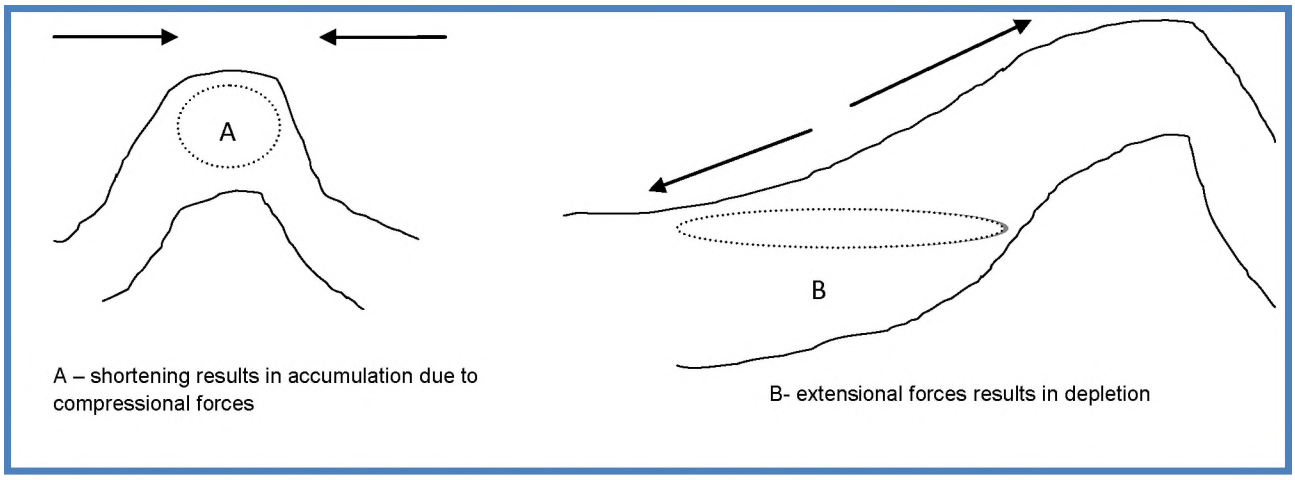

Figure 4.1.5: The distribution of elements in the system as a result of the folding in limbs A and B.

4.7.3. Grade control

For mining purposes the unaltered ore is ideally not the top priority to mine for high grades because the manganese ore minerals are being replaced by the carbonate minerals.

The reason is that as the section progresses to the unaltered ore there is continous enrichment of Mg and Ca which forms kutnohorite and calcite respectively and depletion of K and Na which are the key elements of alteration to form manganomelane and todorokite.

4.7.4. Identification in the field

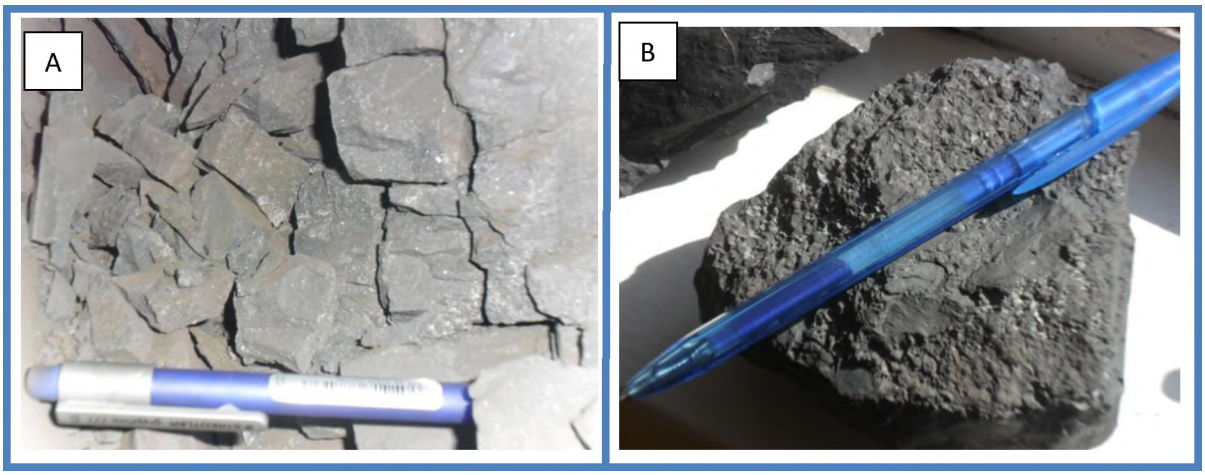

Figure 4.1.7: Two hand specimens differentiating the unaltered ore and altered ore.

From the two images above A which is dull looking and devoid of carbonate ooids is the top priority ore to mine because it is rich in manganomelane, romanechite and todorokite apart from the braunite. As shown in Table 4.2 on the left side these alteration minerals can increase the MnO grade by 18% from the unaltered ore.

Image B shows the typical braunite-lutite rich unaltered rock, the carbonate ovoids seem to replace the interstitial spaces between crystal lattices of the manganses ore.

Braunite becomes the main manganese mineral which becomes interbedded with kutnohorite and dolomite in a fine grained matrix, whereas the Mn rich calcites define the coarse grained part of the ore by the ovoids.

4.7.5. Fissures

The small fissures which are present along the profile such LSW3, LSW6 and RW5 are also microfaults to the the main fault. Figure 2.2.3 in Chapter 2 proves displacement has taken place, however these micro faults dilute the grade of the ore because they contain very low Mn values.

These small scale faults are predominantly carbonate rich with calcite and dolomite dominating the matrix as evidenced in Figure 2.2.2C. However they have a small width of 30cm - 60 cm, if high grade ore is in abundance they will have a very little effect on influencing the overall grade of the ore.

Caution has to be exercised in terms of selecting which ore to mine when these small scale faults are witnessed in the field. As already discussed these micro faults do not cause wall rock alteration on either side and therefore will not cause much bearing in influencing the overall grade of Mn_2O_3. As the ore changes from unaltered ore to altered ore, the mineralogy of the unaltered ore is supposed to consist of braunite II but braunite II was not observed under the microscope. However it is also a major mineral constituent of the unaltered ore in association with Mn rich calcites, kutnohorite and dolomite and braunite.

4.8. The 'SMARTT' event

The Smartt event was named after Smartt Mine which is located approximately 7 km north of Mamatwan Mine on the southern part of the KMF by Gutzmer and Beukes (1996). They described it as the final process which is preceded by the Mamatwan alteration event. Based on the $^{40}Ar/^{39}Ar$ geochronology of the asbestiform manjiroite – todorokite found at Smartt Mine it is believed to have occurred between 35 – 40 Ma ago.

This event involved overprinting of manganese ores along joints and faults as a result of supergene alteration along the unconformity below the Kalahari Formation. These joints and faults were completely altered by ascending low temperature fluids.

The source of the low temperature fluids is postulated to be ground water of a very low temperature. This event is described as being specific to the Southern and Eastern parts of the KMF.

The Mamatwan alteration event is a pre-Karoo process which occurred between 0.55 - 0.60 Ga associated with hydrothermal alteration which is fault controlled and caused reduction and bleaching of the unaltered braunite- carbonate rich manganese ore along these structures.

This event is evidently shown by its exposure through erosional processes through the Hotazel formation which is preceded by the deposition of the KMF. This process is associated with infiltration of fluids which caused brecciation and fracturing along the faults caused by hydrostatic pressure from meteoric waters.

The Smartt Event is described as a process of hydrothermal alteration which is shown by the alteration minerals such as todorkite and manganomelane which replace the typical unaltered ore comprised of Mn-rich calcites, kutnohorite, hausmannite and braunite.

4.9. Conclusions

This study is related to the Smartt Event as summarized in the table below:

Smartt Event	**Study Area**
The event was specifically limited to the Southern and Eastern parts of the KMF.	Mamatwan Mine is located in the Southernmost tip of the KMF.
The event is associated with bleaching and reduction of ores.	Wall rock alteration is evidence of bleached ore and there is reduction of ore.
The event is associated with intense fracturing	The section is associated by intense fracturing which are related to the faults.
The event is characterized by replacement of Mn rich carbonates and braunite by todorokite and manganomelane.	Todorokite and manganomelane are the main alteration minerals that replace the unaltered braunite-carbonate rich ore.
Infiltration of fluids and hydrostatic pressure from meteoric fluids caused brecciation of the fault.	As shown in Figure 4.1.0 graphite within the main fault is brecciated. Graphite is an index mineral of high grade metamorphism which is associated with high pressure.

Table 4.5: Similarities of the study area and the Smartt Event.

This study is a typical example of a faulted (presumably strike slip) and folded block subject to wall rock alteration caused by the Smartt Event in which the metasomatic alteration caused redistribution, enrichment and depletion of various elements within the bleached zone in comparison to the unaltered braunite-carbonate rich ore.

REFERENCES

100th Anniversary Special Paper: Sedimentary Mineral Deposits and the Evolution of the Earth's Near- Surface Environments Economic Geology 2005, 100: 1489 – 1509.

Asbestiform manjiroite and todorokite from the Kalahari manganese field, South Africa, South African Journal of Geology 2000, 103: 163 – 174.

A sugilite- bearing assemblage from the Wolhaarkop breccias, Bruce iron-ore mine, South Africa: Evidence for alkali metasomatism and 40 Ar- 39 Ar dating, Eur J Mineral 2011, 23: 661 – 673.

Beukes, N.J. (1983). Palaeoenvironmental setting of iron formations in the depositional basin of the Transvaal Supergroup, South Africa. In: Trendall, A.F., and Morris, R.C (eds). Iron formations, facts and problems, Elsevier, Amsterdam, 131 - 209.

Beukes, N.J. (1986). Sedimentology and its application. Volume **173**, Rand Afrikaans University, 24 pp.

Beukes, N.J., Kleyenstüber, A.S.E., and Nel, C.J. (1982). Volcanogenic - sedimentary cycles in the Kalahari manganese field. Sedimentology' **82**, Geol.Soc. S.Afr. Extended Abstracts, 93 - 97.

Beukes, N.J., Burger, A.M & Gutzmer,J. (1995). Fault-controlled hydrothermal alteration of Palaeoproterozoic manganese ore in Wessels mine, Kalahari manganese field, South Africa. S.Afr.J., Geol., **98**,430 - 451.

Beukes, N.J., Smith, A. (1987). New evidence for thrust faulting in Griqualand West, South Africa. Implications for stratigraphy and the age of redbeds. Trans.Geol.Soc. S.Afri, **90**: 378 - 394.

Burger, A.M. (1994). Fault controlled hydrothermal alteration of Palaeoproterozoic manganese ore in Wessels mine, Kalahari manganese field. M.Sc. thesis (unpubl.) Rand Afrikaans Univ., Johannesburg, 138 pp.

Cheney E.S, Winter H. de la . (1995). The Late Archaen to Mesoproterozoic major unconformity bounded units of the Kaapvaal Province of South Africa. Precam. Res., **74**, 204 - 223.

Cornell, D.H., Schütte, S.S. (1995). A volcanic - exhalative origin for the world's largest (Kalahari) - manganese field. Mineral. Depos., **30**, 146 - 151.

Deposition, Diagenesis and Secondary Enrichment of Metals in the Paleoproterozoic Hotazel Iron Formation.

Depositional environment and lithostratigrpahy of the Paleoproterozoic Mooidraai formation, Kalahari Manganese field, South Africa. South African Journal of Geology 2014, 117: 173 -192.

De Villiers, J. (1960). Manganese deposits of the Union of South Africa. Handbook 2, Geol. Surv. S.Afr., Pretoria, 280 pp.

De Villiers, J.E (1983). The manganese deposits of Griqualand West, South Africa: Some mineralogical aspects. Econ. Geol., **78**: 1108 -1118.

De Villers, J.E. (1943). A preliminary description of the new mineral patridgeite, Am . Mineral., **28**, 336 - 338.

De Villers, P.R. (1970). The geology and mineralogy of the Kalahari manganese field, north of Sishen, Cape Province. Mem.geol.Surv. S.Afr., **59**, 84 pp.

De Villiers, P.R., Visser, J.N.J. (1977). The glacial beds of the Griqualand West Supergroup as revealed by four deep boreholes between Postmasburg and Sishen. Trans.Geol. Soc. S.Afri., **80**: 1 - 8.

Dixon,R.D.(1989). Sugilite and associated metamorphic silicate minerals from Wessels mine, Kalahari manganese field. Mem.geol.Surv.S.Afr., **93,** 47pp.

Fournier, R.O. (1986). Geology and geochemistry of epithermal systems. Reviews in economic geology, **vol 2**, Society of Economic Geologists.

Fractionation of manganese from iron in Archaen and Proterozoic sedimentary ores; Geological Society, London, Special Publications 1997, 119: 29 – 42.

Frenzel, G. (1980). The manganese ore minerals,In: Varentsov, I.M.& rasselly,G.(Eds.), Geology and Geochemistry of Manganese. Schweizerbart'sche Verlagsbuchhandlung, Stuttgart, **1**, 125 - 127.

Grant, J.A. (1986). The Isocon Diagram - A Simple Solution to Gresens' Equation for Metasomatic Alteration. Econ. Geol., **81**, 1976 - 1982.

Grant, J. A. (2005). Isocon analysis : A brief review of the method and applications. Physics and Chemistry of the Earth., **30**, 997 - 1004.

Gresens, R.L. (1967). Composition - volume relationships of metasomatism. Chem. Geology**, v.2**, p 47 – 55.

Gutzmer, J. (1993). Hydrothermal Alteration von Manganerzen der Nchwaning - Mine, Kalahari Manganerzfeld , Südafrika. Diploma thesis (unpubl.) Technische Universitä t Clausthal, 161 pp.

Gutzmer, J. (1996). Genesis and alteration of the Kalahari and Postmasburg manganese deposits, Griqualand west, South Africa. P.hD. thesis (unpubl.) Rand Afrikaans Univ., Johannesburg, 474 pp.

Gutzmer, J., Beukes, N.J. (1995). Hydrothermal alteration and ferruginization of sedimentary manganese ore at Nchwaning Mine, Kalahari manganese field, Early Proterozoic Transvaal Supergroup, South Africa. Econ. Geol., **90**, 823 - 844.

Gutzmer, J., Beukes, N.J. (1996). Mineral paragenesis of the Kalahari manganese field, South Africa. Ore Geology reviews, **11**, 405 - 428.

Gutzmer, J., Kleyenstüber, A.S.E., Beukes, N.J.& Burger, A.M.(1995). Magnetic hausmannite from hydrothermally altered manganese ore in the Palaeoproterozoic Kalahari manganese deposit, Transvaal Supergroup, South Africa. Min.Mag., **57**, 703 - 706.

Gutzmer, N.J Beukes, H.-W. Yeh. (1997). Fault-controlled metasomatic alteration of Early Proterozoic sedimentary manganese ore at Mamatwan mine, Kalahari manganese field, South Africa. S.Afr.J., Geol.,1997,**100**, 53 - 71.

James, Craig.R (1940). Ore Microscopy and Ore Petrography. Second Edition, New York et al: J Wiley and sons, c 1994, 424 pp.

Jawed, T., Siddiquie, F.N. (2014). Mineragraphic Study of Manganese Ore Deposits of Kandri, Mansar, Beldongri and Satak Mines, Nagpur District (Maharashtra) Central India. International Journal of Geosciences, **5**, 710 - 727.

Khorshinskij, D.S (1970). Theory of metasomatic zoning. Oxford, Claredon Press, 162 pp.

Kleyenstüber, A.S.E (1984). The mineralogy of the manganese bearing Hotazel Foramtion, of the Proterozoic Transvaal Sequence in Griqualand West, South Africa. Trans.geo.Soc.S.Afr., **87**, 257 - 272.

Kleyenstüber, A.S.E (1985). A regional mineralogical study of the manganese bearing Voëlwater Subgroup in the Northern Cape Province . Ph.D thesis (unpubl.), Rand Afrikaans Univ., Johannesburg, 328 pp.

Kleyenstüber, A.S.E (1993). Some significant characteristics of the manganese ores and some of the minerals occurring in the Proterozoic Kalahari manganese field, South Africa, Resource Geol., **17**, 2 -11.

Martini,J.E.J., Eriksson, P.G.& Snyman, C.P.(1995). The Early Proterozoic Mississipi Valley-type-Pb-Zn-F-deposits of the Campbellrand and Malmani Subgroups, South Africa. Min,Depos., **30**, 135 - 145.

Nel, C.J. (1984). Die mineralogie en geochemie van die Mamatwanertsliggam, Kalaharimangaanveld, Transvaal – Supergroep. M.Sc. thesis (unpubl.), Rand Afrikaans Univ., Johannesburg, 119 pp.

Nel, C.J., Beukes, N.J., & De Villiers, J.P.R.(1986). The Mamatwan manganese mine of the Kalahari Manganese field. In : Anhaeusser, C.R., Maske, S., (eds.), Mineral deposits of Southern Africa. Geol. Soc. S.Afri., Johannesburg, **1**, 963 – 978.

Nicholson, K. (1992). Contrasting mineralogical – geochemical signatures of manganese oxides: Guides to metallogenesis. Econ. Geol., **87**, 1253 – 1264.

Paleomagnetic Constraints on Ages of Mineralization in the Kalahari Manganese Field, South Africa; Economic Geology 2001, 96: 621 – 631.

Prehnite from the Kalahari Manganese Field, South Africa, and its possible implications; South African Journal of Geology 2000, 103: 231 – 236.

Preston, R.C.C.P. (2001). Physical and chemical characterization of the manganese ore bed at the Mamatwan Mine, Kalahari Manganese Field. M.Sc. thesis (unpubl.), Rand Afrikaans Univ., Johannesburg, 135 pp.

SAMANCOR, (1993). Welcome to Mamatwan mine. SAMANCOR, Johannesburg, 17 pp.

SAMANCOR, (1994). Brochure describing the manganese and iron interests of the Samancor Group of Companies. SAMANCOR, Johannesburg, 6 pp.

Schütte, S.S (1992). Ongeluk Volcanism in Relation to the Kalahari Manganese Deposits. P.hD.(unpubl) University of Natal, 510 pp.

Söhnge, P.G. (1977). Timing aspects of the manganese deposits of the Northern Cape Province, South Africa. In: Klemn D.D., and Schneider, H.J. (eds.): Time and strata – bound ore deposits, 115 - 122.

Taljaardt, J.J. (1982). Major manganese ore fields, Republic of South Africa. (Unpubl.) SAMANCOR, Johannesburg, 7 pp.

The chemostratigraphy of a Paleoproterozoic MnF- BIF succession the Voelwater Subgroup of the Transvaal Supergroup in Griqualand West, South Africa. South African Journal of Geology 2006, 109: 63 – 80.

Tsikos, H. (1994). The mineralogy and geochemistry of the Voëlwater banded iron - formation, Northern Cape Province. M.Sc (unpubl.), Rhodes University.,190 pp.

Tsikos, H., Moore, J.M. (1997). Petrography and Geochemistry of the Paleoproterozoic Hotazel Iron Formation, Kalahari Manganese Field, South Africa: Implications for Precambrian manganese metallogenesis. Econo. Geol, **92**, 87 - 97.

Tsikos, H., Moore, J.M. (1998). The Kalahari Manganese Field: An enigmatic association of iron and managanese. South African Journal of Geology, **101**, 287 - 290.

Tsikos, H. (1999). Petrographic and Geochemical constraints on the origin and post depositional history of the Hotazel iron - manganese deposits, Kalahari manganese field, South Africa. P.hD. (unpubl.) Rhodes University, 189 pp.

Tsikos, H., Moore, J.M & Harris, C. (2003). Deposition, Diagenesis and Secondary Enrichment of Metals in the Paleoproterozoic Hotazel Iron Formation, Kalahari Manganese Field, South Africa. Econ.Geol., **98**, 1449 - 1462.

National Academies, (1981). Manganese Reserves and Resources of the World. Washington DC, USA, p 334.

Visser, J. N. J, (1971). The deposition of the Griquatown glacial member in the Transvaal Supergroup. Trans. Geol. Soc. S.Afr., **74**, 187 - 199.

Zheng, Y.F & Hoefs, J. (1993). Carbon and oxygen isotopic covariations in hydrothermal calcites. Min. Depos., **28**, 78 - 89.

APPENDICES

Part A: Composition Maps.

Analysis was carried out for the following elements Si, Mg, Na, K, Al, Fe, Ca and Al.

A.1.1. LSW1

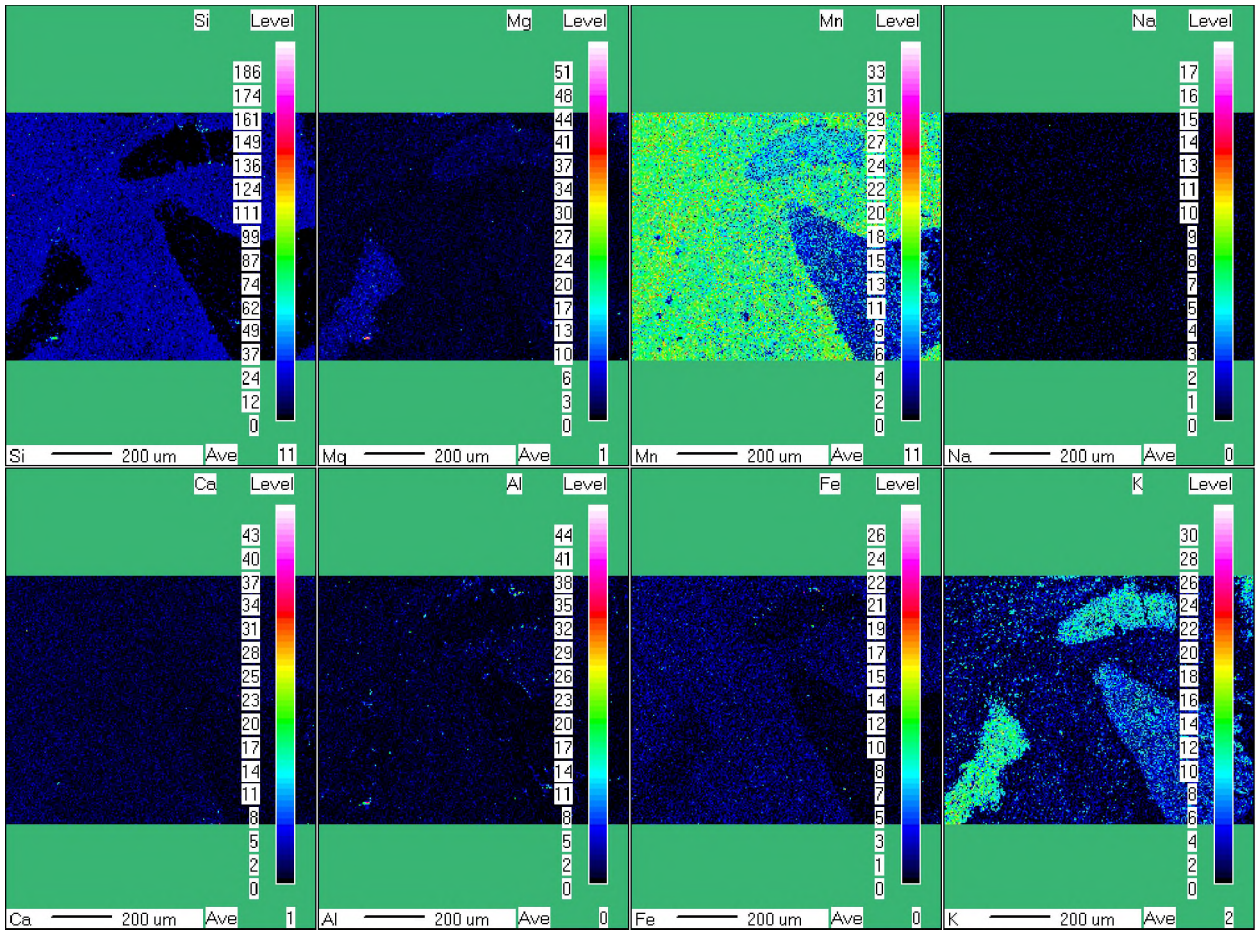

EMPA scan of a thin section from sample LSW1 showing the composition of different elements.

A.1.2. LSW2

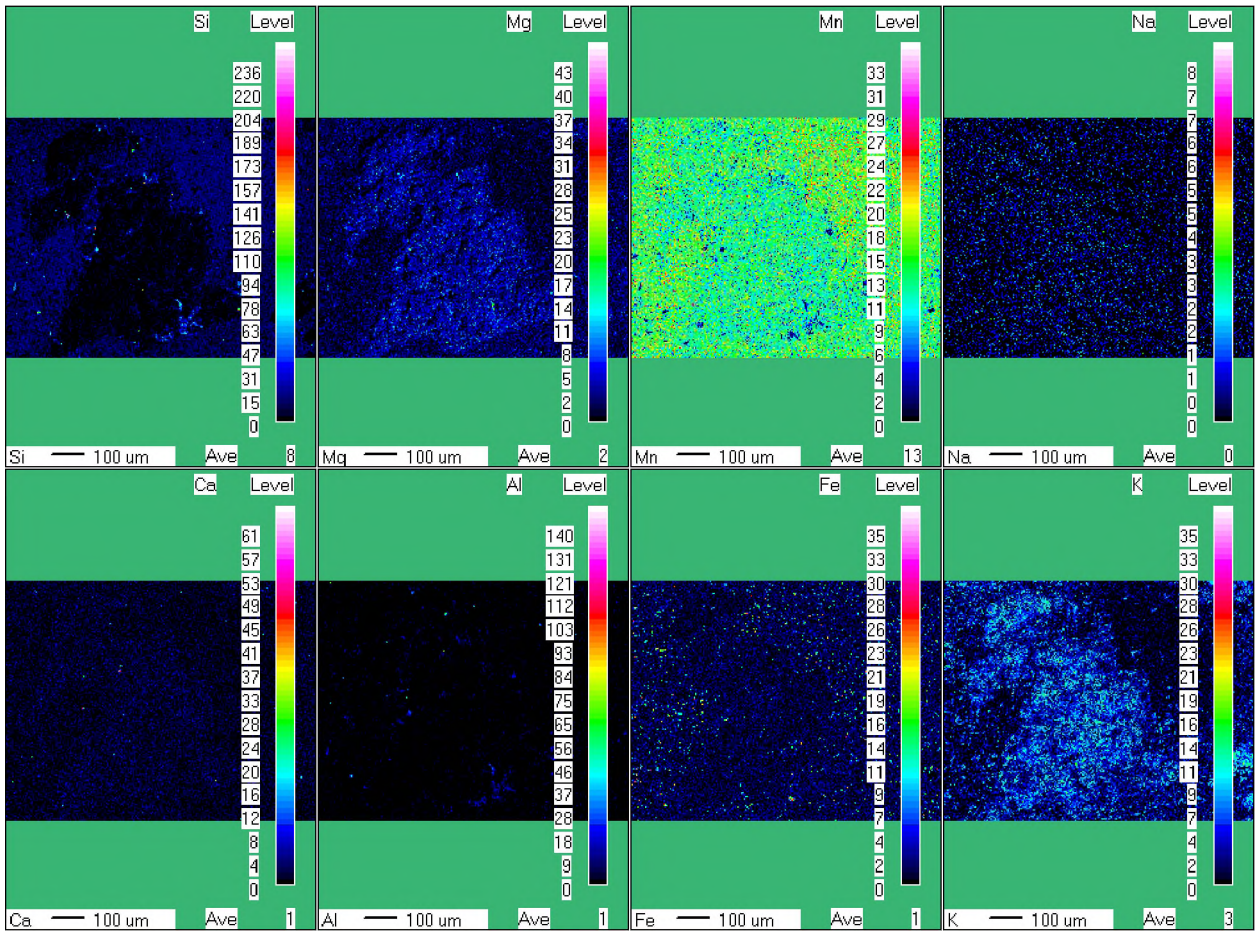

EMPA scan of a thin section from sample LSW2 showing the composition of different elements.

A.1.3. LSW5A

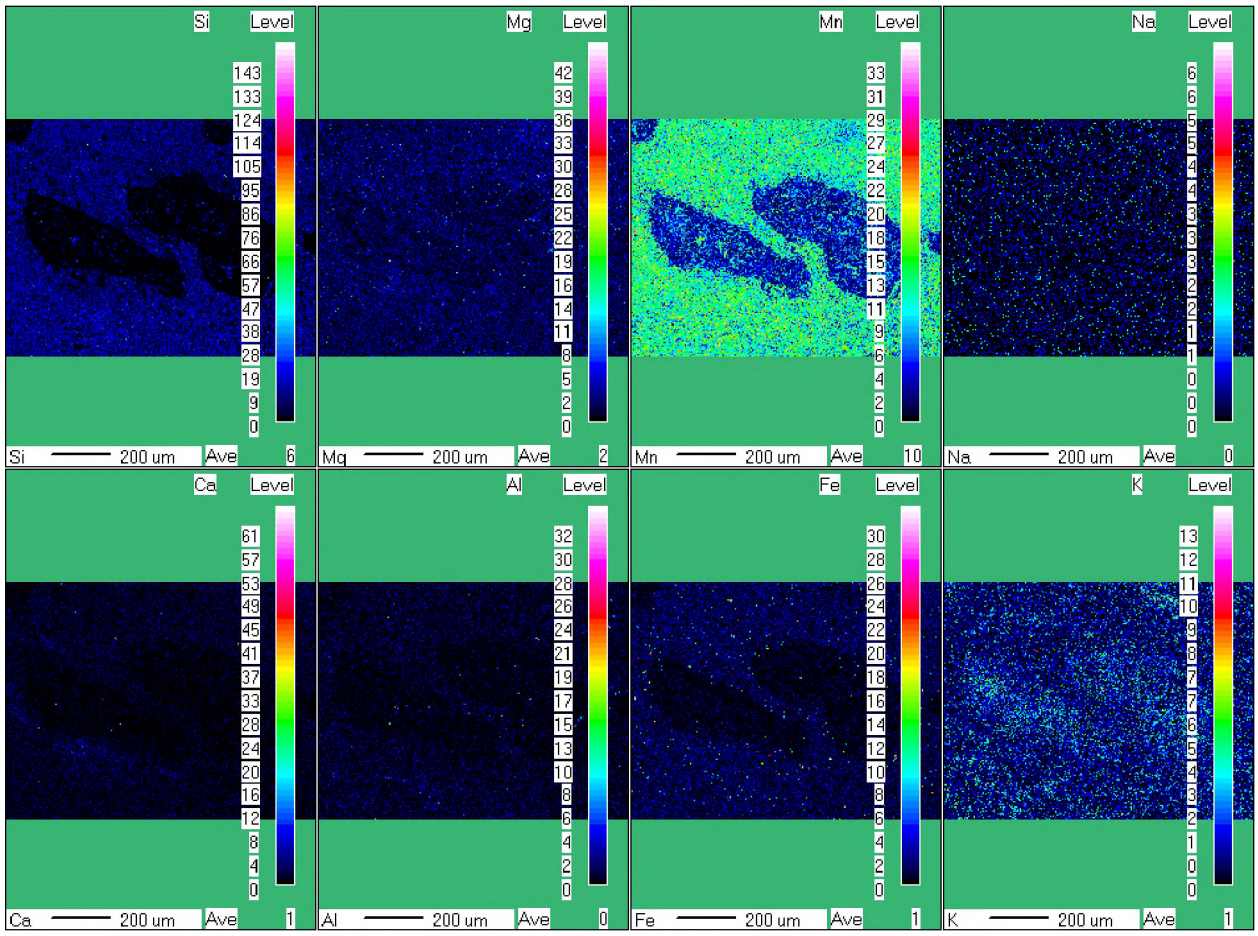

EMPA scan of a thin section from sample LSW5A showing the composition of different elements.

A.1.4. RW1

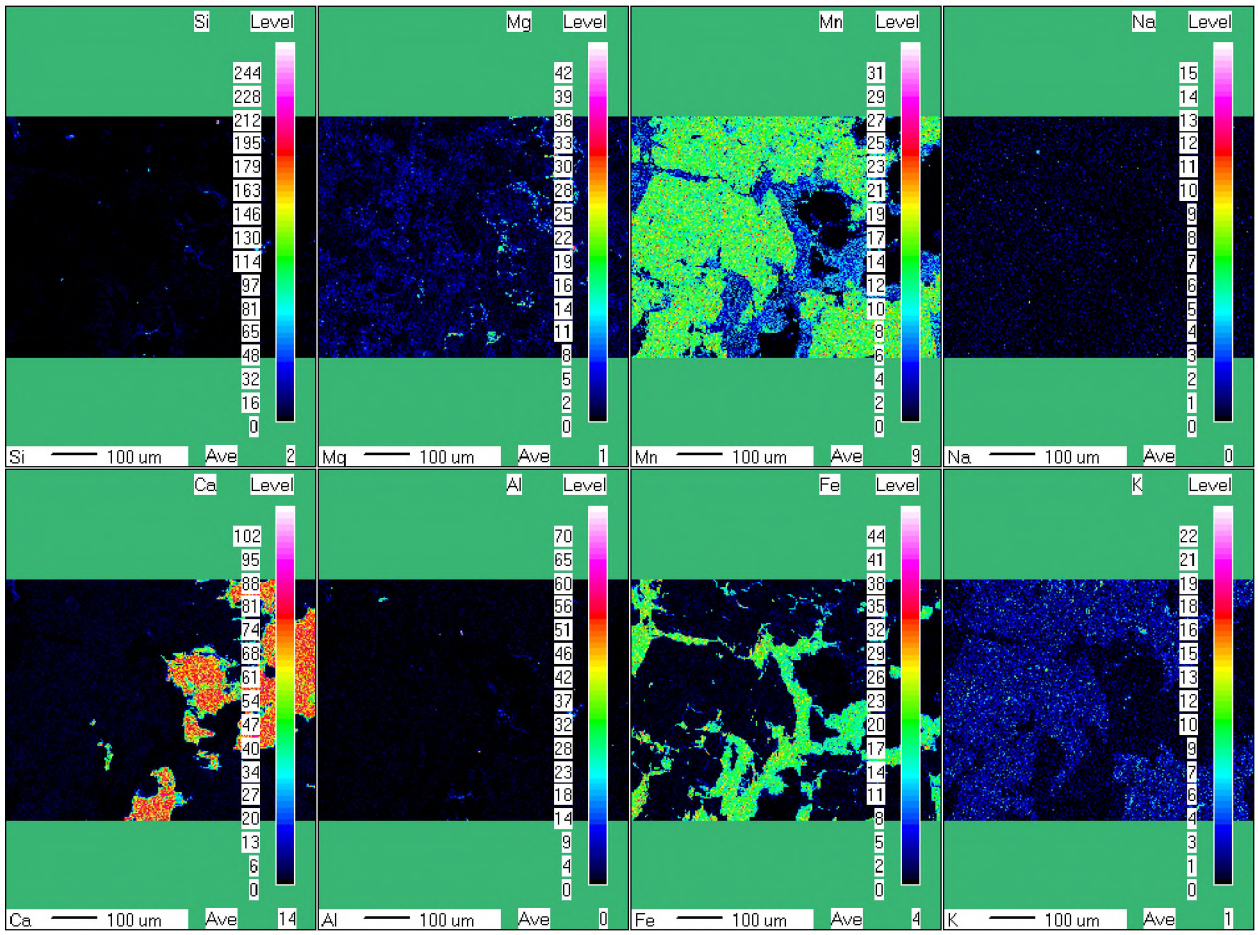

EMPA scan of a thin section from sample RW1 showing the composition of different elements.

A.1.5. RW4

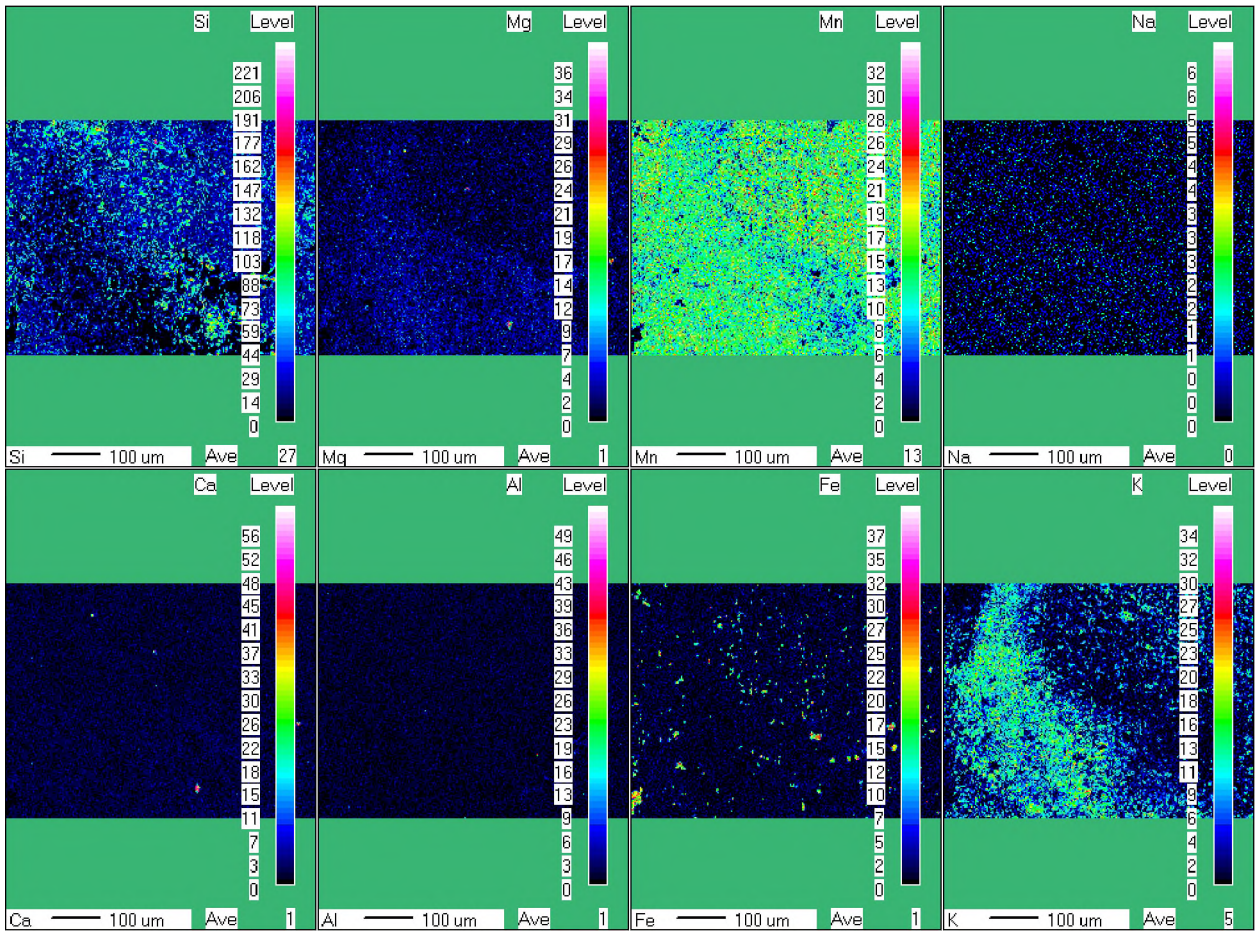

EMPA scan of a thin section from sample RW4 showing the composition of different elements.

A.1.6. RW8

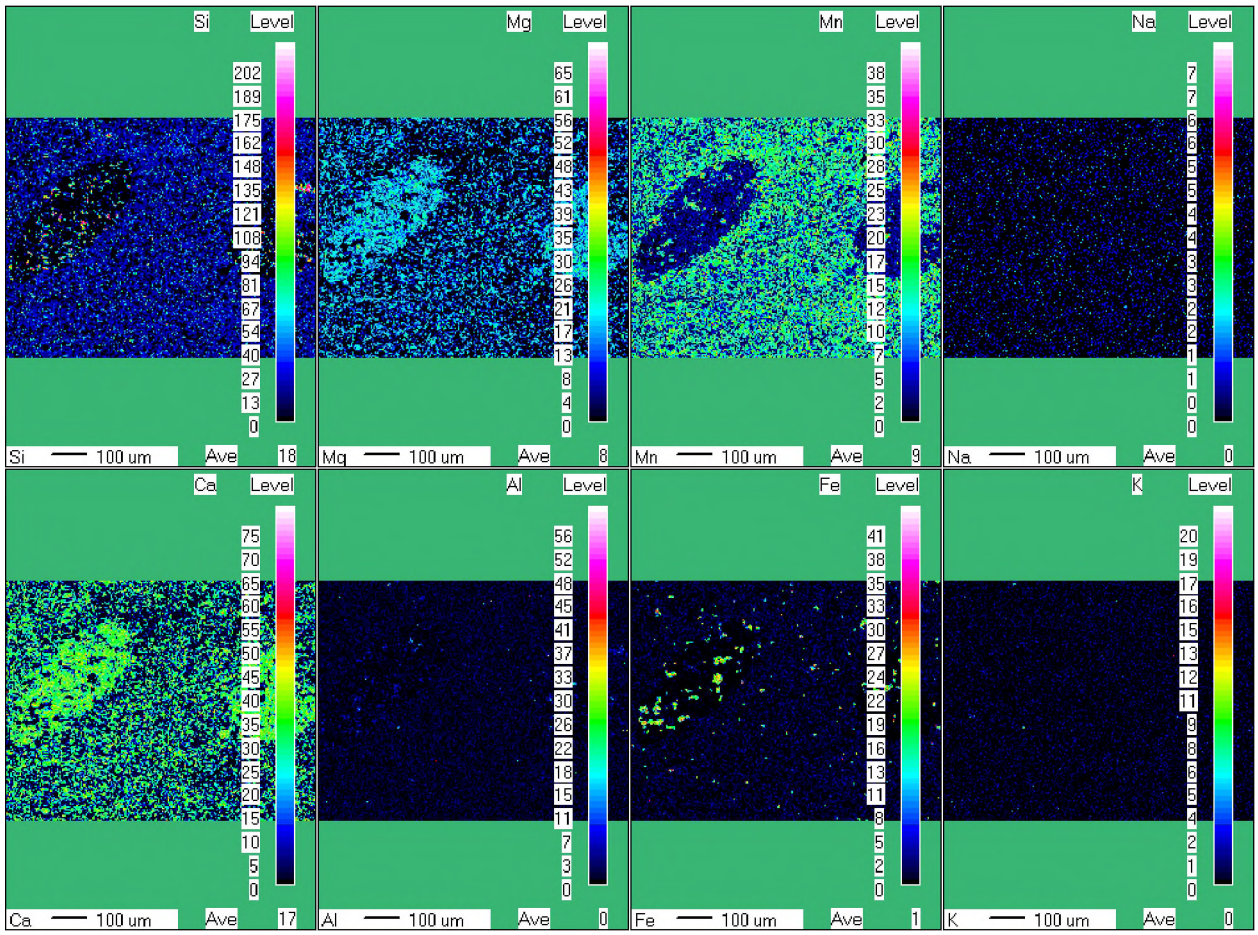

EMPA scan of a thin section from sample RW8 showing the composition of different elements.

A.1.7. RW12

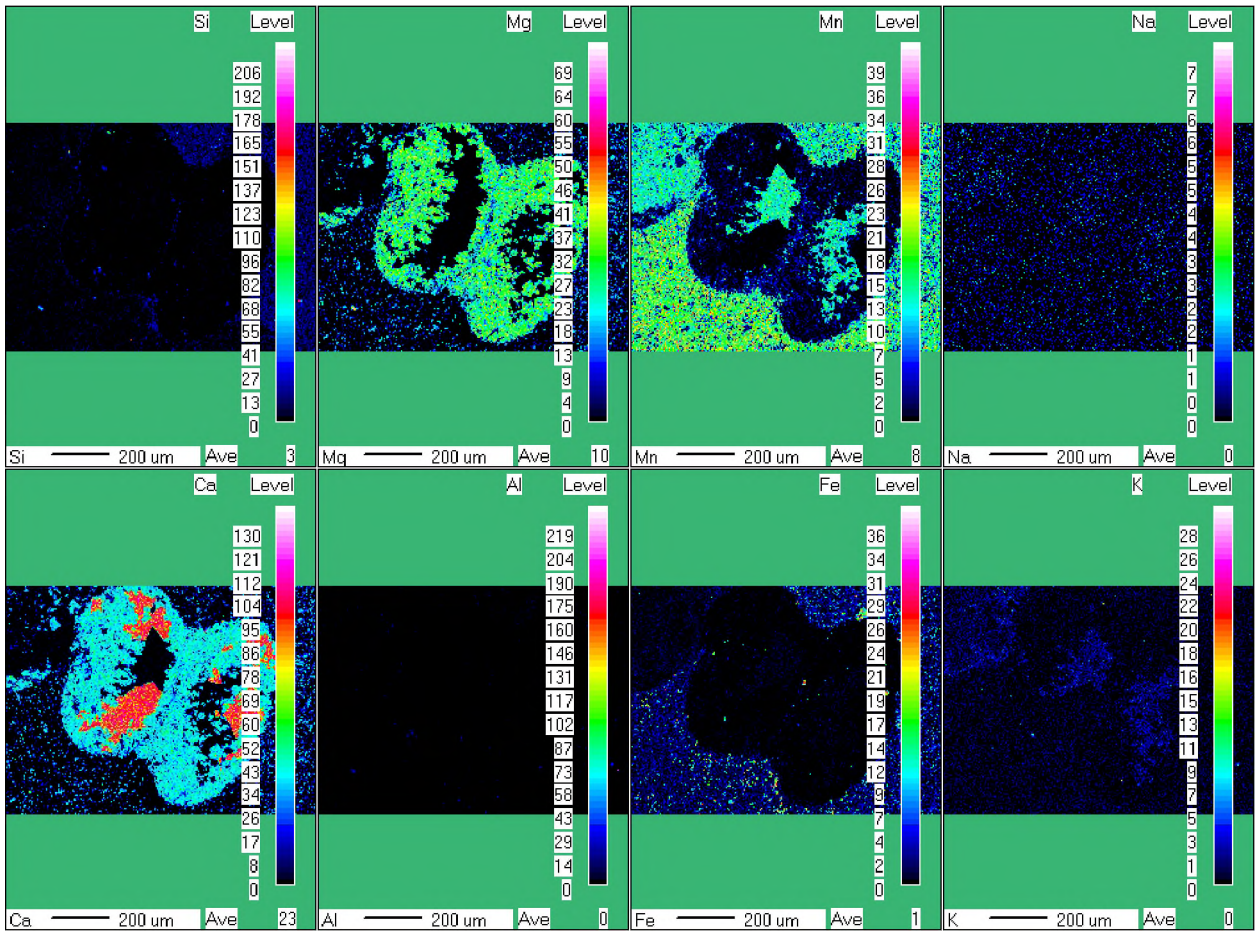

EMPA scan of a thin section from sample RW12 showing the composition of different elements.

A.1.8. RW16

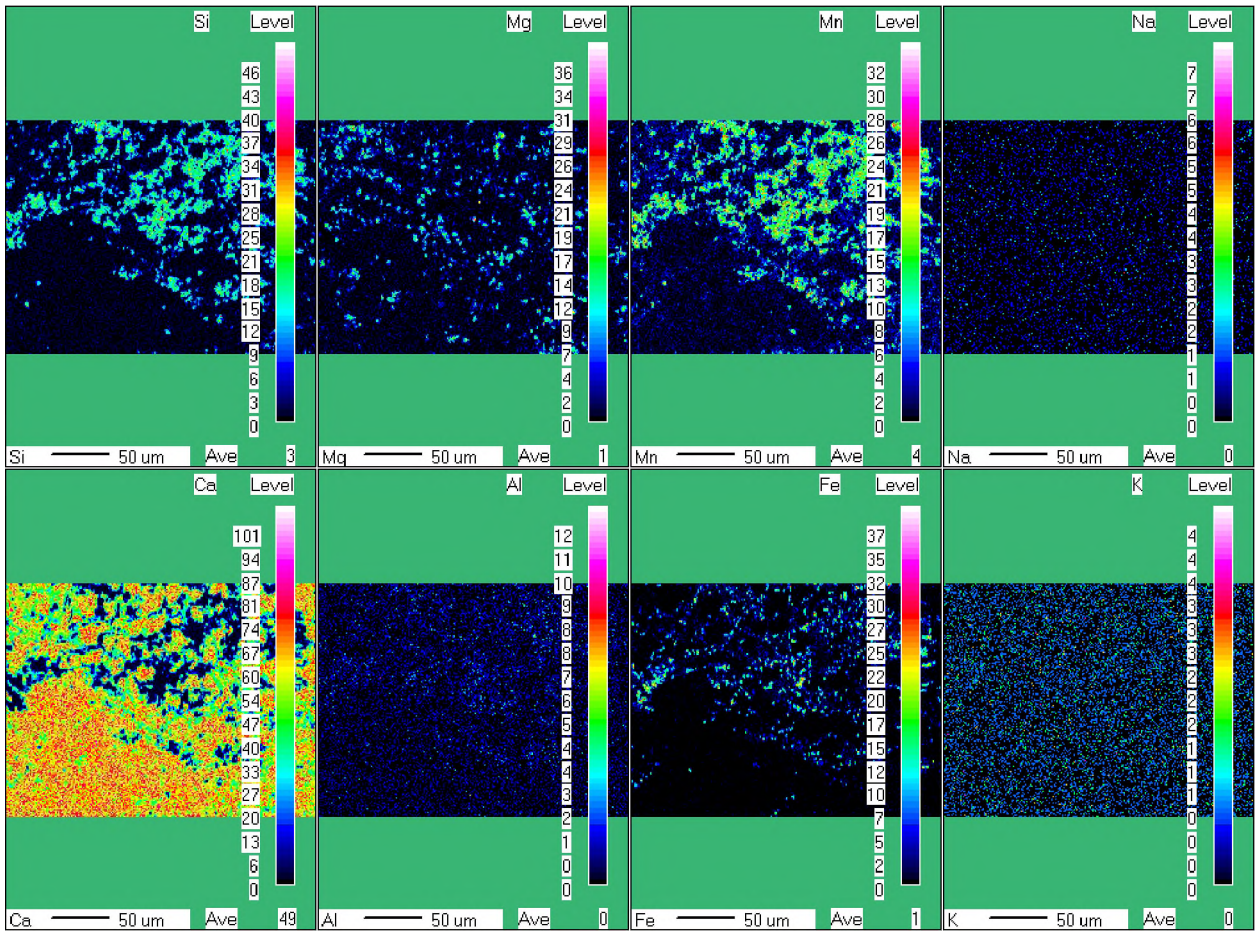

EMPA scan of a thin section from sample RW16 showing the composition of different elements.

Part B: EMPA raw data

B.1.1. Oxides

Comment	CaO Mass%	BaO Mass%	MgO Mass%	MnO Mass%	K_2O Mass%	FeO Mass%	SrO Mass%	P_2O_5 Mass%	CO_2 Mass%	Total Mass%
LSW9D_1b_1	1.288	0.154	3.734	70.502	0.011	0.847	0.025	0	23.439	**100**
LSW9D_1b_2	1.308	0.18	3.161	65.826	0.011	4.715	0	0	24.8	**100.001**
LSW9D_1b_3	1.095	0.125	3.708	72.246	0.017	0.612	0.057	0	22.14	**100**
LSW9D_1b_4	1.511	0.134	3.167	66.364	0.004	2.637	0	0.019	26.163	**99.999**
LSW8_7_1	55.987	0.028	0.404	0.054	0	0.005	0	0	43.521	**99.999**
LSW8_7_2	57.227	0	0.669	0.216	0	0.021	0	0	41.868	**100.001**
LSW8_7_3	56.799	0	0.917	0.12	0	0.023	0	0.028	42.113	**100**
LSW8_7_4	55.712	0	0.386	0.279	0	0.02	0	0.032	43.572	**100.001**
LSW8_7_5	55.654	0	1.195	0.105	0	0.074	0	0.039	42.932	**99.999**
LSW8_7_6	60.139	0	0.307	0.16	0.002	0.002	0	0.021	39.369	**100**
LSW8_7_7	56.589	0	0.369	0	0	0.016	0	0.044	42.981	**99.999**
LSW8_7_8	58.098	0.067	0.2	0.028	0	0	0	0.015	41.59	**99.998**
LSW8_7_9	56.66	0.008	0.645	0	0	0	0	0.068	42.618	**99.999**
LSW8_8_1	38.331	0	20.393	0	0	0.017	0	0	41.26	**100.001**
LSW8_8_2	36.402	0	19.898	0.145	0	0	0	0.023	43.531	**99.999**
LSW8_8_3	36.776	0	19.698	0.026	0	0.01	0	0.014	43.475	**99.999**
LSW8_8_4	36.33	0	19.758	0.043	0.001	0.084	0	0	43.783	**99.999**
LSW8_8_5	36.281	0.043	19.943	0.072	0	0.024	0	0.021	43.617	**100.001**
LSW8_8_6	38.069	0.042	20.432	0.045	0	0	0	0	41.411	**99.999**
LSW8_8_7	37.706	0.01	19.419	0	0	0	0	0	42.865	**100**
LSW8_8_8	35.852	0.023	19.996	0.028	0	0	0	0	44.1	**99.999**
LSW8_8_9	36.275	0.035	19.806	0	0	0	0	0.029	43.856	**100.001**
RW5_18_1	57.943	0	0.015	1.851	0.001	0	0	0.011	40.18	**100.001**
RW5_18_2	54.358	0	0.028	1.939	0.002	0.03	0	0.02	43.623	**100**
RW5_18_3	55.736	0	0.027	5.316	0	0.036	0	0	38.885	**100**
RW5_18_4	58.002	0	0.032	3.95	0	0	0	0.005	38.012	**100.001**
RW5_18_5	54.773	0.012	0.026	2.459	0	0.032	0	0.021	42.676	**99.999**
RW5_18_6	56.26	0.025	0.059	2.012	0	0.034	0	0.038	41.573	**100.001**
LSW9A_24_1	38.817	0	19.54	0	0	0.001	0	0	41.641	**99.999**
LSW9A_24_2	38.105	0.008	19.544	0	0	0.04	0	0.037	42.266	**100**
LSW9A_24_3	37.881	0	20.224	0	0.001	0.007	0	0.038	41.849	**100**
LSW9A_24_4	39.037	0	17.954	0.056	0	0.074	0	0	42.878	**99.999**
LSW9A_24_5	36.808	0.043	19.566	0.007	0.002	0.034	0	0.025	43.513	**99.998**
LSW9A_24_6	38.457	0	19.567	0.061	0	0.056	0	0.004	41.854	**99.999**
LSW6_28_1	58.655	0	0.207	2.265	0	0.103	0	0.023	38.748	**100.001**
LSW6_28_2	55.979	0	0.392	2.436	0	0	0	0.003	41.189	**99.999**
LSW6_28_3	59.955	0	0.263	2.463	0	0.036	0	0.019	37.264	**100**

LSW6_28_4	58.261	0	0.672	2.888	0	0.048	0	0.018	38.113	**100**
LSW3_35_1	53.092	0	0.375	2.325	0	0.566	0	0.072	43.571	**100.001**
LSW3_35_2	56.637	0.048	0.183	0.162	0	0.233	0	0.006	42.729	**99.998**
LSW3_35_3	57.301	0.087	0.367	2.644	0	0.311	0	0.02	39.269	**99.999**
LSW3_35_4	57.255	0	0.139	0.242	0	0.309	0	0.016	42.038	**99.999**
LSW3_35_5	52.263	0	0.874	0.608	0	0.717	0	0	45.537	**99.999**
LSW3_37_1	56.148	0.007	0.469	0.154	0.003	0.144	0	0.022	43.052	**99.999**
LSW3_37_2	55.038	0	0.873	0.026	0	0.203	0	0.017	43.843	**100**
LSW3_37_3	55.729	0	0.497	0.037	0	0.187	0	0.012	43.537	**99.999**
LSW3_37_4	56.141	0.043	0.374	0.126	0	0.385	0	0.003	42.928	**100**
LSW3_37_5	55.189	0	0.249	0.13	0	0.208	0	0.009	44.217	**100.002**
LSW3_39_1	2.242	0.266	2.281	73.809	0.027	0.937	0.208	0	20.23	**100**
LSW3_39_2	2.372	0.171	2.45	70.956	0.029	0.74	0.24	0.006	23.035	**99.999**
LSW3_39_3	2.318	0.312	2.38	67.541	0.028	0.8	0.156	0.006	26.46	**100.001**
LSW3_39_4	2.312	0.207	2.286	70.226	0.023	1.065	0.249	0.035	23.598	**100.001**
LSW3_39_5	2.302	0.187	2.364	71.552	0.023	0.595	0.167	0.024	22.787	**100.001**
RW1_3_1	57.251	0	0.632	0	0	0.066	0	0.035	42.017	**100.001**
RW1_3_2	56.11	0.056	0.434	0.139	0	0	0	0.009	43.253	**100.001**
RW1_3_3	56.617	0	0.221	0.202	0	0	0	0.028	42.933	**100.001**
RW1_3_4	58.179	0	0.604	0.034	0	0	0	0	41.183	**100**
RW1_3_5	56.876	0.025	0.587	0.116	0	0.015	0	0.013	42.368	**100**
RW1_3_6	55.716	0.079	0.555	0.036	0	0	0	0	43.614	**100**
RW1_4_1	38.118	0.025	19.888	0.073	0	0.008	0	0.014	41.875	**100.001**
RW1_4_2	37.514	0	20.698	0.016	0	0	0	0.019	41.752	**99.999**
RW1_4_3	36.093	0	20.1	0.082	0	0	0	0	43.725	**100**
RW1_4_4	36.495	0.005	20.093	0.001	0	0.021	0	0.044	43.341	**100**
RW1_4_5	36.809	0	21.457	0.05	0	0	0	0.05	41.635	**100.001**
RW2_6_1	59.47	0	0.738	0	0	0.048	0	0.027	39.716	**99.999**
RW2_6_2	53.533	0.019	0.21	0.109	0.006	0	0	0.018	46.105	**100**
RW2_6_3	57.2	0	0.27	0	0	0.019	0	0.003	42.508	**100**
RW2_6_4	55.976	0	0.556	0	0.001	0	0	0.016	43.451	**100**
RW2_6_5	58.767	0.014	0.103	0.054	0	0.043	0	0.031	40.986	**99.998**
LSW7_22_1	52.889	0	0	0.263	0	0.028	0	42.483	4.336	**99.999**
LSW7_22_2	52.918	0.028	0	0.536	0.003	0.05	0	40.517	5.949	**100.001**
LSW7_22_3	52.986	0.003	0	0.448	0	0.009	0	41.975	4.579	**100**
LSW7_22_4	52.136	0.039	0	0.453	0.01	0.096	0.352	42.749	4.164	**99.999**
LSW7_22_5	52.954	0.032	0	0.389	0.007	0	0	41.948	4.672	**100.002**
LSW7_22_6	52.4	0	0	2.549	0	0.027	0	41.197	3.827	**100**
LSW7_22_7	52.255	0	0	0.188	0	0.074	0	42.378	5.106	**100.001**
RW9_23_1	52.919	0	0.332	2.656	0	0.017	0	0.01	44.067	**100.001**
RW9_23_2	53.405	0	0.27	6.22	0.011	0.014	0	0.012	40.068	**100**

RW9_23_3	56.516	0	0.229	2.664	0	0	0	0.03	40.562	**100.001**
RW9_23_4	54.32	0	0.27	2.584	0	0.033	0	0.008	42.785	**100**
RW9_23_5	54.599	0	0.282	2.253	0.005	0.05	0	0	42.81	**99.999**
RW9_23_6	54.369	0	0.258	2.245	0	0	0	0.046	43.084	**100.002**
RW10_28_1	56.396	0.056	0.316	2.72	0	0	0	0.025	40.488	**100.001**
RW10_28_2	57.008	0	0.142	2.801	0	0.064	0	0.023	39.961	**99.999**
RW10_28_3	54.476	0.037	0.208	2.391	0	0	0	0.029	42.859	**100**
RW10_28_4	57.326	0.007	0.247	5.989	0	0.079	0	0.015	36.337	**100**
RW10_28_5	54.162	0.021	0.173	2.488	0	0	0	0	43.156	**100**
RW10_28_6	56.584	0.038	0.15	2.503	0	0.078	0	0.033	40.613	**99.999**
RW16_29_1	52.793	0.05	0.28	5.344	0	0.103	0	0.014	41.417	**100.001**
RW16_29_2	54.36	0.003	0.148	4.277	0	0.054	0	0	41.158	**100**
RW16_29_3	53.907	0.05	0.279	5.167	0	0.091	0	0.037	40.469	**100**
RW16_29_4	54.444	0.06	0.29	5.967	0	0	0	0.034	39.205	**100**
RW16_29_5	54.577	0	0.212	3.899	0	0	0	0.037	41.274	**99.999**
RW16_29_6	51.713	0	0.345	5.231	0.012	0.108	0	0.012	42.579	**100**

B.1.2. Carbonates

Comment	**CaO Mass%**	**BaO Mass%**	**MgO Mass%**	**MnO Mass%**	**K_2O Mass%**	**FeO Mass%**	**SrO Mass%**	**P_2O_5 Mass%**	**CO_2 Mass%**	**Total Mass%**
LSW9D_1b_1	1.288	0.154	3.734	70.502	0.011	0.847	0.025	0	23.439	**100**
LSW9D_1b_2	1.308	0.18	3.161	65.826	0.011	4.715	0	0	24.8	**100.001**
LSW9D_1b_3	1.095	0.125	3.708	72.246	0.017	0.612	0.057	0	22.14	**100**
LSW9D_1b_4	1.511	0.134	3.167	66.364	0.004	2.637	0	0.019	26.163	**99.999**
LSW8_7_1	55.987	0.028	0.404	0.054	0	0.005	0	0	43.521	**99.999**
LSW8_7_2	57.227	0	0.669	0.216	0	0.021	0	0	41.868	**100.001**
LSW8_7_3	56.799	0	0.917	0.12	0	0.023	0	0.028	42.113	**100**
LSW8_7_4	55.712	0	0.386	0.279	0	0.02	0	0.032	43.572	**100.001**
LSW8_7_5	55.654	0	1.195	0.105	0	0.074	0	0.039	42.932	**99.999**
LSW8_7_6	60.139	0	0.307	0.16	0.002	0.002	0	0.021	39.369	**100**
LSW8_7_7	56.589	0	0.369	0	0	0.016	0	0.044	42.981	**99.999**
LSW8_7_8	58.098	0.067	0.2	0.028	0	0	0	0.015	41.59	**99.998**
LSW8_7_9	56.66	0.008	0.645	0	0	0	0	0.068	42.618	**99.999**
LSW8_8_1	38.331	0	20.393	0	0	0.017	0	0	41.26	**100.001**
LSW8_8_2	36.402	0	19.898	0.145	0	0	0	0.023	43.531	**99.999**
LSW8_8_3	36.776	0	19.698	0.026	0	0.01	0	0.014	43.475	**99.999**
LSW8_8_4	36.33	0	19.758	0.043	0.001	0.084	0	0	43.783	**99.999**
LSW8_8_5	36.281	0.043	19.943	0.072	0	0.024	0	0.021	43.617	**100.001**
LSW8_8_6	38.069	0.042	20.432	0.045	0	0	0	0	41.411	**99.999**
LSW8_8_7	37.706	0.01	19.419	0	0	0	0	0	42.865	**100**
LSW8_8_8	35.852	0.023	19.996	0.028	0	0	0	0	44.1	**99.999**

LSW8_8_9	36.275	0.035	19.806	0	0	0	0	0.029	43.856	**100.001**
RW5_18_1	57.943	0	0.015	1.851	0.001	0	0	0.011	40.18	**100.001**
RW5_18_2	54.358	0	0.028	1.939	0.002	0.03	0	0.02	43.623	**100**
RW5_18_3	55.736	0	0.027	5.316	0	0.036	0	0	38.885	**100**
RW5_18_4	58.002	0	0.032	3.95	0	0	0	0.005	38.012	**100.001**
RW5_18_5	54.773	0.012	0.026	2.459	0	0.032	0	0.021	42.676	**99.999**
RW5_18_6	56.26	0.025	0.059	2.012	0	0.034	0	0.038	41.573	**100.001**
LSW9A_24_1	38.817	0	19.54	0	0	0.001	0	0	41.641	**99.999**
LSW9A_24_2	38.105	0.008	19.544	0	0	0.04	0	0.037	42.266	**100**
LSW9A_24_3	37.881	0	20.224	0	0.001	0.007	0	0.038	41.849	**100**
LSW9A_24_4	39.037	0	17.954	0.056	0	0.074	0	0	42.878	**99.999**
LSW9A_24_5	36.808	0.043	19.566	0.007	0.002	0.034	0	0.025	43.513	**99.998**
LSW9A_24_6	38.457	0	19.567	0.061	0	0.056	0	0.004	41.854	**99.999**
LSW6_28_1	58.655	0	0.207	2.265	0	0.103	0	0.023	38.748	**100.001**
LSW6_28_2	55.979	0	0.392	2.436	0	0	0	0.003	41.189	**99.999**
LSW6_28_3	59.955	0	0.263	2.463	0	0.036	0	0.019	37.264	**100**
LSW6_28_4	58.261	0	0.672	2.888	0	0.048	0	0.018	38.113	**100**
LSW3_35_1	53.092	0	0.375	2.325	0	0.566	0	0.072	43.571	**100.001**
LSW3_35_2	56.637	0.048	0.183	0.162	0	0.233	0	0.006	42.729	**99.998**
LSW3_35_3	57.301	0.087	0.367	2.644	0	0.311	0	0.02	39.269	**99.999**
LSW3_35_4	57.255	0	0.139	0.242	0	0.309	0	0.016	42.038	**99.999**
LSW3_35_5	52.263	0	0.874	0.608	0	0.717	0	0	45.537	**99.999**
LSW3_37_1	56.148	0.007	0.469	0.154	0.003	0.144	0	0.022	43.052	**99.999**
LSW3_37_2	55.038	0	0.873	0.026	0	0.203	0	0.017	43.843	**100**
LSW3_37_3	55.729	0	0.497	0.037	0	0.187	0	0.012	43.537	**99.999**
LSW3_37_4	56.141	0.043	0.374	0.126	0	0.385	0	0.003	42.928	**100**
LSW3_37_5	55.189	0	0.249	0.13	0	0.208	0	0.009	44.217	**100.002**
LSW3_39_1	2.242	0.266	2.281	73.809	0.027	0.937	0.208	0	20.23	**100**
LSW3_39_2	2.372	0.171	2.45	70.956	0.029	0.74	0.24	0.006	23.035	**99.999**
LSW3_39_3	2.318	0.312	2.38	67.541	0.028	0.8	0.156	0.006	26.46	**100.001**
LSW3_39_4	2.312	0.207	2.286	70.226	0.023	1.065	0.249	0.035	23.598	**100.001**
LSW3_39_5	2.302	0.187	2.364	71.552	0.023	0.595	0.167	0.024	22.787	**100.001**
RW1_3_1	57.251	0	0.632	0	0	0.066	0	0.035	42.017	**100.001**
RW1_3_2	56.11	0.056	0.434	0.139	0	0	0	0.009	43.253	**100.001**
RW1_3_3	56.617	0	0.221	0.202	0	0	0	0.028	42.933	**100.001**
RW1_3_4	58.179	0	0.604	0.034	0	0	0	0	41.183	**100**
RW1_3_5	56.876	0.025	0.587	0.116	0	0.015	0	0.013	42.368	**100**
RW1_3_6	55.716	0.079	0.555	0.036	0	0	0	0	43.614	**100**
RW1_4_1	38.118	0.025	19.888	0.073	0	0.008	0	0.014	41.875	**100.001**
RW1_4_2	37.514	0	20.698	0.016	0	0	0	0.019	41.752	**99.999**
RW1_4_3	36.093	0	20.1	0.082	0	0	0	0	43.725	**100**

RW1_4_4	36.495	0.005	20.093	0.001	0	0.021	0	0.044	43.341	**100**
RW1_4_5	36.809	0	21.457	0.05	0	0	0	0.05	41.635	**100.001**
RW2_6_1	59.47	0	0.738	0	0	0.048	0	0.027	39.716	**99.999**
RW2_6_2	53.533	0.019	0.21	0.109	0.006	0	0	0.018	46.105	**100**
RW2_6_3	57.2	0	0.27	0	0	0.019	0	0.003	42.508	**100**
RW2_6_4	55.976	0	0.556	0	0.001	0	0	0.016	43.451	**100**
RW2_6_5	58.767	0.014	0.103	0.054	0	0.043	0	0.031	40.986	**99.998**
LSW7_22_1	52.889	0	0	0.263	0	0.028	0	42.483	4.336	**99.999**
LSW7_22_2	52.918	0.028	0	0.536	0.003	0.05	0	40.517	5.949	**100.001**
LSW7_22_3	52.986	0.003	0	0.448	0	0.009	0	41.975	4.579	**100**
LSW7_22_4	52.136	0.039	0	0.453	0.01	0.096	0.352	42.749	4.164	**99.999**
LSW7_22_5	52.954	0.032	0	0.389	0.007	0	0	41.948	4.672	**100.002**
LSW7_22_6	52.4	0	0	2.549	0	0.027	0	41.197	3.827	**100**
LSW7_22_7	52.255	0	0	0.188	0	0.074	0	42.378	5.106	**100.001**
RW9_23_1	52.919	0	0.332	2.656	0	0.017	0	0.01	44.067	**100.001**
RW9_23_2	53.405	0	0.27	6.22	0.011	0.014	0	0.012	40.068	**100**
RW9_23_3	56.516	0	0.229	2.664	0	0	0	0.03	40.562	**100.001**
RW9_23_4	54.32	0	0.27	2.584	0	0.033	0	0.008	42.785	**100**
RW9_23_5	54.599	0	0.282	2.253	0.005	0.05	0	0	42.81	**99.999**
RW9_23_6	54.369	0	0.258	2.245	0	0	0	0.046	43.084	**100.002**
RW10_28_1	56.396	0.056	0.316	2.72	0	0	0	0.025	40.488	**100.001**
RW10_28_2	57.008	0	0.142	2.801	0	0.064	0	0.023	39.961	**99.999**
RW10_28_3	54.476	0.037	0.208	2.391	0	0	0	0.029	42.859	**100**
RW10_28_4	57.326	0.007	0.247	5.989	0	0.079	0	0.015	36.337	**100**
RW10_28_5	54.162	0.021	0.173	2.488	0	0	0	0	43.156	**100**
RW10_28_6	56.584	0.038	0.15	2.503	0	0.078	0	0.033	40.613	**99.999**
RW16_29_1	52.793	0.05	0.28	5.344	0	0.103	0	0.014	41.417	**100.001**
RW16_29_2	54.36	0.003	0.148	4.277	0	0.054	0	0	41.158	**100**
RW16_29_3	53.907	0.05	0.279	5.167	0	0.091	0	0.037	40.469	**100**
RW16_29_4	54.444	0.06	0.29	5.967	0	0	0	0.034	39.205	**100**
RW16_29_5	54.577	0	0.212	3.899	0	0	0	0.037	41.274	**99.999**
RW16_29_6	51.713	0	0.345	5.231	0.012	0.108	0	0.012	42.579	**100**

B.1.3. Silicates

Comment	SiO_2 Mass%	Al_2O_3 Mass%	CaO Mass%	MgO Mass%	Cr_2O_3 Mass%	K_2O Mass%	MnO Mass%	FeO Mass%	Na_2O Mass%	TiO_2 Mass%	BaO Mass%	Total Mass%
LSW9D_4_1	24.591	0.055	1.651	2.084	0	0.189	47.325	1.394	0.81	0.021	0.081	**78.201**
LSW9D_4_2	36.032	0.031	1.331	1.735	0	0.132	39.183	1.171	0.72	0	0.022	**80.357**
LSW9D_4_3	44.401	0.041	1.271	1.455	0	0.118	35.145	0.949	0.688	0	0.067	**84.135**
LSW9D_4_4	1.75	0	1.634	3.461	0.15	0.242	64.422	1.555	1.148	0	0.034	**74.396**
LSW9E_16_1	36.953	21.403	21.989	0.115	0.082	0.001	0.167	14.953	0.049	0.034	0.019	**95.765**
LSW9E_16_2	37.095	21.461	22.765	0.014	0	0.003	0.049	15.005	0.045	0.024	0	**96.461**
RW5_19_1	44.552	1.335	0.289	38.742	0	0.017	0.659	0.849	0	0.006	0	**86.449**
RW5_19_2	44.432	0.792	0.29	41.745	0	0.003	0.783	0.676	0	0	0.031	**88.752**
RW5_19_3	40.902	1.236	0.658	26.064	0	0.068	0.965	13.348	0.201	0.012	0.009	**83.463**
RW5_19_4	44.205	0.437	0.277	40.161	0.04	0	0.615	0.532	0	0	0.048	**86.315**
RW5_21_1	54.422	1.932	0.631	23.407	0	0.046	2.597	1.915	0.141	0.007	0.033	**85.131**
RW5_21_2	51.671	1.478	0.484	23.74	0.015	0.047	1.599	2.052	0.149	0.008	0.033	**81.276**
RW5_21_3	45.661	1.499	0.484	19.253	0.037	0.037	1.259	1.683	0.115	0.05	0	**70.078**
RW5_21_4	51.534	2.044	0.578	23.476	0.017	0.03	1.239	1.658	0.116	0.013	0.031	**80.736**
RW5_21_5	51.613	2.174	0.563	22.476	0	0.04	1.145	1.719	0.11	0	0.03	**79.87**
RW2_7_1	6.876	0.579	0.852	1.019	0.033	0.063	32.154	33.749	0.325	0.1	0.05	**75.8**
RW2_7_2	14.334	0.701	0.454	0.523	0.013	0.01	23.576	45.889	0	0.09	0	**85.59**
RW2_7_3	7.864	1.173	0.957	1.636	0.02	0.059	35.212	37.59	0.52	0.066	0.067	**85.164**
RW2_7_4	9.687	1.085	0.636	1.077	0.028	0.055	29.201	43.233	0.182	0.043	0.056	**85.283**
RW2_7_5	12.234	2.507	0.862	1.379	0	0.067	25.777	34.296	0.302	0.087	0.014	**77.525**
LSW1_10_1	9.64	0.083	1.01	0.275	0	0.001	78.896	5.623	0	0	0.051	**95.579**
LSW1_10_2	9.344	0.061	0.981	0.204	0	0.016	75.216	5.051	0	0.015	0.007	**90.895**
LSW1_10_3	9.243	0.053	0.734	0.261	0	0.042	76.779	5.597	0.04	0	0	**92.749**
LSW1_10_4	9.439	0.057	0.973	0.19	0	0.011	76.394	5.092	0.162	0.026	0	**92.344**
LSW1_10_5	9.491	0.025	1.026	0.302	0.068	0	76.576	6.108	0.006	0	0	**93.602**
LSW1_14_1	0.085	0.126	0.722	0.546	0.078	2.537	47.531	2.098	0.625	0.018	0	**54.366**
LSW1_14_2	0.07	0.097	0.643	0.518	0.009	2.049	38.708	1.537	0.522	0.026	0.024	**44.203**
LSW1_14_3	0.07	0.075	0.522	0.49	0.026	1.955	33.466	1.484	0.576	0.008	0.002	**38.674**
LSW1_14_4	0.08	0.092	0.995	0.651	0	3.286	68.901	3.411	0.834	0.022	0.007	**78.279**
LSW1_14_5	0.08	0.064	0.715	0.544	0.006	2.609	46.612	1.944	0.733	0	0.059	**53.366**
LSW1_14_6	0.069	0.064	0.922	0.839	0.039	3.208	61.096	2.429	0.66	0.006	0.01	**69.342**
LSW1_14_7	1.309	0.071	0.654	0.535	0.097	1.911	45.808	2.289	0.685	0.002	0.023	**53.384**
LSW4_15_1	8.99	0.12	0.915	0.115	0	0.016	78.333	3.031	0.019	0	0.035	**91.574**
LSW4_15_2	9.399	0.079	1.078	0.182	0.114	0.011	65.458	4.936	0	0	0	**81.257**
LSW4_15_3	9.165	0.317	1.033	0.155	0.105	0	75.972	3.855	0	0	0	**90.602**
LSW4_15_4	9.289	0.054	0.993	0.218	0.173	0	73.908	4.509	0	0.029	0	**89.173**
LSW4_15_5	9.028	0.049	1.106	0.194	0	0.027	72.142	5.707	0	0	0	**88.253**
RW9_24_1	9.299	0.066	1.296	0.214	0	0	70.786	5.321	0	0	0	**86.982**

RW9_24_2	9.75	0.062	1.102	0.439	0	0.002	72.835	5.156	0	0.01	0	**89.356**
RW9_24_3	9.198	0.489	1.121	0.186	0	0	73.349	4.025	0	0.019	0	**88.387**
RW9_24_4	9.537	0.186	1.213	0.227	0	0	72.014	4.972	0	0.009	0	**88.158**
RW9_24_5	8.466	0.086	0.758	0.179	0.005	0.016	70.816	5.665	0	0.045	0.019	**86.055**
RW16_30_1	8.783	0.253	1.624	0.073	0.008	0	75.897	3.055	0	0.033	0	**89.726**
RW16_30_2	8.205	0.231	1.224	0.136	0.061	0	78.147	2.521	0	0	0	**90.525**
RW16_30_3	8.482	0.22	1.394	0.373	0	0.002	77.011	2.567	0	0	0.054	**90.103**
RW16_30_4	8.163	0.274	1.138	0.084	0.057	0	76.296	2.499	0	0.021	0	**88.532**
RW16_30_5	8.896	0.415	0.716	0.007	0	0	76.157	2.817	0	0.029	0	**89.037**